

# Blood pressure waveform characteristics exposed by spectral analysis and neural nets

**Citation for published version (APA):**

Prentza, A. (1997). *Blood pressure waveform characteristics exposed by spectral analysis and neural nets*. [Phd Thesis 1 (Research TU/e / Graduation TU/e), Electrical Engineering]. Technische Universiteit Eindhoven. <https://doi.org/10.6100/IR495052>

**DOI:**

[10.6100/IR495052](https://doi.org/10.6100/IR495052)

**Document status and date:**

Published: 01/01/1997

**Document Version:**

Publisher's PDF, also known as Version of Record (includes final page, issue and volume numbers)

**Please check the document version of this publication:**

- A submitted manuscript is the version of the article upon submission and before peer-review. There can be important differences between the submitted version and the official published version of record. People interested in the research are advised to contact the author for the final version of the publication, or visit the DOI to the publisher's website.
- The final author version and the galley proof are versions of the publication after peer review.
- The final published version features the final layout of the paper including the volume, issue and page numbers.

[Link to publication](#)

**General rights**

Copyright and moral rights for the publications made accessible in the public portal are retained by the authors and/or other copyright owners and it is a condition of accessing publications that users recognise and abide by the legal requirements associated with these rights.

- Users may download and print one copy of any publication from the public portal for the purpose of private study or research.
- You may not further distribute the material or use it for any profit-making activity or commercial gain
- You may freely distribute the URL identifying the publication in the public portal.

If the publication is distributed under the terms of Article 25fa of the Dutch Copyright Act, indicated by the "Taverne" license above, please follow below link for the End User Agreement:

[www.tue.nl/taverne](http://www.tue.nl/taverne)

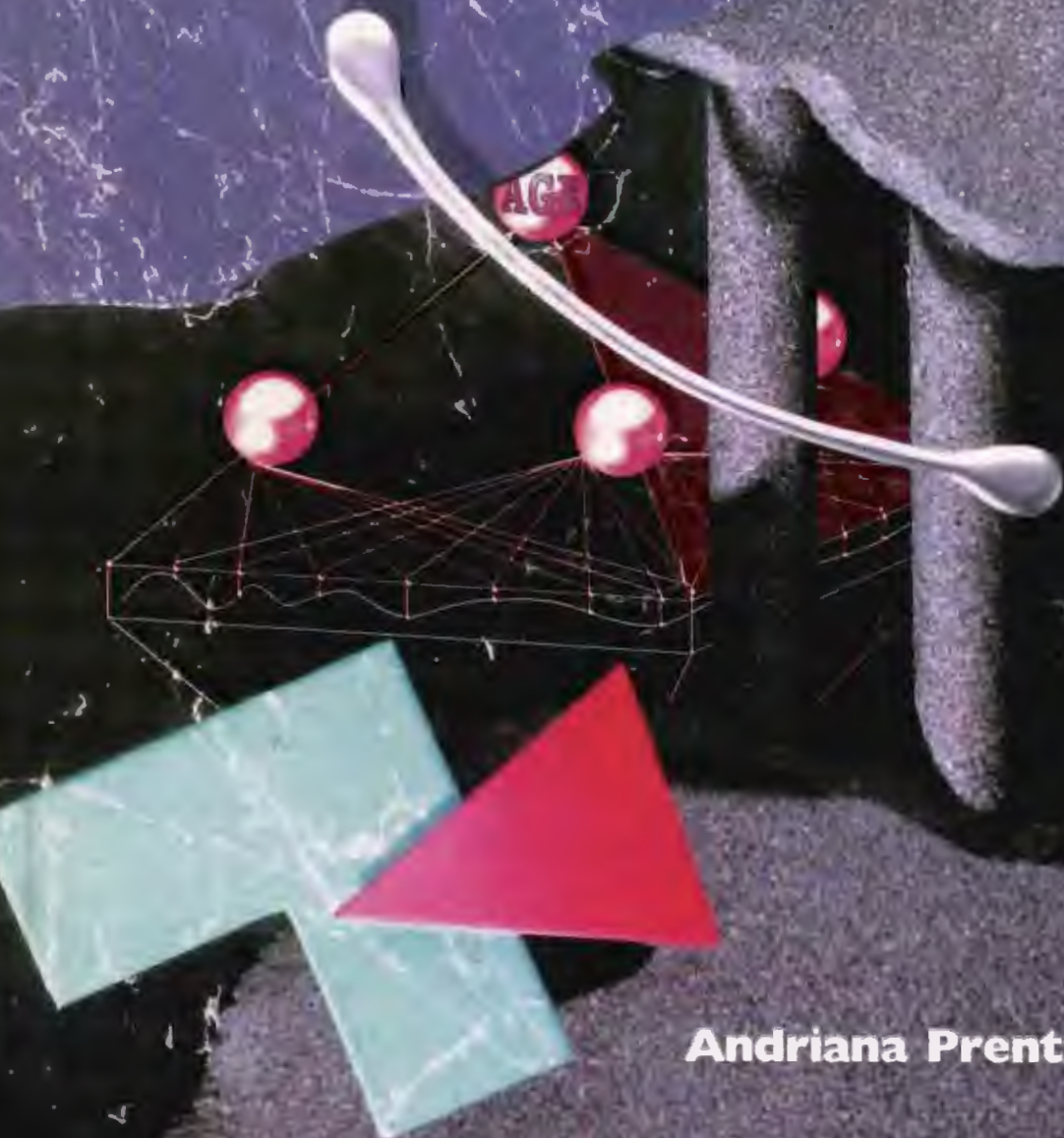
**Take down policy**

If you believe that this document breaches copyright please contact us at:

[openaccess@tue.nl](mailto:openaccess@tue.nl)

providing details and we will investigate your claim.

**Blood pressure waveform  
characteristics exposed  
by spectral analysis  
and neural nets**



**Andriana Prentza**

**Blood pressure waveform characteristics  
exposed by  
spectral analysis and neural nets**

**PROEFSCHRIFT**

ter verkrijging van de graad van doctor aan de  
Technische Universiteit Eindhoven, op gezag van de  
Rector Magnificus, prof.dr. M. Rem, voor een  
commissie aangewezen door het College van  
Dekanen in het openbaar te verdedigen  
op donderdag 3 juli 1997 om 16.00 uur

door

**Andriana Prentza**

geboren te Sydney, Australië

Dit proefschrift is goedgekeurd door de promotoren:

prof.ir. K.H. Wesseling  
en  
prof.dr.ir. P. Gizdulich

Copromotor: dr.ir. P.J.M. Cluitmans

CIP-DATA LIBRARY TECHNISCHE UNIVERSITEIT EINDHOVEN

Prentza, Andriana

Blood pressure waveform characteristics exposed by spectral analysis  
and neural nets / by Andriana Prentza. - Eindhoven : Technische  
Universiteit Eindhoven, 1997.

Proefschrift. - ISBN 90-386-0360-6

NUGI 743

Trefw.: bloeddrukmetingen / bloeddruk / neurale netwerken /  
spectraalanalyse / patientbewaking.

Subject headings: blood pressure measurement / neural nets /  
spectral analysis / patient monitoring.

Druk: Universiteitsdrukkerij, Technische Universiteit Eindhoven

*To my parents*

The work presented in this thesis has been carried out in the Division of Medical Electrical Engineering, Faculty Electrical Engineering, Eindhoven University of Technology, the Netherlands, in collaboration with TNO-TPD Biomedical Instrumentation, Academic Medical Centre, Amsterdam, the Netherlands. The research was supported in part by TNO-TPD Biomedical Instrumentation.

# Contents

<b>I</b>	<b>Introduction</b>	<b>1</b>
<b>II</b>	<b>Artificial Neural Networks</b>	<b>3</b>
1	General description . . . . .	3
2	Different types of neural nets . . . . .	4
2.1	Topology . . . . .	4
2.2	Learning algorithms . . . . .	5
3	Applications of neural nets . . . . .	6
3.1	Why use neural nets . . . . .	6
3.2	Where to use neural nets . . . . .	7
3.3	Application of neural nets in the medical area . . . . .	8
4	Backpropagation trained neural nets . . . . .	8
4.1	Transfer Functions . . . . .	10
4.2	Variations on the standard algorithm . . . . .	11
5	Practical Considerations . . . . .	13
5.1	Training and testing data sets . . . . .	13
5.2	Network size . . . . .	14
5.3	Scaling of data sets . . . . .	14
5.4	Input representation . . . . .	14
5.5	Software implementations of neural nets . . . . .	14
6	Conclusion . . . . .	15
	References . . . . .	15
<b>III</b>	<b>Detection of damped blood pressure waveforms</b>	<b>21</b>
1	Damped blood pressure waveforms detected by neural nets . . . . .	21
1.1	Introduction . . . . .	22
1.2	Methods . . . . .	23
	Subjects . . . . .	23
	Measurements . . . . .	23
	Data processing . . . . .	24
	Neural nets . . . . .	26
	Performance evaluation . . . . .	27

	Statistical significance of classification . . . . .	27
	Useful dimensionality of input vector . . . . .	27
1.3	Results . . . . .	28
	Damped / adequate classification . . . . .	28
	Error in clinically relevant parameters . . . . .	30
	Dimensionality of input data . . . . .	30
1.4	Discussion . . . . .	32
	Clinical applicability . . . . .	33
	Parameter vectors or waveforms . . . . .	34
	Quality factor . . . . .	35
	Neural nets . . . . .	35
1.5	Conclusion . . . . .	36
2	Damped blood pressure waveforms detected during exercise . . . . .	36
2.1	Methods . . . . .	36
	Subjects and Measurements . . . . .	36
	Data processing . . . . .	37
	Neural nets . . . . .	38
	Evaluating performance . . . . .	39
2.2	Results . . . . .	41
2.3	Discussion . . . . .	42
2.4	Conclusion . . . . .	44
3	Damped blood pressure waveforms detected by experts . . . . .	44
3.1	Introduction . . . . .	44
3.2	Methods . . . . .	45
3.3	Results . . . . .	46
3.4	Discussion . . . . .	47
	References . . . . .	48
<b>IV Brachial to finger pressure modelling</b>		<b>51</b>
1	Introduction . . . . .	52
2	Methods . . . . .	53
2.1	Subjects . . . . .	53
2.2	Pressure measurements . . . . .	53
2.3	Signal processing . . . . .	55
2.4	Model identification . . . . .	55
2.5	Inverse modelling . . . . .	57
2.6	Level correction . . . . .	57
2.7	Random subgroups . . . . .	57
3	Results . . . . .	57
3.1	Waveform distortion model . . . . .	58
3.2	Dependencies of model coefficients . . . . .	60
3.3	Inverse distortion model . . . . .	61



3.4	Level correction . . . . .	62
4	Discussion . . . . .	63
4.1	Waveform distortion . . . . .	64
4.2	Pressure levels . . . . .	65
5	Conclusion . . . . .	66
	Appendix . . . . .	67
	References . . . . .	70
<b>V</b>	<b>Human age estimated from finger pressure waveforms</b>	<b>73</b>
1	Human age estimated from finger pressure waveforms . . . . .	73
1.1	Introduction . . . . .	74
1.2	Methods . . . . .	75
Subjects	. . . . .	75
Measurements	. . . . .	77
Neural nets	. . . . .	77
Data processing	. . . . .	78
Reconstructed aortic waveforms	. . . . .	79
Composition of the train and the test selection	. . . . .	79
Statistics . . . . .		81
1.3	Results . . . . .	82
Performance of the neural nets . . . . .		84
Performance per subject group . . . . .		85
1.4	Discussion . . . . .	85
Generality of results . . . . .		85
Earlier efforts at age estimation with neural nets . . . . .		87
Comparison of finger and aorta waveforms . . . . .		87
Causes for waveform changes with age . . . . .		87
Vaso-active substances . . . . .		88
The possible meaning of pressure pulse estimated age . . . . .		89
1.5	Conclusions . . . . .	90
2	Neural net estimated age during 24hr . . . . .	90
2.1	Introduction . . . . .	90
2.2	Methods . . . . .	91
Subjects . . . . .		91
Measurements . . . . .		92
Data processing . . . . .		93
Statistics . . . . .		93
2.3	Results . . . . .	94
2.4	Discussion . . . . .	95
2.5	Conclusions . . . . .	96
	Appendix . . . . .	97
	References . . . . .	97

<b>Summary</b>	<b>101</b>
<b>Samenvatting</b>	<b>104</b>
<b>Acknowledgments</b>	<b>109</b>
<b>Curriculum vitae</b>	<b>110</b>

# Chapter I

## Introduction

This thesis is about blood pressure. Not the blood pressure that is read by a cuff and a stethoscope from your upper arm, but the blood pressure that represents the dynamic process of heart contraction (systole) and relaxation (diastole) and the ejection of blood in the arterial system. The continuously rising and falling pressure thus generated contains diagnostic information for example about your age, the condition of your heart, the state of your arterial system, the state of the baroreflex system that controls your blood pressure day in, day out, during your life.

When you are ill and on the operating table or in an intensive care unit this blood pressure is so important that it is often justified to measure it invasively. This is done by bringing into your arterial bloodstream a thin plastic tube filled with slightly salted and sweetened water, connected at the other end to an electronic manometer. More often than not, however, there is an extreme interest in your blood pressure but no sufficient justification to penetrate your skin and place the cannula. Until some 10 years ago nothing could be done about this dilemma but near that time a device became available that allows the noninvasive measurement of this blood pressure at the finger, the Finapres.

The availability of this device has created new possibilities for new research about blood pressure, its shape, its dynamics, its control, and its variability. At first this research was mainly methodological. Doctors had to become familiar with the device and the pressures it measured, with the accuracy of the measurements and with its limitations. An important number of studies, therefore, appeared on the comparison of blood pressure measured invasively at the upper arm and noninvasively at the finger. Accurate and reliable invasive recordings were necessary, but proved not easy to obtain. In this thesis we will develop, in Chapter III, a method based on the application of artificial neural networks to judge and to monitor a certain aspect of invasive blood pressure recording, its degree of linear distortion of the waveforms. From the studies, it appeared that arterial pressure at the finger differed in waveform and slightly in level from arterial pressure in the upper arm so they could not be compared directly. In Chapter IV of this thesis, we will study these differences between finger and brachial artery pressures, model them, and then apply inverse models to remove the differences.

From the blood pressure recordings, it is possible to extract on a beat-to-beat basis

certain parameters of diagnostic importance such as the systolic pressure as the highest pressure reached in each heart beat, the diastolic or lowest pressure, the heart rate, even the stroke volume of the left ventricle, the amount of blood that the heart presses into the arteries at each beat. Such parameters can now be extracted from the finger pressure record with increased accuracy, using the inverse models.

It has also become possible to challenge a subject's blood pressure, to record the responses to the challenge, and to diagnose aspects of blood pressure control such as the ability to redress with speed and effectiveness the evoked blood pressure changes and to stabilize blood pressure. An electric power plant has the similar task to stabilize the electric voltage in your home but it solves this problem quite differently. It has also been demonstrated that it is possible to record the blood pressure responses to physical stress such as when a person exercises on a bicycle. Mental stress, such as occurs during the defence of a PhD Thesis, or while lecturing to students, or reading aloud, or taking logical decisions, sometimes dramatically affects blood pressure control and this is now being recorded by numerous experimental psychologists providing new insight. This field of research we have left to the experts.

However, the shape of the blood pressure waveform in rest is interesting also. It has been known for a long time that these pulsations change with the increasing age of a subject. It has been speculated that these changes had to do with the aging of the arterial vessels which lose much of their elasticity with age. In Chapter V we shall use neural nets to detect the subtle changes in the arterial pulse with age, recorded at the finger. The changes in the waveform during the aging process can be attributed largely to the age of a subject, but not entirely. Some subjects will appear to have young waveforms for their age and some will appear with rather older waveforms. This differentiation seems absent below 30 years of age.

No longer is the recording of blood pressure limited to occasional numbers extracted from phenomena under an upper arm cuff, but the shape and the changes of the blood pressure wave can be recorded continuously and under the application of some new techniques partially developed in this thesis with increasing reliability, for as long as is necessary. This possibility we have used in this thesis to develop new techniques of hopefully diagnostic importance. Of course, we have only scratched the surface.

# Chapter II

## Artificial Neural Networks

This chapter is a general introduction to the subject of artificial neural networks (further called neural nets) which we use in some of the following chapters. We will describe the various types, their properties, and their suitability for certain tasks. One particular type, the multilayer feedforward neural net is described in more detail, since it was the network we selected for our purposes.

### 1 General description

Neural nets are networks of artificial "neurons". These neurons are linked with connections which have a certain intensity multiplier, called "weight". The weight determines the amount of effect that one neuron has to the one it is connected with.

A neuron receives input signals via the input connections (Fig. II.1). The input signals are summed and put to the transfer function of the neuron. The transfer function can be a linear function, but it is usually a nonlinear threshold or half bell-shaped, which passes information only if the input reaches a certain range of values. The output of the transfer function is forwarded to the input of further neurons through subsequent connections. There is also an extra input to the neuron called "bias". The bias is used to shift the position of the threshold function along the input-axis.

There is a schematic representation of a simple neural net in Fig II.2. The neurons are organized into layers. When all the neurons of one layer are connected with all the neurons of the next layer, then this neural net is called fully connected. Neurons of the *input layer* have only one input and fan their information out to the neurons of the intermediate – so called *hidden layer*. Neurons of the *output layer* are presenting the resultant output of the neural net to the user.

The essential feature of neural nets is their learning property. Example inputs are iteratively fed to the neural nets, together with the desired outputs to adjust the connections between the neuron layers. The way this adjustment is done is treated later.

Neural nets can detect relationships between the input variables implicitly and generate rules that control these relationships. Once these internal adjustments are well

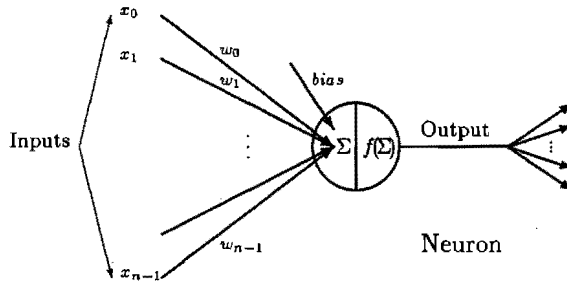


**Figure II.1:** A schematic representation of a neuron, where  $x_0, x_1, x_{n-1}$  are the inputs to the neuron coming from the outputs of other neurons,  $w_0, w_1, w_{n-1}$  are the weights of the connections between the current neuron and the corresponding to the inputs neurons,  $bias$  is the bias of the neuron,  $\Sigma$  stands for the weighted summation of the inputs :  $\sum_{i=0}^{n-1} w_i x_i$ , and  $f$  is the transfer function of the neuron.

learned, training stops, and the neural net is ready to provide answers to learned or novel inputs. With novel inputs, we mean inputs that do not belong to the examples used for training the net, but are still within the range that the training examples covered. This ability of the neural nets to respond correctly even to novel inputs is called *generalization*. More is mentioned later in section 5.1 of this chapter.

In many cases, weights do not change after training, though neural nets exist that continue to adjust to changing conditions thus responding more effectively in situations that differ from those on which they were trained.

## 2 Different types of neural nets

The differentiation between the various types of neural nets rests on the 1) *topology* of a neural net – that is the way the connections between neurons are arranged, and on the 2) *learning algorithm* used to adjust the connections between the neurons to achieve the desired behavior [1]. This results in many different networks, each suitable for certain applications.

### 2.1 Topology

Topologically, neural nets can be divided in the two categories of *feedforward* and *recurrent* neural nets.

**Feedforward neural nets.** In this topology information flows only from the input layer, via zero or more hidden layers to the output layer (Fig. II.3, left panel). There is no

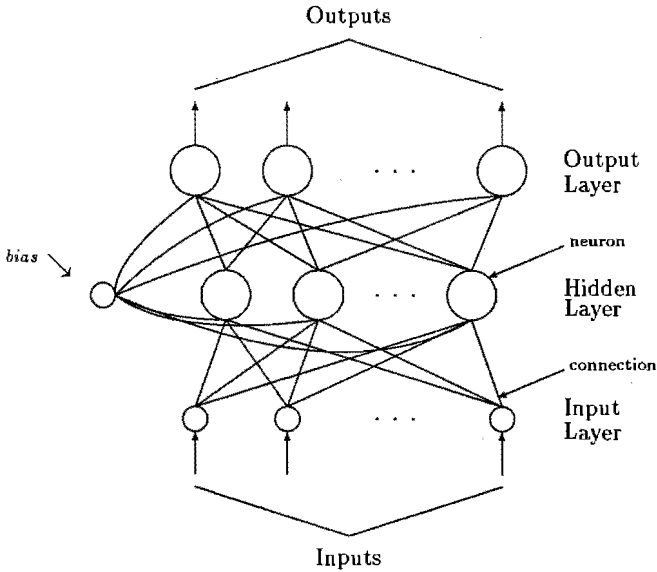


**Figure II.2:** . The circles represent the neurons and are connected to the other neurons in the net with solid lines.

feedback. There are also no connections between neurons of the same layer. Feedforward neural nets perform static mappings between inputs and outputs, meaning that application of a given input always produces the same output.

**Recurrent neural nets.** In this topology connections between neurons of the same layer or with previous layers are also present, in addition to the connections described in the feedforward neural nets. Information flows from input to output and back (Fig. II.3, right panel). Recurrent (feedback) neural nets can perform dynamic mappings between input and output vectors, where the output produced depends upon remembered previous, as well as current inputs and/or outputs.

## 2.2 Learning algorithms

Learning can be considered as an optimization process, as a "search" in a multidimensional parameter (weight) space, for a solution which optimizes a desired behavior [2]. There are two main categories of learning algorithms: *supervised* learning and *unsupervised* learning.

**Supervised Learning.** During training the inputs are presented to the net together with their desired outputs, which are compared with the actual outputs. The weights are adjusted to minimize the difference between the desired and actual output. Inputs and desired outputs are applied to the neural net repeatedly until no further improvements are obtained.

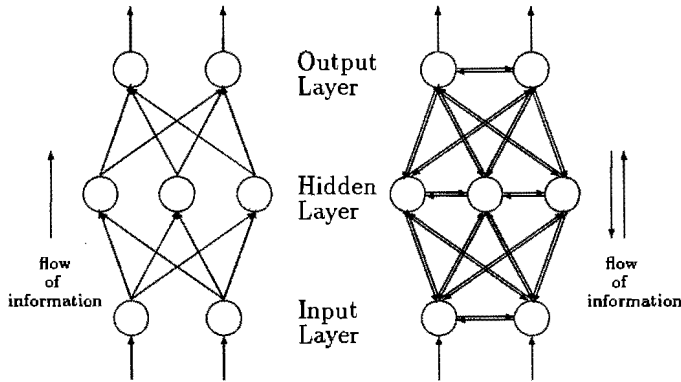


**Figure II.3:** Schematic representation of a feedforward neural net where information flows only in one direction from input to output (left panel) and a recurrent neural net where information flows in both directions (right panel).

An example of supervised learning is the backpropagation algorithm [3], which is performed on multilayered feedforward neural nets. These neural nets will be further called *backpropagation trained neural nets*. During the training with the backpropagation algorithm, the actual output of the neural net is compared with the desired one each time, and the weights are changed to reduce the difference between the actual and the desired output. Input information is always propagated forward to the output of the neural net (feedforward topology). It is the error between the desired and the actual output that is propagated backwards to adjust the weights. This has given the name to this learning algorithm (backpropagation algorithm). Details are given later in section 4 of this chapter.

**Unsupervised Learning.** Only the input signals are fed to the neural net. The weights are now adjusted so as similar inputs produce similar outputs. Similarity is based upon some distance measure. The learning algorithm thus adjusts the connections among the neurons on the basis of the input patterns. The weights and the outputs of the neural net tend to converge to values that capture the statistical regularities of the input data.

### 3 Applications of neural nets

#### 3.1 Why use neural nets

Neural nets are good for dealing with situations that cannot easily be described by sets of rules or formulae [4]. It is not necessary to develop models of behavior or rules of detection,



because the training algorithm does that for us. No *a priori* assumptions are necessary about the underlying statistics of the data [5]. With neural nets, it is possible to reveal patterns that are hidden in the data which cannot easily be found by statistical methods without knowing the details of the mechanisms governing a process. An algorithm to solve the problem, which could be difficult or even impossible to develop, especially in cases when the problem is not well understood, is not necessary. This non-algorithmic nature of neural computing differentiates it from statistical analysis methods [6, 7].

Even for very complex neural nets, real-time performance can be achieved by chip implementation and parallel information processing [8]. Such implementations are low-cost and can be added to existing systems to improve their performance.

Neural nets should not be used when existing mathematical techniques or algorithms offer a solution, since much time and effort is often spent to choose the proper kind of neural net for the problem, to choose an optimal configuration, and to assemble the examples set to train the nets. This data set should be chosen carefully to represent the whole domain of the problem (more details in section 5 of this chapter). In our experience, working with neural nets is time consuming, but especially satisfying results can be achieved.

### 3.2 Where to use neural nets

Neural nets are widely used in the field of pattern recognition and pattern classification. They are able not only to recognize a pattern, but also to associate a pattern with a diagnostic class (classification). Applications include character recognition (e.g. recognition of handwritten digits) [9], image recognition, speech analysis and recognition, speech synthesis and text to speech conversion [10], classification of radar signals [11, 12, 13], function approximation, image compression, or searching large databases for specific knowledge [14]. Refenes and coworkers [15] use neural nets as alternative to classical statistical techniques for stock performance modeling, and show that neural nets can do better than multiple linear regression. The smooth interpolation properties of the neural nets allow them to fit better models to the data and to generalize significantly better.

An extended bibliography is available to define the type of neural net suitable for an application, though it is not always clear which is the best topology and the best learning algorithm. One of the most used learning algorithms is backpropagation. Fields of primary application of backpropagation trained neural nets are pattern recognition and classification, and function approximation[4]. It has been proved that this type of net is capable of approximating any continuous multivariate function of the input data to any desired degree of accuracy [16, 17, 18]. In applications where the relationships between the variables are nonlinear and high-order correlations are involved, backpropagation trained neural nets have produced accurate results.

Major problem with neural nets is that they are unable to explain their conclusions. This is due to the many distributed weights and nonlinear thresholds, whose detailed effects can only be understood in the simplest of cases. Neural nets are thus limited to

interpreting patterns where no explanation or justification for selecting a conclusion is necessary [19].

### 3.3 Application of neural nets in the medical area

In medicine, neural nets have been used predominantly for pattern matching and computer aided diagnosis [20] – [27]. Traditional methods have not been very successful, since biological signals are characterized by substantial variability, caused either by spontaneous internal (reflex) mechanisms or by external stimuli. Here neural nets have been more successful.

Miller *et al.* [28] present a comprehensive review of applications of neural networks in the area of medical imaging and signal processing. They conclude that neural nets represent a major advance in this field, that the backpropagation trained neural net has been used in most of the applications, and that, however, there are still basic problems to be addressed, such as collecting and classifying sufficient training and testing data, choosing a valid data presentation strategy, choosing an appropriate network architecture, and implementing the network on a sufficiently powerful computer system to achieve net convergence in reasonable time. Some of these problems are addressed later in this chapter (see section 5).

In particular, backpropagation trained neural nets have proved successful in many classification tasks, including biomedical signal classification and diagnosis [29] – [34]. Nekovei and Sun [29] detect vascular structures in angiograms, and demonstrate that neural nets outperform both the classic method based on maximum likelihood estimation and the modern method based on iterative ternary classification. Guo *et al.* [33] report superior results in comparison with the Bayes classifier to classify valve sounds to detect spontaneous degeneration of prosthetic heart valves. Kennedy *et al.* [34] demonstrate that neural nets are suitable to analyze clinical data in relation to the diagnosis of acute myocardial infarction, and results are superior to those obtained with linear discriminant analysis.

## 4 Backpropagation trained neural nets

A typical multilayer feedforward neural net has an input layer, an output layer and at least one hidden layer. Theoretically, there is no limit on the number of hidden layers but in practice there are only one or two hidden layers. The neurons of one layer are usually fully connected with the neurons of the succeeding layer.

The neural net has to learn to produce the right output for a certain input. A set of input patterns is required for the learning procedure. The desired output has to be presented together with the corresponding input.

In more detail, the training algorithm acts as follows: An input pattern  $p$  is presented to the neurons of the input layer of the neural net. This pattern is transmitted via the

weights to the neurons of a hidden layer. The output of each neuron in a hidden layer is transformed by a transfer function,  $f$ , usually a sigmoid or hyperbolic tangent function:

$$I_{pj} = \sum_i w_{ji} * x_{pi} + b_j \quad (\text{II.1})$$

$$O_{pj} = f(I_{pj}) \quad (\text{II.2})$$

where  $I_{pj}$  is the weighted sum of the inputs  $x_{pi}$ ,  $w_{ji}$  is the weight from neuron  $i$  of the previous layer to neuron  $j$ ,  $O_{pj}$  is the output of the neuron  $j$  after pattern  $p$  is applied,  $b_j$  is the bias for neuron  $j$ , and  $f$  is the transfer function.

After the actual values of the output neurons have been calculated, the pattern error is calculated as in the following equation [3]:

$$E_p = \frac{1}{2} \sum_{k=1}^M (d_{pk} - O_{pk})^2 \quad (\text{II.3})$$

where  $d_{pk}$  is the desired output for pattern  $p$  at the output neuron  $k$ ,  $O_{pk}$  is the actual output at this neuron for this certain pattern, and  $M$  is the number of output neurons. The overall error on the whole set of patterns is simply the sum, across patterns, of the pattern error.

The backpropagation algorithm, as defined in [3], is an algorithm that uses a *gradient descent* method to adjust the weights between the neurons so that the error between the desired output and the output signal of the network is minimized. The gradient descent method acts on an energy surface, where the dimension of this energy surface equals the number of the weights in the network and the "energy" is the overall error on the set of patterns. The gradient descent method explores the slope of this multidimensional error surface near the current error, to estimate the direction to the location of minimal error. A step is taken in this direction, by adjusting the weights, after which the procedure is repeated.

The derivative of the error measure with respect to each weight is proportional to the weight change with negative constant of proportionality:

$$\Delta_p w_{ji} \propto -\frac{\partial E_p}{\partial w_{ji}} \quad (\text{II.4})$$

Updating of the weights is being done according to the formula:

$$\Delta_p w_{ji} = a * \delta_{pj} * O_{pi} \quad (\text{II.5})$$

and for the biases, where  $O_{pi} = 1$ :

$$\Delta_p b_j = a * \delta_{pj} \quad (\text{II.6})$$

where  $a$  is the learning coefficient, and  $\delta_{pj}$  is the error signal for neuron  $j$ . The error signal for an output neuron is calculated from the difference between the actual and the desired output for this neuron:

$$\delta_{pj} = (d_{pj} - O_{pj}) * f'_j(I_{pj}) \quad (\text{II.7})$$

where  $f'$  is the derivative of the transfer function with respect to the weighted sum  $I$  of the inputs of a neuron.

The error signal for a hidden neuron  $j$  depends on the error signals of the neurons in the next higher layer which neuron  $j$  is connected to and the weights of those neurons:

$$\delta_{pj} = f'_j(I_{pj}) * \sum_k \delta_{pk} * w_{kj} \quad (\text{II.8})$$

Explanation why the error signals can be calculated by the equations II.7 and II.8 can be found in [3]. The previous steps of the learning algorithm are repeated until the error becomes smaller than a predetermined value, or until a certain number of iterations. Once the training of the neural net stops, the weights for the training set have been optimized and remain constant and a test set may be applied. During this phase, the output is calculated via the equations II.1, and II.2.

The updating of the weights can be done either after each pattern is presented to the neural net (*on-line*), or after several patterns have been presented to the neural net (*batch*). This number of patterns, called "epoch", can correspond either to the whole set of patterns, or to a subset. When the batch way of updating weights is used, the error derivatives are averaged over the epoch, the weight adjustment is done toward reducing the overall error function, and this may lead to a more accurate estimate of the overall gradient and smoother convergence. On the other hand, the on-line method introduces a randomization to the weight steps that may help to avoid being trapped in local minima. No conclusive evidence has been presented to prefer either alternative [35].

## 4.1 Transfer Functions

The most common transfer function used with backpropagation trained neural nets is the *sigmoid* transfer function. The sigmoid is a continuous monotonic mapping of the input variable,  $x$ , onto the value  $f(x)$  between zero and one:

$$f(x) = 1/(1 + e^{-x}) \quad (\text{II.9})$$

It can be considered a smooth version of a [0,1] step function. One important advantage of this function is that its derivative - which is needed for the calculation of the error signals in the equations II.7, and II.8, is easily calculated:

$$f'(x) = f(x) * (1 - f(x)) \quad (\text{II.10})$$

Another transfer function also used is the *hyperbolic tangent* which is a bipolar version of the sigmoid function:

$$f(x) = (e^x - e^{-x})/(e^x + e^{-x}) \quad (\text{II.11})$$

It can be considered a smooth version of a [-1,1] step function. The derivative of this transfer function can also be expressed in terms of the transfer function itself:

$$f'(x) = 1 - (f(x))^2 \quad (\text{II.12})$$

The shape of the sigmoid and the hyperbolic tangent transfer functions is shown in Fig. II.4.

In most cases, it has been found that the exact shape of the sigmoidal transfer function has little effect on the performance of the neural net, though it can have great impact on speed [36].

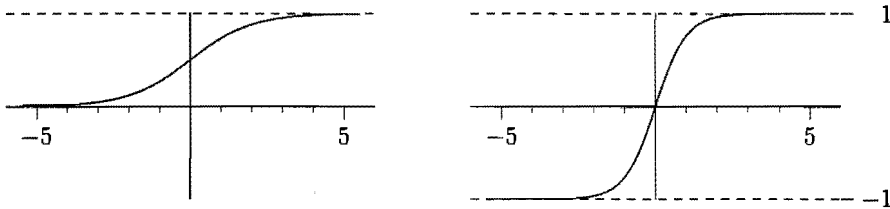


**Figure II.4:** Transfer functions used in the backpropagation algorithm. The function on the left is the sigmoid transfer function, and the one on the right is the hyperbolic tangent transfer function.

## 4.2 Variations on the standard algorithm

Learning with the backpropagation algorithm is quite slow. The error surface is usually harsh with a lot of flat or extremely steep surfaces but not much in between [37]. The size of the change of the weights depends on the learning coefficient of the learning rule. A large value of the learning coefficient would lead to faster convergence (larger steps on the error surface towards the minimum), but might cause oscillations during the search, bouncing between two opposite sides of a steep valley of the error surface, without reaching the bottom – minimum. On the other hand, too small a value would slow convergence and would prevent the system from making reasonable progress across an almost long flat surface.

One way to solve this problem is to include a *momentum* term [3] in the learning rule :

$$\Delta_p w_{ji}(n+1) = a * \delta_{pj} * O_{pi} + \mu * \Delta_p w_{ji}(n) \quad (\text{II.13})$$

where  $\mu$  is the momentum term,  $\Delta_p w_{ji}(n+1)$  is the current delta weight, and  $\Delta_p w_{ji}(n)$  is the previous delta weight. It smoothes high frequency fluctuations of the error surface in the weight-space and it improves the speed of convergence by augmenting weight changes when consecutive changes have the same sign (that means that the weight changes are moving towards the right direction in the weight space), and by damping when they have different signs.

This variation was used for training the neural nets described in chapter III.

There is no automatic way to choose the proper values of the learning coefficient and the momentum. The selection is frequently empirical [3, 38]. It depends very much on

the problem, but also on the training set size, on the hidden layer size, etc. An unlucky choice can cause slow convergence or can stop learning too early. The neural net can also be trapped in some local minimum and give a solution that is not close to the best one.

Another variation of the learning rule, which was used in the study described in chapter IV, has been developed by Vogl *et al.* [39]. They introduce a variable learning rate depending on the local topography: if a weight adjustment results in reduced error, then the learning rate increases ( $a = a * incr$  with  $incr > 1$ ), otherwise if a weight adjustment results in an error more than a few percent over the previous value, then the learning rate decreases ( $a = a * decr$  with  $decr < 1$ ), the weights do not change, momentum becomes zero and the step is repeated. Only after the network takes a useful step, that means a step that reduces the total error, then the momentum gets again a non-zero value.

The rationale behind this variation is that error surfaces have different properties along different regions. To take the right steps as the weights vary, the learning coefficient needs to change accordingly. As long as the surface is rather uniform and the descent is relatively smooth, then the momentum term helps convergence. If, however, a step results in a decrease of the performance of the system, then that means that a change is necessary in the direction of the optimization, and prior experience (incorporated in the term in momentum) will be more misleading than beneficial.

There exist more techniques that aim at speeding up backpropagation learning. Details can be found in the corresponding references [38], [40]– [50], but the literature lacks extensive comparative research in the performance of these methods [40].

**Initialization of weights.** The learning should be repeated starting with different initialization weights to avoid assuming a local minimum to be the correct global one. Backpropagation is sensitive to initial weights. In practice, the weights are normally initialized to small random values [3]. This is because large weights tend to prematurely saturate processing neurons in a neural net and make them insensitive to the learning process [51].

Nguyen and Widrow [52] have formulated a method of initialization of the weights and biases of the neural nets that leads to a decrease in necessary training time. They consider that each hidden neuron is responsible for approximating only a small part of the desired function, and the complete approximation of the desired function is formed by summing the outputs of the hidden neurons, which are piece-wise linear approximations to the desired function. Linearity is considered, because the sigmoid function is approximately linear for inputs between 0 and 1. The weights need to move in such a way that the region of interest is divided into small intervals. So the initial weights of the hidden layer are being set so that each hidden neuron is assigned its own interval at the beginning of the training. The network is trained as before. Nguyen and Widrow have used this method to initialize weights over different training problems and they report that they have managed to improve the learning speed in every case.

## 5 Practical Considerations

There are numerous neural network algorithms present in the literature. To choose a suitable type we based ourselves upon the nature of the problem, and on the success of a certain type of neural net in previous similar applications.

This resulted in our choosing the backpropagation algorithm to train multilayer feed-forward neural nets. It can be used both for classification (see Chapter III) or continuous mapping (see Chapter V). In both studies, sufficient training data was available for performing supervised learning. However, much time and computing power was required :

- to assemble training and testing data sets,
- to size the network,
- to find good learning coefficients, momentum,
- to select proper nonlinear functions, and
- to obtain optimal input representations.

To these processes there is little guidance available in literature. As a result, time consuming training has to be repeated over and over again.

### 5.1 Training and testing data sets

The performance of a neural net depends strongly on the patterns used for training, which should therefore be selected very carefully. The training set should be representative, in the sense of containing all the different variants of patterns that characterize the problem to solve [53]. The set should be complete and represent the entire domain of the problem, or a suboptimal solution might result. A trained neural net can only be as good and complete as the data used to train it. Extrapolation is usually not indicated. When we tried (in Chapter V) to train neural nets to estimate age from blood pressure waveforms of subjects ranging in age from 25 to 65 years, the performance deteriorated significantly on subjects younger or older than the ones in the training set. The neural nets showed a preference for outputs in the range 25 to 65 years and tended to over- and underestimate, respectively, the ages of the younger and older subjects.

The desired outputs in the training sets can either be obtained subjectively, based, for example, on the judgement of human experts, or objectively. Since human experts often do not agree amongst themselves, are hesitant, uncertain, or insensitive, training a neural net and evaluating its performance can be severely compromised. In section 3 of chapter III, we show how human experts scored on the detection of damping in arterial pressure waveforms. Their score was not significantly different from a chance scoring, whereas the neural net, that was trained on objective data, performed significantly better than random.

## 5.2 Network size

The number of the hidden layers and the number of neurons in each layer may have a significant influence on the performance of the neural net. The optimal number of hidden neurons has to be approached by trial and error but depends on the complexity of the problem, and the diversity and size of the training set. A small number of neurons may lead to underfitting and may fail to represent a complex problem. On the other hand, too many neurons in a layer slows training and requires a large size training set to generalize well on novel inputs. A neural net with too many neurons may recognize all individual inputs thus losing the ability to make generalizations. Such nets may act as a look-up table giving correct answers only on the training data but producing large errors at novel inputs.

Detailed discussions of these aspects with theoretical and practical results can be found in [54, 55].

## 5.3 Scaling of data sets

Scaling of the data sets is not really necessary for training backpropagation trained neural nets, but it is usually a good approach since large input values can result in saturation of the transfer function. Saturation impedes the adjustment of the weights. Often, in practice, input data is normalized to the range 0 to 1 or -1 to 1, when the transfer function used is the sigmoid or the hyperbolic tangent, respectively.

## 5.4 Input representation

A proper representation of the input data should include the information critical for a successful application of the neural nets. This may result in many input nodes, that require long training time. Preprocessing of the input data is then advantageous to extract a small set of essential features. This procedure should be used with care, since underlying relationships may be unknown and important information may have been discarded leading to suboptimal performance.

## 5.5 Software implementations of neural nets

Neural nets can be implemented in hardware or software. Hardware implementations allow network training to be carried out fast, but there is little flexibility in choosing the network architecture and the learning algorithm. Software implementations, on the other hand, are flexible, but training times are long and large computer facilities are required. There are different software packages available. In our studies, the following packages were used to develop our neural nets:

*NeuralWorks* is a powerful neural network development tool capable of generating a broad array of common network types. Its user-friendly graphical interface in combination with its very good documentation makes it relatively easy to use.



*SNNS* — *Stuttgart Neural Network Simulator* is a luxurious simulator which supports many network topologies and learning algorithms, but is difficult to get acquainted with. The documentation is not very helpful.

*MATLAB Neural Network Toolbox* is a great collection of *MATLAB* functions for the design, and training of neural nets, accompanied with excellent documentation. It supports a wide range of network architectures with virtually unlimited numbers of neurons and interconnections (up to operating system constraints). All the algorithms and implementations are available to the users for understanding as well as for trying out alternative ideas and creating new functions. The preprocessing of the data sets and the postprocessing of the outputs of the neural nets is also very easy in this environment.

## 6 Conclusion

The development of the neural nets has come to a point where methods are available to do special things not easily, or not at all, possible in other ways. However, theoretical support and practical experience is limited often requiring a trial and error approach. If time is taken to explore the many possibilities, results can be obtained that have not been achieved with other methods. Two cases will be described in chapters III and V. With faster computers trial and training will become easier and special purpose hardware is under development at various places including this university.

## References

- [1] Hecht-Nielsen R. Neurocomputing: picking the human brain. *IEEE Spectrum*, 35(3):35–41, March 1988.
- [2] Hassoun MH. *Fundamentals of artificial neural networks*. The MIT Press, Cambridge, Massachusetts, 1995.
- [3] Rumelhart DE, Hinton GE, and Williams RJ. Learning internal representations by error propagation. In DE Rumelhart and JL McClelland, editors, *Parallel distributed processing: Explorations in the microstructure of cognition, Volume 1: Foundations*. MIT Press Cambridge, MA, 1986.
- [4] Maren A, Harston C, and Pap R. *Handbook of neural computing applications*. Academic Press, London, 1990.
- [5] Ciaccio EJ, Dunn SM, and Akay M. Biosignal pattern recognition and interpretation systems, part 3 of 4: Methods of classification. *IEEE Engineering in Medicine and Biology*, pages 129–135, February/March 1994.

- [6] Ciaccio EJ, Dunn SM, and Akay M. Biosignal pattern recognition and interpretation systems, part 1 of 4: Fundamental concepts. *IEEE Engineering in Medicine and Biology*, pages 89–97, September 1993.
- [7] Schalkoff R. *Pattern Recognition : Statistical, structural, and neural approaches*. John Wiley & Sons, Inc, New York, 1992.
- [8] Masa P. *Neuroclassifier analog VLSI neural network for very high speed pattern classification*. PhD thesis, Twente University of Technology, 1994.
- [9] Le Cun Y, Boser B, Denker JS, Henderson D, Howard RE, Hubbard W, and Jackel LD. Backpropagation applied to handwritten ZIP code recognition. *Neural Computation*, 1:541–551, 1989.
- [10] Sejnowski TJ and Rosenberg CR. Parallel networks that learn to pronounce English text. *Complex Systems*, 1:145–168, 1987.
- [11] Anderson JA, Gately MT, Penz PA, and Collins DR. Radar signal categorization using a neural network. *Proc. IEEE*, 78(10):1646–1657, October 1990.
- [12] Vrckovnik G, Chung T, and Carter CR. Classifying impulse radar waveforms using principal component analysis and neural networks. In *International Joint Conference on neural networks*, volume I, pages 69–74, San Diego, CA, 1990.
- [13] Gorman RP and Sejnowski TJ. Analysis of hidden units in a layered network trained to classify sonar targets. *Neural Networks*, 1:75–89, 1988.
- [14] Muñoz A. Creating term associations using a hierarchical ART architecture. In von der Malsburg C, von Seelen W, Vorbrüggen JC, and Sendhoff B, editors, *Proceedings of the International Conference on Artificial Neural Networks*, pages 171–177, Bochum, Germany, July 1996. Springer Verlag.
- [15] Refenes AN, Zapranis A, and Francis G. Stock performance modeling using neural networks : A comparative study with regression models. *Neural Networks*, 7(2):375–388, 1994.
- [16] Funahashi K. On the approximate realization of continuous mappings by neural networks. *Neural Networks*, 2:183–192, 1989.
- [17] Hornik K, Stinchcombe M, and White H. Multilayer feedforward networks are universal approximators. *Neural Networks*, 2:359–366, 1989.
- [18] Cybenko G. Approximation by superpositions of a sigmoidal function. *Mathematical Control Signals Systems*, 2:303–314, 1989.
- [19] Hutton P and Prys-Roberts C. *Monitoring in Anaesthesia and Intensive Care*. WB Saunders Company Ltd, London, 1994.

- [20] Akay YM, Akay M, Welkowitz W, and Kostis JB. Noninvasive detection of coronary artery disease using wavelet-based fuzzy neural networks. *IEEE Engineering in Medicine and Biology*, pages 761–764, November-December 1994.
- [21] Micheli-Tzanakou E, Yi C, Kostis WJ, Shindler DM, and Kostis JB. Myocardial infarction : Diagnosis and vital status prediction using neural networks. In *IEEE Computers in Cardiology*, pages 229–232, 1993.
- [22] Höher M, Kestler HA, Bauer S, Weismüller P, Palm G, and Hombach V. Neural network based analysis of the signal-averaged electrocardiogram. In *Computers in Cardiology*, pages 257–260, 1995.
- [23] Yeap TH, Johnson F, and Rachniowski M. ECG beat classification by a neural network. In *Proceedings of the 12th Annual International Conference of the IEEE Engineering in Medicine and Biology Society*, volume 3, pages 1457–1458, Philadelphia, Pennsylvania, USA, November 1–4 1990.
- [24] Sebald AV. Use of neural networks for detection of artifacts in arterial pressure waveforms. In *Proceedings of the 11th Annual International Conference of the IEEE Engineering in Medicine and Biology Society*, volume 6, pages 2034–2035, Seattle, Washington, USA, November 9–12 1989.
- [25] Pike T and Mustard RA. Automated recognition of corrupted arterial waveforms using neural network techniques. *Computers in Biology and Medicine*, 22(3):173–179, 1992.
- [26] Prentza A and Wesseling KH. Catheter–manometer system damped blood pressures detected by neural nets. *Medical and Biological Engineering and Computing*, 33:589–595, July 1995.
- [27] Pattichis C, Schizas C, and Middleton L. Neural network models in EMG diagnosis. *IEEE Transactions on Biomedical Engineering*, 42(5):486–496, May 1995.
- [28] Miller AS, Blott BH, and Hames TK. Review of neural network applications in medical imaging and signal processing. *Medical and Biological Engineering and Computing*, 30:449–464, September 1992.
- [29] Nekovei R and Sun Y. Back-propagation network and its configuration for blood vessel detection in angiograms. *IEEE Transactions on Neural Networks*, 6(1):64–72, January 1995.
- [30] Rayburn DB, Klimasauskas CC, Januszkievicz AJ, Lee JM, Ripple GR, and Snapper JR. The use of back propagation neural networks to identify mediator-specific cardiovascular waveforms. In *International Joint Conference on Neural Networks*, volume 2, pages 105–110, 1990.

- [31] Gindi GR, Darken CJ, O'Brien KM, Sterz ML, and Deckelbaum LI. Neural network and conventional classifiers for fluorescence-guided laser angioplasty. *IEEE Transactions on Biomedical Engineering*, 38(3):246–252, March 1991.
- [32] Dawant BM, Ozkan M, Sprenkels H, Aramata H, Kawamura K, and Margolin RA. A neural network approach to magnetic resonance imaging tissue characterization. In Arikan E, editor, *Communication, Control, and Signal Processing*, volume 2, pages 1803–1809, Bilkent University, Ankara, Turkey, 2nd-5th July 1990. Elsevier, Amsterdam.
- [33] Guo Z, Durant LG, Lee HC, Allard L, Grenier MC, and Stein PD. Artificial neural networks in computer-assisted classification of heart sounds in patients with porcine bioprosthetic valves. *Medical and Biological Engineering and Computing*, 32:311–316, May 1994.
- [34] Kennedy LR, Harrison RF, Burton AM, Fraser HS, Hamer WG, MacArthur D, McAlum R, and Steedman DJ. An artificial neural network system for diagnosis of acute myocardial infarction (AMI) in the accident and emergency department: evaluation and comparison with serum myoglobin measurements. *Computer Methods and Programs in Biomedicine*, 52:93–103, 1997.
- [35] Wasserman PD. *Advanced Methods in Neural Computing*. Van Nostrand Reinhold, New York, 1993.
- [36] Master T. *Practical Neural Network Recipes in C++*. Academic Press, London, 1993.
- [37] Hush DR and Horne BG. Progress in supervised neural networks, what's new since Lippmann? *IEEE Signal Processing Magazine*, pages 8–39, January 1993.
- [38] Watrous R. Learning algorithms for connectionist networks: Applied gradient methods for nonlinear optimisation. Technical Report MS-SIS-88-62, University of Pennsylvania, USA, 1988.
- [39] Vogl TP, Mangis JK, Rigler AK, Zink WT, and Alkon DL. Accelerating the convergence of the back-propagation method. *Biological Cybernetics*, 59:257–263, 1988.
- [40] Tollenaere T. SuperSAB: Fast Adaptive Back Propagation with Good Scaling Properties. *Neural Networks*, 3:561–573, 1990.
- [41] Jacobs R. Increased rates of convergence through learning rate adaptation. *Neural Networks*, 1:295–307, 1988.
- [42] Fahlman SE. An empirical study of learning speed in back-propagation networks. Technical Report CMU-CS-88-162, Carnegie-Mellon University, June 1988.
- [43] Schmidhuber J. Accelerated learning in back-propagation nets. Technical report, Institut für Informatik, Technische Universität München, Germany, 1989.

- [44] Chan LW and Fallside F. An adaptive training algorithm for back propagation networks. *Computer Speech and Language*, 2:205–218, 1987.
- [45] Devos MR and Orban GA. Self adaptive backpropagation. In *Proceedings NeuroNimes*, Nanterre, France, EZ 1988.
- [46] Franzini MA. Speech recognition with back propagation. In *Proceedings of the 9th Annual International Conference of the IEEE Engineering in Medicine and Biology Society*, volume 3, pages 1702–1703, Boston, MA, USA, November 13–16 1987.
- [47] Kruschke JK and Movellan JR. Benefits of gain: Speeded learning and minimal hidden layers in back-propagation networks. *IEEE Transactions on Systems, Man, and Cybernetics*, 21(1):273–280, January/February 1991.
- [48] Yu X, Loh NK, and Miller WC. A new acceleration technique for the backpropagation algorithm. In *1993 IEEE International Conference on Neural Networks*, volume 3, pages 1157–1161, San Francisco, California, March 28 – April 1 1993.
- [49] Battiti R. Optimization methods for back propagation: Automatic parameter tuning and faster convergence. In *Proceedings of International Joint Conference on Neural Networks*, volume 1, pages 593–596, 1990.
- [50] Minai AA and Williams RD. Acceleration of back propagation through learning rate and momentum adaptation. In *Proceedings of International Joint Conference on Neural Networks*, volume 1, pages 676–679, 1990.
- [51] Hush D, Salas JM, and Horne B. Error surfaces for multi-layer perceptrons. *IEEE Transactions on Systems, Man and Cybernetics*, 22(5):1152–1161, 1992.
- [52] Nguyen D and Widrow B. Improving the learning speed of 2-layer neural networks by choosing initial values of the adaptive weights. In *International Joint Conference on Neural Networks*, volume 3, pages 21–26, July 1990.
- [53] Sanchez R, Riquenes A, and Perez-Abalo M. Automatic detection of auditory brainstem responses using feature vectors. *International Journal of Bio-Medical Computing*, 39(3):287–297, June 1995.
- [54] Kruschke JK. Creating local and distributed bottlenecks in hidden layers of back-propagation networks. In Touretzky D, Hinton G, and Sejnowski T, editors, *Proc. 1988 Connectionist Models Summer School*, pages 120–126, San Mateo, CA, USA, 1989. Morgan Kaufmann.
- [55] Denker J, Schwartz D, Wittner B, Solla S, Hopfield J, Howard R, and Jackel L. Automatic learning, rule extraction, and generalization. *Complex Systems*, 1:877–922, 1987.



# Chapter III

## Detection of damped blood pressure waveforms

### 1 Catheter–manometer system damped blood pressures detected by neural nets

*Andriana Prentza<sup>a</sup>, Karel H Wesseling<sup>a,b</sup>*

<sup>a</sup> Department of Electrical Engineering, Technical University Eindhoven, P O Box 513, 5600 MB Eindhoven, The Netherlands

<sup>b</sup> TNO–TPD BioMedical Instrumentation, Academic Medical Centre, Suite L0-002, Meibergdreef 9, 1105 AZ Amsterdam, The Netherlands

*Medical and Biological Engineering and Computing, July 1995; 33:589-595*

#### Abstract

Degraded catheter–manometer systems cause distortion of blood pressure waveforms, often leading to erroneously resonant or damped waveforms, requiring waveform quality control. We have tried multilayer perceptron back-propagation trained neural nets of varying architecture to detect damping on sets of normal and artificially damped brachial arterial pressure waves. A second order digital simulation of a catheter–manometer system was used to cause waveform distortion. Each beat in the waveforms is represented by an 11 parameter input vector. From a group of normotensive or (borderline) hypertensive subjects, pressure waves are used to statistically test and train the neural nets. For each patient and category 5–10 waves are available. The best neural nets correctly classified about 75–85% of the individual beats as either adequate or damped. Using a single majority vote classification per subject per damped or adequate situation, the best neural nets correctly classify at least 16 of the 18 situations in nine test subjects (binomial  $P=0.001$ ). More importantly, these neural nets can always detect damping before clinically relevant parameters such as systolic pressure and computed stroke volume are reduced by more than 2%. Neural nets seem remarkably well adapted to solving such subtle problems as detecting a slight damping of arterial pressure waves before it affects waveforms to a clinically

relevant degree.

## Keywords

Arterial pressure monitoring, Artificial neural nets, Back-propagation, Catheter-manometer systems, Damped pressure waves, Quality control.

### 1.1 Introduction

To diagnose a patient's hemodynamic state, invasive arterial pressures are routinely measured via cannulae, liquid-filled tubing systems and external pressure transducers. The limited dynamic performance of such systems alters the waveforms. Waveform alteration for well maintained, continuously flushed systems with proper damping is usually acceptable clinically although regular testing is always required. If systems become degraded, however, pressure waveforms may become distorted to a clinically significant degree, leading to errors in derived parameters such as systolic and diastolic pressure levels. Degradation is not an occasional event but often occurs. It may be caused by tiny air bubbles developing gradually over time, by kinking of connecting tubes, and by clotting and fibrin deposits at the tip of the cannula.

Subsequent distortions are of two kinds:

- (i) resonance, causing waveform oscillations and systolic overshoot.
- (ii) damping, causing slower rising pulsations with systolic underestimation and, in severe cases, diastolic over-estimation.

Resonance is often quite easily detected by inspection of the waveform. To detect damping, however, a mere look at the waveform will not usually be sufficiently informative. For example, waveforms that do not have clear dicrotic notches may lead a critical observer to think that the recording system is overdamped; however, such waveforms may also be physiological since peripheral pressure waves become distorted due to transmission and reflection of the pressure pulse over peripheral arteries.

Furthermore, in catheterization and experimental laboratories, the monitoring and maintenance of the quality of the waveforms should not require continuous attention from the staff who have other matters to attend to. Since an immediate response to damping is considered important and deterioration of a system *in situ* tends to develop gradually, an automated damping detection and alerting system is desirable. A quick flush may then correct the damping.

Artificial neural networks (neural nets), can be considered digital filters with nonlinear, fuzzy decision making properties. They are good for dealing with situations that cannot easily be described by a set of rules or formulae [1]. Instead, neural nets are trained by presenting them with examples. Supervised learning, in addition, presents the neural nets with desired outputs for each training input example. In our case adequate and damped pressure waveforms are required for this purpose but are simple to obtain. We decided,



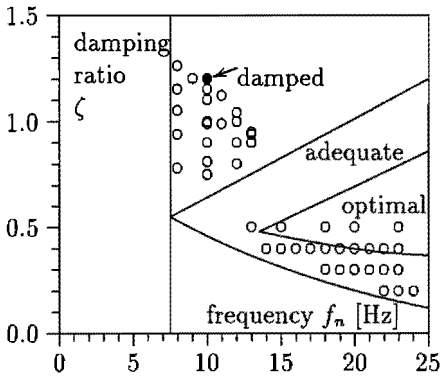


**Figure III.1:** Natural frequency damping ratio pairs of the simulated second-order systems used to distort the pressure waves; closed dot = pair used to damp all pressure waves; open dot pairs used on one patient's waveforms.

therefore, to apply neural nets to the problem of detecting damped, in this study brachial, arterial pressure waves.

## 1.2 Methods

### Subjects

Brachial arterial pressure waves were used to train and test the neural nets. Data was collected from 25 subjects, ranging in age from 22 to 65 years, recorded for other purposes and published elsewhere [2, 3]. Seven subjects were normotensive volunteers and eighteen were (borderline) hypertensive patients. Eleven of the patients were taking anti-hypertensive medication. This data set provided us with high and low blood pressures, old and young subjects and blood pressure measurements through carefully checked hardware. The study protocol for the normotensive volunteers was approved by the Ethical Committee of the Erasmus University Hospital, and for the hypertensive patients by the Medical Ethics Committee of the Academic Medical Centre of the University of Amsterdam.

### Measurements

The way of recording intrabrachial pressure has been previously described [3]. Briefly, all subjects were resting supine during cannulation and measurement. After local anaesthesia with a 2% lidocain solution, a cannula<sup>1</sup> is inserted with the Seldinger technique into the brachial artery of the non-dominant arm. The cannula is connected to a Gould-Statham P23 IO for the volunteer group and to a Hewlett-Packard 1290A transducer for the patient group. The transducer is strapped to the mid upper arm at heart level. A 10 cm section of polyethylene tubing is used to connect the cannula and transducer, and a continuous flush system is installed. The resonance frequency of each of these systems is checked *in vivo* with the fast flush method [4] and after measurements in the laboratory. The *in vivo* measurements range from 11 Hz with adequate damping to 50 Hz underdamped, but

<sup>1</sup>Travenol Quick Cath, N113, 20 gauge, 11 cm long Teflon

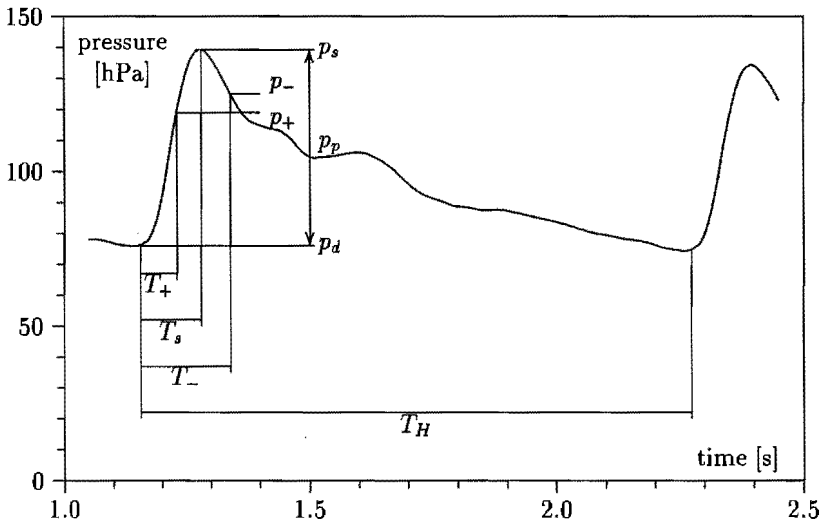


**Figure III.2:** One pressure pulsation indicating various pressure levels and instants of 11-dimensional input vector; symbol meanings are in Table III.1; instead of the beat's duration,  $T_H$ , its inverse heart rate is used; lines to indicate steepest positive and negative slopes are not shown.

still adequate, response in individual cases. These waveforms are considered as clinically acceptable, as adequate recording systems are used and their performance tested and monitored during the sessions.

The pressure signals are recorded<sup>2</sup> and digitized off-line at 100 Hz sample rate and 33.25 Pa (0.25 mmHg) resolution. Waveform sample files of about 10 s duration are thus obtained for each subject, spanning at least one but usually two full respiratory cycles.

### Data processing

Gardner classified catheter-manometer systems as optimal, adequate, resonant or damped according to the natural frequency and damping ratio pair of a system (Fig. III.1) [4]. We have adopted this classification but called a system adequate if it was either in the optimal or the adequate region. The original waveforms are accepted as a set of adequate waveforms. Next, these waveforms are artificially distorted using a second-order low-pass digital simulation<sup>3</sup> of a catheter-manometer system with selectable natural frequency,  $f_n$ , and damping ratio,  $\zeta$ . Second-order systems are a good approximation of catheter-manometer system behavior [5].

To obtain a first set of damped waveforms, the original waveforms are sent through

<sup>2</sup>Hewlett-Packard FM Instrumentation recorder

<sup>3</sup>CATH program, available from TNO

**Table III.1:** 11 derived signal parameters used as input vector to neural nets. Instants within a beat are measured relative to the starting upstroke instant; diastolic pressure is taken at the starting upstroke and thus has no associated delay.

number	symbol	meaning
1	$p_s$	systolic pressure
2	$T_s$	instant of $p_s$
3	$p_d$	diastolic pressure
4	$p_p$	pulse pressure ( $p_s - p_d$ )
5	$f_H$	heart rate
6	$\dot{p}_+$	maximum positive systolic slope
7	$p_+$	pressure level at $\dot{p}_+$
8	$T_+$	instant of $\dot{p}_+$
9	$\dot{p}_-$	maximum negative systolic slope
10	$p_-$	pressure level at $\dot{p}_-$
11	$T_-$	instant of $\dot{p}_-$

filters with an arbitrarily chosen frequency and damping ratio pair, taken from the region marked 'damped' in Gardner's diagram. A second set of damped waveforms is obtained by sending the original waveforms through filters with a fixed frequency of 10 Hz and damping ratio 1.2. These two damped sets are pooled. To balance the filtering, a second set of adequate waveforms is obtained by sending the original waveforms through filters with arbitrarily chosen frequency and damping ratio taken from the regions marked 'adequate' or 'optimal'. Both adequate sets are also pooled.

For input to the neural nets, we have decided not to use entire waveforms but to parameterize each heart beat [6]. Parameters were obtained with the BEATFAST program [7]. This program filters the input signal with a low-pass filter [8] cutting off at 17 Hz, being 60 dB down at 50 Hz. Next, it identifies for each beat (Fig. III.2) the instant of the beginning of the systolic upstroke as the reference for timing within a beat; systolic pressure as the maximum pressure in systole; diastolic pressure as the minimum pressure in diastole just before the starting upstroke; true integrated mean pressure; the instant of the dicrotic notch; and a relative measure of stroke volume via simulation of a nonlinear, time-variant model of arterial input impedance [9]. A first derivative signal computation is added to BEATFAST for this study as the difference between pressure samples 20 ms apart. Maximum and minimum first derivative values in systole and their instants relative to starting upstroke are detected and output. A further program NNPARAM adds the pressure levels belonging to the maximum derivative instants, computes instantaneous heart rate from the pulse interval and prepares this 11-dimensional beat derived parameter vector (Table III.1) for input to the neural nets.

Two subject selections are prepared, one for training the neural nets, and one for assessing trained performance. The subjects are ordered according to age first and then alphabetically according to last name. A random number source then produces numbers from 1 to 25 until nine different subjects are selected. This became the test selection not to be used for any other purpose. The remaining subjects formed the training selection. This process is repeated twice to obtain two further selections to verify results obtained with the first selection. Each selection is tested for randomness at significance level  $\alpha = 0.05$  by the runs test [10], and passed. The first training selection contains input and desired output data of 564 beats (282 adequate, 282 damped). The first test selection contains data of 196 beats (98 adequate and 98 damped). The other selections had similar numbers.

### Neural nets

Back-propagation trained neural nets have been well studied [11] and many successful applications have been reported. We therefore concentrate on multi-layer perceptron back-propagation trained architectures. As a development tool, NeuralWorks Professional II/PLUS<sup>4</sup> was selected. This software supports several variants of back-propagation algorithms.

Our neural nets consist of an input layer of 11 nodes equal to the size of the input vector of parameters (Table III.1), an intermediate or hidden layer of various numbers of nodes, and an output layer of two nodes. All neural nets are fully connected with weights initially randomized in the range from  $-0.1$  to  $0.1$ . Each node in the hidden and output layer consists of a summing junction and a nonlinear transfer function, suitably biased. Using Kolmogorov's heuristic, the upper limit for nodes in the hidden layer  $N_H$  is taken as  $2N + 1 = 23$ , with  $N = 11$  the number of input nodes. The lower limit for nodes in the hidden layer is taken as the number of output nodes  $N_H = 2$  [12, 13, 1].

The sigmoid and the hyperbolic tangent transfer functions are used to transform the weighted sum of the inputs of a node. The sigmoid is a continuous monotonic mapping of the summed input  $I$  onto a value  $T$  between zero and one:  $T = 1/(1 + e^{-I})$ . It can be considered a smooth version of a  $[0,1]$  step function. The hyperbolic tangent is a bipolar version of the sigmoid function:  $T = (e^I - e^{-I})/(e^I + e^{-I})$ . It can be considered a smooth version of a  $[-1,1]$  step function. As the sigmoid transfer function gave uniformly inferior results in this case, it is not discussed further in this paper.

Input and desired output data vectors are scaled before presentation to the network. Each parameter is independently scaled. Minimum and maximum values are computed for the combined data of the training and test selections. The values are then linearly mapped to a scale from  $-1$  to  $1$ . During training, the correct output for a beat of a given damping class is to be 1 for the node corresponding to the beat's class, and 0 for the other node. Thus, the desired output was (1, 0) for an adequate beat and (0, 1) for a damped beat. These desired outputs are similarly scaled.

The back-propagation algorithm is used to train the neural nets, and both single beat

---

<sup>4</sup>NeuralWare, Inc., Pittsburgh, Pennsylvania, USA

learning and batched input learning are tried (see NeuralWare Manual). The neural nets are trained with a number of random order presentations of the training selection until no further improvement in classification can be obtained. Batched input learning usually provides faster learning.

### **Performance evaluation**

During testing, the network is considered to have correctly classified a beat if the output node with the greatest activation is associated with the beat's class [14]. Counts are made of the correctly and incorrectly classified beats and converted to percentages. As the waveforms per subject do not vary significantly, a majority vote per subject is also taken to obtain statistics for significance testing. If the majority of the beats of a subject are classified correctly, they are counted as a correctly classified situation and counted as one result (one degree of freedom).

In addition to evaluating performance in terms of classification error, performance is evaluated in terms of reduction in the clinically relevant systolic pressure and stroke volume. For corresponding damped and adequate beats, we compute the reductions in these parameters and averaged the reductions over all beats per subject. This results in two numbers per subject, one for each clinical parameter, for comparison with the neural net's output. A quality factor  $Q$  is defined as the output value of the node that should have a high value when waveforms are adequate.

### **Statistical significance of classification**

If a neural net has no effect, then 50% of the classifications, on average, would be correct due to chance. To test if a percentage correct classification is significantly different from a chance classification, we use the binomial distribution. The size of the test selection (i.e. 9) is taken such that it would allow a smooth grading of probabilities (see Table D, [10]) concurrent with as large as possible a training selection. After taking a majority vote of the network's output over all beats of a subject in a category, the classification is considered correct if this output corresponds to the desired output.

### **Useful dimensionality of input vector**

An 11 parameter vector is used as input to the neural nets. However, parameters can be interdependent. In the case that interdependence is significant, a more limited choice of parameters reduces the size of the input vector and network complexity. The dimensionality of the input vector is estimated by studying the neural network's trained weights, by multiple regression and by principal component analysis.

– **Network weights** : from the best network, we compute mean and standard deviations of the absolute values of the weights from each input parameter, and mark the mean weights greater than half the maximum mean weight. In addition, the number of times a single weight to any of the hidden nodes is greater than a level is counted, in order to get

an impression of the distribution of weights. Low weights from a scaled input parameter point to a lesser degree of importance of that parameter to the neural net.

– **Multiple regression** [15]: for each of the 16 subjects of the training selection, the average parameter vector of two situations is considered, one adequate and one damped, and linear correlations computed between parameters. In the case that two parameters appear highly correlated, one can be eliminated. Multiple linear regression is computed between the 11 beat-derived parameters as the independent variables and damping ratio  $\zeta$  as the dependent or predicted variable. Then, one by one, the parameters are eliminated that contribute least to the total variance explained.

– **Principal components** [16, 17]: after normalization for zero mean and unit variance, the individual parameter vectors of the training selection are projected onto their set of eigenvectors [18]. Only those eigenvectors are retained that corresponded to the principal eigenvalues of the set. If only a few of the eigenvectors contain the majority of the variance, then the useful dimensionality of the data is reduced.

### 1.3 Results

For each subject, the position of the natural frequency damping ratio pair is entered in Gardner's diagram (Fig. III.1). For the adequate waveforms, natural frequencies range from 13 to 24 Hz with mean (SD) of 19.6 (3.2) Hz and damping ratios from 0.2 to 0.5 with mean 0.37 (0.1). For the first damped set, natural frequencies range from 8 to 13 Hz with mean of 10.6 (1.8) Hz and damping ratios range from 0.75 to 1.26 with mean 1.0 (0.13). The second damped set is filtered with a frequency of 10 Hz and damping ratio of 1.2.

#### Damped / adequate classification

Table III.2 presents the result of classifying beats into the damped and adequate categories for 2 to 23 nodes in the hidden layer. The bipolar hyperbolic tangent transfer function and batched learning are used. Average performance on the training selection varies from 82.5 to 90.5%; on the test selection it varies from 75.5 to 86.5%. For the best neural net on the test selection, by a majority vote, we obtain one false classification out of 18, which is significantly different from a random result ( $P=0.0005$ ).

The best results (Table III.2) seem to favor either a very small number of hidden nodes, about equal to the number of output nodes, or an intermediate number of hidden nodes about equal the number of input nodes. On the test selection alone, a very good and simple network appears to be the one with three hidden nodes. There is no clear overall winner.

Training and testing are repeated with the two other selections and two, three, and four hidden nodes. The results are presented in Table III.3. There is little difference between the selections. The network with three hidden nodes performs best.

**Table III.2:** Results of classifying damped and adequate waveforms. Bipolar transfer function and batched learning used in a network with 11 input nodes and 2 output nodes;  $N_H$  = number of nodes in the hidden layer; CA = percentage of waveforms correctly classified as adequate from the pool of adequate waveforms; remainder were incorrectly classified as damped; CD = percentage of waveforms correctly classified as damped from the pool of damped waveforms, with remainder incorrectly classified as adequate; avg. = average of CA and CD which, since we have equal numbers of adequate and damped waveforms, represents the accuracy of the classifier; ca and cd = corresponding numbers obtained per subject by majority vote; P = probability that a result could have been obtained by chance.

$N_H$	first train selection			first test selection			majority vote		
	CA	CD	avg	CA	CD	avg	ca	cd	P
2	82	90	86.0	76	83	79.5	8	8	0.001
3	92	85	88.5	85	86	85.5	9	8	0.0005
4	90	91	90.5	68	88	78.0	6	8	0.015
5	70	95	82.5	81	86	83.5	6	8	0.015
6	76	95	85.5	69	95	82.0	7	8	0.004
7	78	94	86.0	66	92	79.0	6	8	0.015
8	86	94	90.0	68	86	77.0	6	8	0.015
9	89	90	89.5	79	84	81.5	7	8	0.004
10	88	88	88.0	76	75	75.5	8	6	0.015
11	86	93	89.5	83	89	86.0	7	8	0.004
12	78	95	86.5	79	91	85.0	7	8	0.004
13	92	87	89.5	88	85	86.5	8	8	0.001
14	77	91	84.0	80	90	85.0	7	8	0.004
15	85	90	87.5	82	90	86.0	7	8	0.004
16	81	88	84.5	83	81	82.0	8	8	0.001
17	74	94	84.0	77	87	82.0	6	8	0.015
18	88	86	87.0	83	82	82.5	8	8	0.001
19	79	90	84.5	77	88	82.5	7	8	0.004
20	80	89	84.5	81	87	84.0	7	8	0.004
21	85	93	89.0	67	93	80.0	6	8	0.015
22	86	93	89.5	68	91	79.5	7	8	0.004
23	72	94	83.0	72	90	81.0	7	8	0.004

**Table III.3:** Results of classifying the waveforms into damped and adequate. This table is similar to Table III.2 but shows the three test selection results for comparison.

$N_H$	Waveforms			Majority vote		
	CA	CD	avg	ca	cd	P
2	76	83	79.5	8	8	0.001
3	85	86	85.5	9	8	0.0005
4	68	88	78.0	6	8	0.015
2	90	63	76.5	9	7	0.001
3	88	67	77.5	8	8	0.001
4	89	64	76.5	9	7	0.001
2	65	83	74.0	6	8	0.015
3	91	60	75.5	9	7	0.001
4	58	86	72.0	6	9	0.004

### Error in clinically relevant parameters

We have studied systolic pressure and stroke volume reduction due to damping versus the network's average quality factor per subject for all the neural nets developed. For the configuration with three hidden nodes, bipolar hyperbolic tangent transfer function and batched learning, the first test selection's results are shown in Fig. III.3. By inspection, this configuration appeared to be an overall optimal one for this criterion. As it also belongs to the four best neural nets in terms of classification error, this network is further called the 'best network'. As shown, a high quality factor means negligible parameter reduction without exception. A low quality factor means slight to significant parameter value reduction. A quality factor of 0.5 seems to delimit these regions. The upper left and bottom right areas in Fig. III.3 are nearly empty, as desired.

### Dimensionality of input data

For the best network, the network's weights, their average absolute value and standard deviation are listed in Table III.4. Weights range from  $-4.6$  to  $+4.4$ . Absolute averages range from  $0.47$  to  $3.67$ . The six weights with absolute values greater than  $1.8$  are marked. The smallest weights are associated with bias and parameter  $T_s$ . All weights except for  $T_s$  assume a value greater than one at least once. The six largest average weights assume values greater than three at least once. Apparently, only one input parameter can be omitted ( $T_s$ ) and input dimensionality is 10.

Omitting this least important input parameter, a network is trained on the first train-



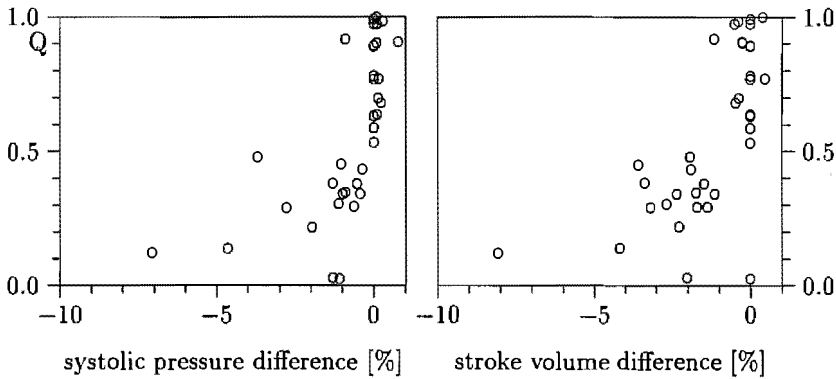


**Figure III.3:** Quality factor determined by best neural net (with three hidden nodes) and average percentage systolic pressure and stroke volume reduction per subject and situation; high quality implies little waveform distortion; two outlier points with almost zero quality, yet almost without pressure and stroke volume degradation, upon inspection represent truly damped waveforms but of such full rounded systolic shape that damping hardly affects clinical parameters; i.e. damping is detected correctly and in a clinical situation a warning should have been issued.

ing selection with ten input nodes, three hidden nodes and two output nodes. Batched learning is used. Average performance on the test selection is 85.5%, with a correct adequate classification performance of 82% and a correct damped performance of 89%, similar to the network with 11 input nodes.

– **Multiple regression:** strong correlations with  $r > 0.9$  and  $P < 0.002$ , are found between  $p_d$  and  $p_+$ , between  $p_d$  and  $p_s$ , between  $p_d$  and  $p_-$ , between  $p_s$  and  $p_+$ , between  $p_s$  and  $p_-$ , between  $p_s$  and  $p_p$ , and between  $p_+$  and  $p_-$ . In other words, all of the pressure levels in a beat show strong correlation to the extent that two pressure levels, for example  $p_d$  and  $p_s$ , seem a reasonable representation. Correlation between the pressure derivatives and the relative timing information is not so strong. This suggests an approximate dimensionality of the input data of eight.

Prediction of the damping ratio  $\zeta$  of the simulated catheter–manometer systems with multiple linear regression, using 11 beat derived parameters, explained only 69% of the variance in  $\zeta$ . Reducing the number of input variables to the best eight in order ( $\dot{p}_+$ ,  $p_+$ ,  $T_+$ ,  $\dot{p}_-$ ,  $p_p$ ,  $f_H$ ,  $p_s$ , and  $T_s$ ) reduces the explained variance to 67%. Removing the last two parameters in the list results in the best six parameters and an explained variance of 61%. Removing one more parameter  $f_H$  from the input vector reduces the explained variance substantially, to 38%. This suggests an input dimensionality of between six and eight.

Using the six best input parameters, a network was trained with six input nodes, three hidden nodes and two output nodes. Batched learning is used. Average performance on the test selection is 84.5%, with a correct adequate classification performance of 81% and

**Table III.4:** Weights of the network with three nodes in the hidden layer. First three numeric columns = network weights to the three hidden nodes; their absolute values are averaged in the next two columns; average values greater than half the maximum average are marked by ( $\Delta$ ); last two columns indicate with  $\times$  how often absolute weight is greater than 1 or 3, respectively.

	W to H1	W to H2	W to H3	mean	SD	$ \overline{W} $ >1.8	$ W $ >1	$ W $ >3
bias	-0.587	0.825	0.031	0.48	0.4			
$p_s$	-0.355	0.581	1.886	0.94	0.8		$\times$	
$T_s$	0.761	0.419	-0.239	0.47	0.3			
$p_d$	1.019	-3.726	-0.869	1.87	1.6	$\Delta$	$\times \times$	$\times$
$p_p$	-1.162	4.198	3.738	3.03	1.6	$\Delta$	$\times \times \times$	$\times \times$
$f_H$	-3.444	-0.729	1.691	1.95	1.4	$\Delta$	$\times \times$	$\times$
$\dot{p}_+$	2.130	-4.224	-4.642	3.67	1.3	$\Delta$	$\times \times \times$	$\times \times$
$p_+$	0.364	-1.954	-1.213	1.18	0.8		$\times \times$	
$T_+$	-1.825	4.430	1.139	2.46	1.7	$\Delta$	$\times \times \times$	$\times$
$\dot{p}_-$	-0.625	2.300	0.557	1.16	1.0		$\times$	
$p_-$	0.744	0.615	1.884	1.08	0.7		$\times$	
$T_-$	2.190	3.606	-0.312	2.04	1.7	$\Delta$	$\times \times$	$\times$

a correct damped performance of 88%, slightly worse than the best neural nets on the full input vector.

– **Principal components:** this analysis produces eigenvalues as listed in Table III.5. Using the criterion of Jain and Dubes that 95% of the variance should be retained in the new space [19], the useful dimensionality is reduced to five; retaining 99% of the variance requires a seven-dimensional transformed vector.

When we use a five-dimensional transformed input vector to train a network with five input nodes, three hidden nodes and two output nodes, we obtain an average performance on the first training selection of 83%, with a correct adequate classification performance of 72% and a correct damped performance of 94%.

## 1.4 Discussion

For a recording system of human blood pressure waves Frank considered as adequate a frequency response of at least 30 Hz [20]. This corresponds to the ability to record the tenth harmonic of a pressure wave at a heart rate of 180 beat/min or 3 Hz. Such high heart rates are not commonly encountered clinically, and peripheral pressure waves in particular do not always contain the tenth harmonic to such an amplitude that it affects

axis	Eigenvalue	% variance
1	6.2794	57.08
2	2.6126	80.84
3	0.9669	89.63
4	0.5247	94.40
5	0.2622	96.78
6	0.2273	98.85
7	0.0694	99.48
8	0.0522	99.95
9	0.0033	99.98
10	0.0019	99.99
11	0.0001	100.00

**Table III.5:** Results of principal component analysis. Eigenvalues listed in order of importance; largest Eigenvalue explains the greatest amount of variance; percentage of the variance explained is the cumulative total variance explained; at least the last three and at most the last six principal components are redundant.

clinically relevant waveform parameters such as systolic pressure. Such considerations have led to a definition of areas of clinically acceptable natural frequencies and damping ratios [4].

In testing catheter-manometer system response, the more obvious choice is to test the system itself by applying some test waveform. The fast flush valve can be a component of such a system [4]. However, these systems are not automatic, require a non-obvious flush response detection and computation, and are sub-optimal in detecting damping. In our classification experiment, we use naturally occurring pressure waveforms of unknown shape and frequency content for input, and Gardner's criteria for (artificially) damped reproduction of waveforms. This is an indirect approach, as certain natural frequency and damping ratio pairs have different effects on different waveforms and their derived parameters. As we use a waveform parameter vector to estimate damping, this creates an uncertainty in the classification. As a result, the performance of the neural nets in terms of error in clinically relevant parameters is better than in terms of classification error. It is the result in terms of error in the clinical parameters that is the most relevant for quality control.

### Clinical applicability

For monitoring in the operating room or the intensive care unit, it is systolic, diastolic pressure, and mean pressure and computed stroke volume that are probably the most clinically relevant parameters. However, in these clinical areas, radial arterial pressure is typically monitored and only occasionally is brachial pressure used. The neural nets we developed work on radial pressures but have not been trained on such waveforms and consequently are sub-optimal for this application. In internal medicine and cardiology,

brachial artery pressure is predominantly used for research, 24 h blood pressure monitoring, exercise stress testing, diagnosis of the autonomic nervous system, detecting cuff hypertension, and in the catheterization laboratory. We have developed our neural nets for these human applications with the same relevant clinical parameters. Of these, systolic pressure and computed stroke volume are affected most by damping.

We have used waveforms obtained from a variety of volunteer subjects and patients, with a wide range of ages and blood pressures. The clinically obtained waveforms are obtained with well maintained systems and can serve as adequate reference waveforms. The artificial damping applied to the adequate waveforms has the same effect on waveforms as actual damping of a catheter-manometer system. The artificially damped waveforms can therefore serve as clinically damped waveforms, with the added advantage that the damping characteristics are precisely known. Damped waveforms can also occur for (patho-)physiological reasons. We expect that they will be detected as damped by our neural net. However, in our system, we do not reject damped waveforms but just attach a label and place a suggestion on the screen to flush the system. When a flush does not cure the damping, the observer at least has better assurance that the damped waveforms are (patho-)physiologic.

Between clinical measurement systems, and for any system over time, a large scatter is found in the natural frequencies and damping ratios measured *in situ* by the fast flush method. This is the reason we selected a series of different pairs of natural frequencies and damping ratios to produce half of the adequate and all the artificially damped waveforms. Some of the pairs hardly provide any damping, some give more substantial damping, as might have occurred in a clinical environment. As a result, some of the individual waveform classifications are unavoidably incorrect, i.e. in cases when the (slight) damping inflicted was insufficient to have an effect on the waveforms. However, in terms of detecting clinically relevant effects such as systolic pressure deterioration, the neural nets perform better, as shown in Fig. III.3. Given a quality factor greater than 0.5, waveform errors are less than 2% and clinically unimportant.

Our optimal neural net with three nodes in the hidden layer has been implemented in the MODELFLO program of the FAST-mf system [7]. This program is an on-line version of BEATFAST. MODELFLO displays the quality factor on-line in real time on inexpensive personal computers. Programming the neural net requires an extra 40 multiplications and three function computations for each heart beat, which does not slow down the program visibly.

### Parameter vectors or waveforms

The selection of input parameters to the neural nets may seem rather arbitrary. Indeed, other parameters or the entire waveform might have been chosen for input. Using entire waveforms presents the problem of scaling the time axis, as beats of widely varying duration are normal. However, scaling the time axis has consequences for the steepness of the waveforms. In addition, a much larger number of input nodes is then required or

waveform detail is lost. Parameterization, on the other hand, requires pre-computation of the needed parameters, which implies the presence of a program that can recognize beats in a continuous presentation of samples. We have previously developed such a program [7] making the route via the parameters feasible.

The choice of input parameters was that used by Johnson *et al.* [6]. This set includes pulse rate, pressure level and pressure slope parameters. For the latter, simple first derivative peak values do not suffice, as on waveforms of equal quality a pulse pressure of 200 mmHg has five times the slope of a pulse of 40 mmHg amplitude. Therefore, pulse pressure and the relative instants of the peak derivatives and the pressure levels at which they occur were included in the set. All parameters are systolic. In arterial diastole, pressure slowly decreases, a process that usually can be followed even by slowly responding systems. In systole, the fastest changes occur and, to detect damping, attention should focus on parameters in this period. Of the 11 parameters, only one ( $T_s$ ) seems redundant to the neural net. Three or more are redundant if some degradation in detection performance is traded for a network of reduced complexity. We were not prepared to make this trade-off.

Johnson *et al.* developed an artificial neural network to predict the natural frequency and the damping ratio of the measurement system from parameterized pressure waveforms. The prediction accuracy is high enough to provide some useful alerting capabilities for damped and resonant artifacts. In our study, we focus on the detection of damping as the more difficult to detect and subtle problem. Resonance may affect systolic pressure as much as or more than damping, but is usually more easily detected visually and by computer. The stroke volume computation is usually little affected by resonance and much more by damping because the pulse systolic area is integrated for stroke volume. Damping has a tendency to develop gradually and can remain undetected for long periods.

### Quality factor

We found it difficult to explain to clinicians the importance of natural frequency and damping ratio without the use of Gardner's diagram and showing the current position of these parameters. Even then, the scatter in the neural network's estimation of these parameters (not discussed here) was considered confusing at times. Waveform quality factor, on the other hand, was a concept more easily accepted. Using the quality factor, the absence of damping is quite reliably presented as a quality factor greater than 0.5 and no systolic pressure reduction, although a quality factor less than 0.5 does not always result in systolic pressure reduction, depending on waveform shape.

### Neural nets

The neural network approach offers such advantages as to make it the method of choice in many application areas. Learning is a most attractive feature of neural nets. With it, neural nets learn to perform certain tasks by being trained with examples. It is not necessary to develop models of behavior or rules of detection. No assumptions are necessary

about the underlying statistics of the data, except range for scaling purposes. On the other hand, to work with neural nets, it is necessary that a designer develops a database of training patterns and experiments with network architectures and training methods. Compared to somewhat similar approaches as multiple regression and principal components, it is our impression that, by drawing multiple intermediate nonlinear conclusions in the hidden layer, neural nets do a better job by extracting more from the input information. The disadvantage is a greater computational burden and more experimentation in the design stage.

## 1.5 Conclusion

We conclude that neural nets can classify brachial arterial pressure waveforms as adequate or damped from parameterized data, and can append a waveform quality label which translates directly either into absence or probably presence of degradation of clinically relevant parameters. The best neural nets do this reliably, continuously, and easily in real time.

## 2 Damped blood pressure waveforms detected during exercise

We demonstrated in the previous section that neural nets can detect subtle changes in waveform as occur when brachial arterial pressure recordings suffer instrumental damping, even though waveforms show substantial differences between subjects. We then wondered if a neural net could do the same when waveform differences occurred within subjects, for example during physical exercise, where large increases in blood pressure, heart rate and vasomotor tone are involved [2, 21].

### 2.1 Methods

#### Subjects and Measurements

Data were collected from 7 healthy normotensive male volunteers aged 22 to 40 years (mean age 30 years), recorded for other purposes and published elsewhere ([2], chapter III.3 in [21]). The study protocol was approved by the Ethics Committee of the University Hospital Dijkzigt in Rotterdam.

The exercise was performed on a bicycle ergometer with the subject in sitting position. After a pre-exercise phase of one minute, the load was increased in steps of 20W/min until exhaustion. The subjects then remained quiet in the sitting position on the ergometer for another 3 minutes, while blood pressure recording continued. Table III.6a lists the ages of the subjects and the maximal exercise level for each individual.

Intrabrachial pressure was recorded in supine position. The non dominant arm was used for cannulation. After local anesthesia with a 2% lidocaine solution, a Travenol Quick Cath, N113, 20 gauge, 11 cm long Teflon cannula was inserted into the brachial artery with the Seldinger technique and was connected to a Gould-Statham P23 ID transducer

**Table III.6:** a) Age of subjects and maximum exercise load (in watts) b) Training - Testing Combinations.  $TR_A$ ,  $TR_B$ ,  $TR_C$ , and  $TR_D$  are the different training sets and  $TE_A$ ,  $TE_B$ ,  $TE_C$ , and  $TE_D$  are the different testing sets. Each set includes the data of those subjects that are marked with  $\times$  in its column.

#	a)		b)							
	Age	Load	Set A		Set B		Set C		Set D	
			$TR_A$	$TE_A$	$TR_B$	$TE_B$	$TR_C$	$TE_C$	$TR_D$	$TE_D$
1	22	300	$\times$		$\times$			$\times$	$\times$	
2	28	260		$\times$	$\times$		$\times$		$\times$	
3	28	300		$\times$	$\times$		$\times$			$\times$
4	30	200	$\times$			$\times$	$\times$		$\times$	
5	30	300	$\times$		$\times$			$\times$	$\times$	
6	36	320	$\times$		$\times$		$\times$			$\times$
7	40	280	$\times$			$\times$	$\times$		$\times$	

by means of a 10 cm long polyethylene tube. The transducer was strapped to the mid upper arm, approximately at heart level. A continuous flush system was installed. The resonance frequency ranged from 17 to 50 Hz, the damping ratio from 0.2 to 0.5. The pressure signal was recorded on a four channel Hewlett-Packard FM Instrumentation recorder. The tape recorded signal was digitized at 100 Hz sample rate and 33.25 Pa (0.25 mmHg) resolution.

### Data processing

Epochs of 10 seconds were extracted each minute, from one-minute before exercise until 3 minutes post exercise, free of motion artifacts. These epochs were accepted as adequate. Next, the recordings were artificially distorted using the second order low pass digital simulation of a catheter-manometer system with selectable natural frequency,  $f_n$ , and damping ratio,  $\zeta$  (see section 1.2 of this chapter).

**Table III.7:** 11 derived signal parameters used as input vector to neural nets. Instants within a beat are measured relative to the starting upstroke instant; diastolic pressure is taken at the starting upstroke and thus has no associated delay

number	symbol	meaning
1	$p_s$	systolic pressure
2	$T_s$	instant of $p_s$
3	$p_d$	diastolic pressure
4	$p_p$	pulse pressure ( $p_s - p_d$ )
5	$f_H$	heart rate
6	$\dot{p}_+$	maximum positive systolic slope
7	$p_+$	pressure level at $\dot{p}_+$
8	$T_+$	instant of $\dot{p}_+$
9	$\dot{p}_-$	maximum negative systolic slope
10	$p_-$	pressure level at $\dot{p}_-$
11	$T_-$	instant of $\dot{p}_-$

To obtain the inputs to the neural nets, we employed a preprocessor to extract key features from the waveforms. Table III.7 presents the features that were extracted from the waveforms. The way they have been extracted is mentioned in detail in the previous section.

The parameterized set contained data of 4164 waveforms - 2082 of which were adequate and 2082 were damped. Because of the small number of subjects included, the data set of the 7 subjects was divided into 4 training/testing set combinations [22]. The data of 2 subjects formed the testing set and the data of the remaining 5 subjects formed the training set. The sets were mutually exclusive. Neural nets were trained using the data of one training set and the trained performance was tested using the correspondent testing set. The procedure was repeated 3 more times. Table III.6b lists the different training/testing sets. In this way, the waveforms of each patient are used as testing waveforms for one of the networks.

### Neural nets

NeuralWorks Professional II/PLUS (NeuralWare, Inc. Pittsburgh PA) was selected for training and testing the neural nets.

Multilayer feedforward neural nets were used. They consisted of an input layer of 11 nodes equal to the number of the input parameters, a hidden layer of various numbers of nodes, and an output layer of one node. All neural nets were fully connected with weights initially randomized in the range from -0.1 to 0.1. The hyperbolic tangent transfer function



was used as transfer function of the nodes in the hidden and the output layer, since it produced the best results as reported in section 1 of this chapter.

All input data, before presenting them to the neural nets, were normalized to the range -1 to 1. The range -1 to 1 was chosen, because the hyperbolic tangent function was used as transfer function. The scaling was necessary since high values of the data could lead to saturation of some processing units. Scaling was done off-line using a pre-processing facility of NeuralWorks. Each parameter was scaled independently. Its minimum value was transformed to -1 and its maximum value was transformed to 1. The values in between were transformed linearly in the region (-1, 1). The minimum and maximum values of the parameters were determined on the whole data set. The output data were also normalized to range 0 to 1.

The back propagation algorithm with a momentum term was used for training (see section 4 of chapter II). The neural nets were trained with a number of random order presentations of the training selection of up to  $10^4$  iterations. To check how the performance on both the training and testing sets is improving during learning, the weights of the network were saved every 5000 iterations. Different numbers of hidden nodes were used varying from 3 to 10.

Back propagation is known to be sensitive to the initial values of weights [23]. On the way to find the global minimum in the weight space, being trapped in a local minimum can occur. To avoid this, for each different combination of hidden nodes and training duration, training and testing was repeated 5 times with a different set of initial values of weights for each training session, to average over variations in performance because of the different initial weights. Batch learning was used.

During training, the correct output for a beat of the adequate class was to be 1, and for a beat of the damped class it was to be 0. The aim was to adapt the values of the weights of the networks so that they performed well also for waveforms which did not belong to the training set.

## Evaluating performance

The output of the network was distributed between 0 and 1 with a value which was showing the closeness of the input waveform to the adequate waveform. The network, initially, was considered to have correctly classified an adequate beat if the output node had an output greater than 0.5, and correctly classified a damped beat if the output node had an output less than 0.5. Thus for each answer we get from the classifier's output node four possible alternatives exist [24]: true damped ( $td$ ) — when the system correctly detects a damped waveform, false damped ( $fd$ ) — when the system fails to detect an adequate waveform, true adequate ( $ta$ ) — when the system correctly detects an adequate waveform, and false adequate ( $fa$ ) — when the system fails to detect a damped waveform. To evaluate the trained performance of the different neural nets on the testing set, the following percentages have been calculated:

$$AC = (td + ta)/N * 100 \quad (\text{III.1})$$

$$FD = fd/(ta + fd) * 100 \quad (\text{III.2})$$

$$FA = fa/(td + fa) * 100 \quad (\text{III.3})$$

$$SE = td/(td + fa) * 100 \quad (\text{III.4})$$

$$SP = ta/(ta + fd) * 100 \quad (\text{III.5})$$

where  $N$  is the total number of adequate and damped waveforms,  $FD$  is the percentage of waveforms incorrectly classified as damped from the pool of adequate waveforms,  $FA$  is the percentage of waveforms incorrectly classified as adequate from the pool of damped waveforms,  $SE$  is sensitivity — percentage of waveforms correctly classified as damped from the pool of damped waveforms,  $SP$  is specificity — percentage of waveforms correctly classified as adequate from the pool of adequate waveforms and  $AC$  is accuracy of the detection. It reflects the percentage of the correct classifications and the percentage of the error rate is 100 - accuracy.

$N_H$	AC	FD	FA	SE	SP
3	73.3	28.3	25.1	74.9	71.7
4	73.1	28.6	25.2	74.8	71.4
5	75.9	24.6	23.6	76.4	75.4
6	76.9	25.0	21.3	78.7	75.0
7	74.2	26.9	24.7	75.3	73.1
8	74.6	28.1	22.7	77.3	71.9
9	74.5	26.8	24.2	75.8	73.2
10	74.4	26.7	24.5	75.5	73.3

**Table III.8:** Results of classifying the waveforms into damped and adequate. The bipolar transfer function and batched learning were used in a network with 11 input nodes and 1 output node.  $N_H$  is the number of nodes in the hidden layer.  $AC$  represents the accuracy of the classifier.  $FD$  represents the percentage of waveforms which were incorrectly classified as damped, and  $FA$  represents the percentage of waveforms incorrectly classified as adequate.  $SE$  represents the sensitivity of the classifier (the percentage of waveforms correctly classified as damped of the pool of damped waveforms).  $SP$  represents the specificity of the classifier (the percentage of waveforms correctly classified as adequate of the pool of adequate waveforms).

To obtain an overall estimate of the performance, the average network performance over the 4 training/testing set pairs was calculated [25]. Network performance on each of the 4 training/testing sets was computed as the average performance of 5 separately trained networks (with different weight initializations).

As another way to measure the performance of the trained neural nets, we use the Receiver Operating Characteristic (ROC) curves [24, 26]. The percentage of damped

**Table III.9:** Error rate of testing set A ( $TE_A$ ) for the different initialization weights.

Run	Error
1	0.195
2	0.198
3	0.189
4	0.206
5	0.186
Mean	0.195
Std	0.008

**Table III.10:** Average error rate for the different testing sets. The error rate for each testing set is the average of the error rates of the networks trained with different initialization weights.

Test Set	Error
$TE_A$	0.195
$TE_B$	0.366
$TE_C$	0.183
$TE_D$	0.180

waveforms which are correctly classified as damped ( $SE$ ) is plotted versus the percentage of adequate waveforms which are incorrectly classified as damped ( $FD$ ) for different values of threshold (0.01, 0.05, 0.1 up to 0.9 with a step of 0.01, 0.95, and 0.99). We repeat the procedure for different number of hidden nodes, resulting in 5 ROC curves corresponding to 4,5,6,7, and 8 hidden nodes. The area under each ROC curve is calculated using the trapezoidal rule.

## 2.2 Results

Table III.8 presents the average results on the four testing sets after the networks have been trained for  $10^4$  iterations.

As we can see from Table III.8, different numbers of nodes in the hidden layer do not seem to have a significant effect on the accuracy of the classifier. Only the neural net with 6 nodes in the hidden layer performs slightly better than the other ones.

The initial weights do not have much effect on the network training process. The maximum variability of the error rate is 0.008 for testing set A -  $TE_A$  (Table III.9).

Testing set B ( $TE_B$ ) gives an error rate around 0.37, whereas the other three testing sets give an error rate around 0.19 (Table III.10).

Subject 3 (see  $TE_A$  and  $TE_D$  in Table III.6) is included twice in a testing set. The performance of the two neural nets, trained on partly different waveforms, on the waveforms of this subject is not significantly different.  $TA$  equals 0.94, and  $TD$  equals 0.60, when the weights of the neural net trained on  $TR_A$  are applied on the waveforms of subject 3, and  $TA$  equals 0.95, and  $TD$  equals 0.56, when the weights of the neural net trained on  $TR_C$  are applied on subject 3.

In Fig. III.4, the ROC curves for different number of hidden nodes are plotted (4 to 8 hidden nodes). The performance of the network is affected by the value of the threshold. As the threshold becomes higher, the number of correctly classified damped waveforms

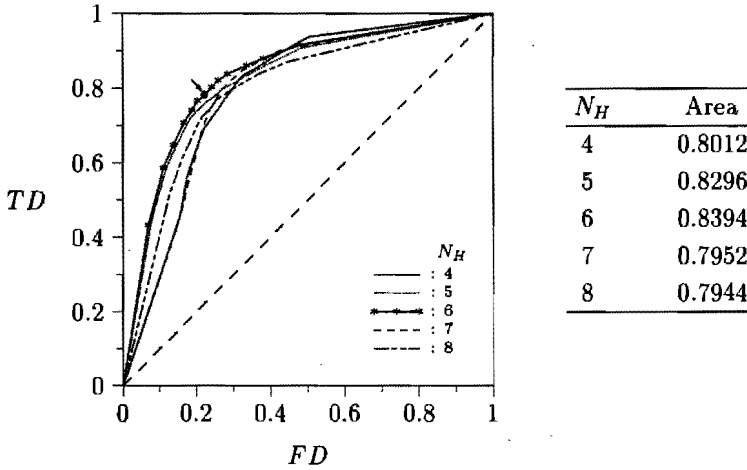


**Figure III.4:** Receiver Operating Characteristic (ROC) curves and their areas for different number of hidden nodes ( $N_H$ ). • = the threshold is equal to 0.5.

increases, however, the number of adequate waveforms incorrectly classified as damped also increases. On the other hand, the number of false damped waveforms and the number of true damped waveforms will become lower as the threshold becomes lower. The area under each ROC curve is given in Fig. III.4. The neural net with the 6 nodes in the hidden layer seems to be the best one, since the area under its ROC curve is the largest. The dashed line drawn along the major diagonal where the true damped and false damped ratios are equal represents a random detection of waveforms. A system could achieve this performance simply by chance.

### 2.3 Discussion

We have developed a software technique for detecting the distortion due to instrumental waveform damping with which we may monitor the reliability of the intra-arterial measurements. Damping is a phenomenon that develops gradually, and it is difficult to be detected. It can remain undetected for long periods, affecting the waveforms and their clinically relevant parameters.

We have adopted the neural network technique for the detection of damping in catheter-manometer system intra-arterial waveforms. Neural nets are being used widely for monitoring the quality of invasively registered arterial pressure waveforms [27, 6, 28].

When a given blood pressure waveform is damped, it is not easy to detect because of the large variability of the arterial waveforms. Klee and coworkers [29] tried to detect damping using the curvature technique. They define as curvature "the ratio of functions of the first and second derivatives" which "has inherent normalizing features that make it less sensitive to the differences among wave forms". According to their results, the

curvature technique could effectively discriminate between the moderately damped signals and the control group, but was not able to distinguish the signals with minute amounts of distortion. The quantitative value of the curvature index (summing the curvature at all points on a pulse beat) allows one to optimize discrimination between clean and distorted signals.

Pike and Mustard [28] have trained a neural network to discard corrupted arterial pressure waveforms. The waveforms that they use to train and test the network are classified manually by the authors according to their own judgement. Moreover, the waveforms have strong artifacts which can be detected with a mere look at the waveform, which is not the case with the detection of slight damping. They use clinical information about the patient as well as inspection of the entire 15 sec signal tracing in order to determine the correct label on each peak. They feed the network with subjective information. The neural net cannot do better than what it is taught to. It will simply produce what the clinicians see. When we asked human observers to classify the waveforms we have been using to test the trained neural net, they did not perform better than the neural net. On the contrary, the results were not significantly different than random. Details are to be found in section 3 of this chapter.

Many of our beats belong into a zone between the two classes: adequate and damped waveforms. This makes the classification more difficult, and it obviously decreases the accuracy of our nets. Some of the waveform classifications are unavoidably incorrect, for example, when the slight damping imposed is not sufficient to have an effect on the waveforms.

The neural nets we have described in the previous section are suitable for blood pressure waveforms that have a heart rate not higher than 100 beats/min. The waveforms we are trying to classify in this study, are coming from subjects that reach heart rates of 200 beats/min.

The adequate waveforms have been recorded through carefully checked hardware. Still at high heart rates the nets detect damped waveforms when in fact there is no added damping. It seems that the undamped blood pressure pulse at the high heart rate changes shape physiologically as if it were damped by a catheter-manometer system. The diagram of Gardner [4] is valid only for operating room and intensive care unit, and not for recording waveforms of subjects during exercise, where the heart rates increase substantially and reach 200 beats/min.

We have tried different number of nodes in the hidden layer. It does not seem to affect the performance of the classifier much. We have not tried a large number, since a network with too many nodes in the hidden layer leads to memorization of the individual data rather than generalization. It will learn to fit the training set well but it will not work well at other data. According to Hanson and Pratt [30], when there are too many hidden nodes, "then the underlying feature relations determining the output surface and category separation are arbitrary, more complex than necessary, and may result in anomalous generalizations". We have used the method of ROC curves analysis, which is recognized as objective and comprehensive way [26] to evaluate performances independent of decision

biases.

Unfortunately, there is no technology available to determine which is the best network topology and the appropriate learning parameters. Thus networks have to be designed by trial and error [31], which is a time consuming and heavily computational task.

The data sets we have used to assess the performance of the different neural nets came from different subjects with a large range of blood pressures and heart rates. During bicycle exercise, the heart rate and the blood pressure increase threefold. There is a large variability of blood pressure and heart rate within subjects.

## 2.4 Conclusion

We have demonstrated the feasibility of neural nets in classifying catheter-manometer system arterial pressure waveforms to adequate and damped during physical exercise when large increases in blood pressure and heart rate are involved.

# 3 Damped blood pressure waveforms detected by experts; a comparison of performances

## 3.1 Introduction

In many cases of neural network engineering an artificial neural net is designed to mimic a certain facility of a human expert. In particular the recognition of waveforms or features of waveforms is often desired by a neural net. Since human experts at times do not agree amongst themselves, or are hesitant, or uncertain, or not able to detect subtleties, training a neural net and evaluating its performance is no easy task.

In the case of the detection of damping in brachial arterial pressure waves this was not a problem since we could start from well recorded waveforms and apply known amounts of damping for the network to detect. Examples of adequate and damped brachial artery waveforms that were used to train and test the networks are shown in Fig. III.5. There was never an uncertainty, neither in the training nor in the testing phase of the performance required from the network. Having thus successfully trained a neural net it occurred to us to *a posteriori* compare the network performance to the expert performance and to investigate how well a human observer could detect damping.

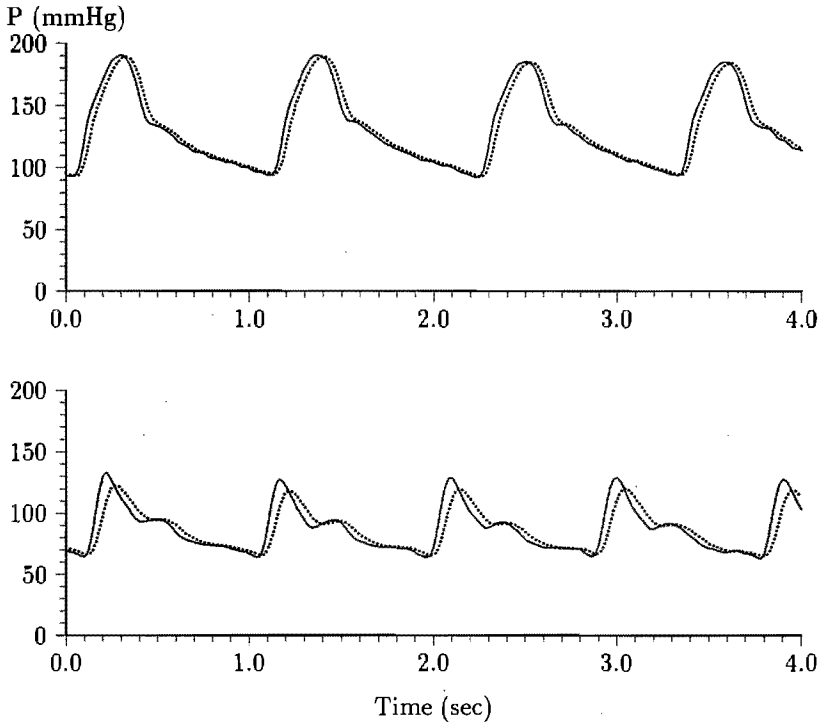


**Figure III.5:** *Examples of adequate (solid line) and damped (dotted line) brachial artery waveforms (slightly damped waveform in the upper panel, more damped in the lower panel). All the four waveforms were correctly classified by the best neural net, described in section 1 of this chapter.*

### 3.2 Methods

We prepared two sets of waveform epochs presenting on a clear amplitude and time scale (an example is shown in Fig. III.6, as exactly presented to the experts) several brachial artery pulsations. One set consisted of 18 adequate (undamped) pulsation epochs coming from nine subjects in the test set of section 1 of this chapter. The other set consisted of exactly the same epochs but with the pulsations more or less damped according to the protocol of section 1 of this chapter. All epochs received a random number that was used for later scoring. The sets were shuffled and offered as a group to the experts.

Twelve experts were asked to do the rating. They were recruited from a group of experienced clinicians, physiologists, and medical physicists. They were told that half of the waves were damped. A time limit was not imposed.

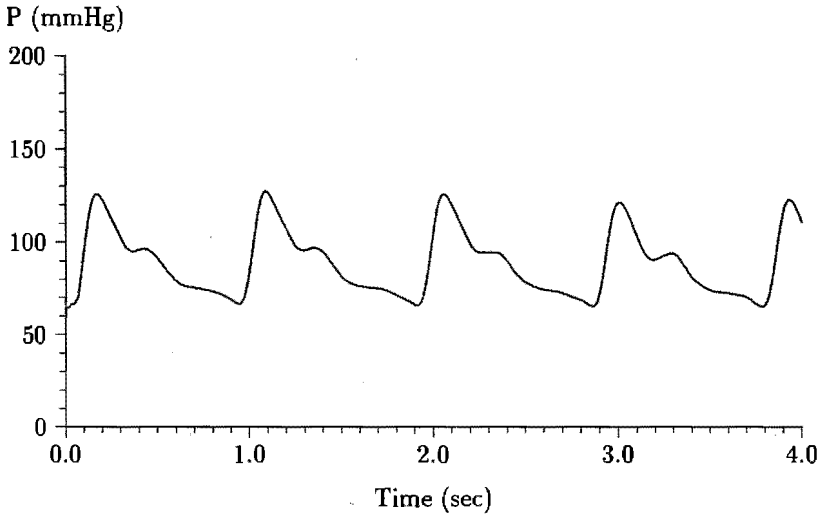


**Figure III.6:** *An example of brachial artery wave that was shown to the human experts. Only 3 of the 11 experts detected that the above waveform was damped.*

### 3.3 Results

We made a table presenting the scoring of the truly damped wave as damped by the eleven experts. One expert, a physiologist, discovered that the waveforms were paired. He paired the waveforms, and placed them on a glass plate illuminated from behind. This facilitated the detection of damping to such a degree that his score was perfect. He was, however, excluded from this analysis.

Of the remaining 11 experts all except expert 2, a clinician, indeed declared 18 waves as damped. Expert 2 scored only 6 waves as damped, of which 4 were correctly identified. The results of the scoring of the truly damped waveforms are shown in Table III.11. The subject waveforms are listed vertically according to age. Of each subject the two epochs are separately shown. The experts are listed horizontally in the order they performed the rating. Only experts 5 (14 out of 18 waveforms) and 10 (13 out of 18 waveforms) scored—slightly—better than purely by chance. Expert 5 worked together with another person for several hours making various measurements on the waveforms. Expert 10 had observed arterial pulsations for over 30 years and was possibly the most experienced. He was also aware of the fact that rise time of the pulse wave is a most important parameter to use to detect damping. His scoring took about 10 minutes. On average the eleven experts scored 10 out of 18 damped waveforms correct, which is not significantly different from a chance scoring. The neural net scored 17 of the 18 damped waveforms correctly as damped.



### 3.4 Discussion

If we had been dependent on human observers to train our neural nets, we would have to have the waveforms damped much more severely than we actually did, to allow human experts to achieve a good, non random, score. Since as it was shown in the previous section, already slight damping causes loss in systolic pressure and stroke volume computation accuracy, the usefulness of the resulting much less sensitive neural net would have been less useful clinically, although probably as good as a human expert.

**Table III.11:** Damped waveforms being detected by expert human observers.  $(f_n, \zeta)$  = natural frequency, damping ratio pairs used to distort the pressure waves;  $\times$  indicates which damped waves were correctly detected as damped by a certain observer; TD = number of human observers who correctly detected the certain waveform of a subject; Correct = number of waveforms that each human observer correctly detected as damped.

Age	$(f_n, \zeta)$	1	2	3	4	5	6	7	8	9	10	11	TD
22	(13, 0.90)					×					×		2
22	(10, 1.20)					×	×		×			×	4
30	(8, 0.94)	×			×	×		×			×	×	6
30	(10, 1.20)	×		×		×				×			4
34	(8, 1.15)				×	×		×		×	×		5
34	(10, 1.20)				×		×			×	×	×	5
36	(8, 1.26)	×		×	×	×			×		×	×	7
36	(10, 1.20)			×							×	×	3
40	(10, 0.99)					×	×	×	×				4
40	(10, 1.20)						×	×	×	×	×	×	6
40	(10, 0.90)	×	×	×	×	×	×	×	×	×	×	×	10
40	(10, 1.20)	×		×	×	×			×		×	×	8
52	(10, 1.10)	×	×	×	×	×			×	×	×		9
52	(10, 1.20)	×		×	×	×	×	×	×	×	×	×	10
52	(10, 1.15)	×	×	×	×	×	×	×	×	×	×	×	11
52	(10, 1.20)	×	×	×	×	×	×	×	×	×	×	×	11
65	(12, 1.0)					×			×				2
65	(10, 1.2)			×				×	×				3
Correct		9	4	10	10	14	10	9	12	9	13	10	110

This observation is in tune with what we can often observe in clinical monitoring of

intraarterial pressure waves in the environment of an operating room or intensive care. It was reported [32] previously that damping of intraarterial waves could be detected quite early in the case that the arterial wave was superposed on a waveform recorded noninvasively on a finger of the same hand. Finger pressure recording does not usually suffer from instrumental damping and is therefore quite suited for this purpose. However, just having to maintain another instrument in the operating room to be able to visually detect the damping state of another instrument cannot be considered practical. Thus, a neural net algorithm such as developed in section 1 of this chapter, but adapted for radial artery pulsations, could prove a more useful solution for this persistent problem, in particular also since it outperforms human experts.

## References

- [1] Maren A, Harston C, and Pap R. *Handbook of neural computing applications*. Academic Press, London, 1990.
- [2] Idema RN, Van den Meiracker AH, Imholz BPM, Man in 't Veld AJ, Settels JJ, Ritsema van Eck HJ, and Schalekamp MADH. Comparison of Finapres non-invasive beat-to-beat finger blood pressure with intrabrachial artery pressure during and after bicycle ergometry. *Journal of Hypertension*, 7(suppl 6):S58-S59, 1989.
- [3] Van Montfrans GA, Van der Hoeven GMA, Karemaker JM, Wieling W, and Dunning AJ. Accuracy of auscultatory blood pressure measurement with a long cuff. *Br. Med. J.*, 295:354-355, 1987.
- [4] Gardner RM. Direct blood pressure measurements — dynamic response requirements. *Anaesthesiology*, 54:227-236, 1981.
- [5] McDonald DA. *Blood flow in arteries*. Edward Arnold, London, second edition, 1974.
- [6] Johnson RW, Scanlon TS, Smith NT, and Mulier JP. A neural network for identification of damped or resonant blood pressure waveforms. In *Proceedings of the 13th Annual International Conference of the IEEE Engineering in Medicine and Biology Society*, volume 3, pages 1413-1414, Orlando, Florida, USA, October 31 - November 3 1991.
- [7] Wesseling KH. *FAST system User Manual*. TNO-Biomedical Instrumentation, Academic Medical Centre, Amsterdam, The Netherlands, 1993.
- [8] Hamming RW. *Digital filters*. Prentice Hall, Inc., Englewood Cliffs, NJ, 1977.
- [9] Wesseling KH, Jansen JRC, Settels JJ, and Schreuder JJ. Computation of aortic flow from pressure in humans using a nonlinear three-element model. *J. Appl. Physiol.*, 74(5):2566-2573, 1993.

- 
- [10] Siegel S and Castellan NJ. *Nonparametric statistics for the behavioral sciences*. McGraw-Hill Book Company, New York, 1988.
- [11] Rumelhart DE, Hinton GE, and Williams RJ. Learning internal representations by error propagation. In DE Rumelhart and JL McClelland, editors, *Parallel distributed processing: Explorations in the microstructure of cognition, Volume 1: Foundations*. MIT Press Cambridge, MA, 1986.
- [12] Hecht-Nielsen R. Kolmogorov's mapping neural network existence theorem. In *Proc. First IEEE International Joint Conference on Neural Networks*, volume 3, San Diego, CA, June 21-24 1987.
- [13] Lippmann RP. An introduction to computing with neural nets. *IEEE ASSP Magazine*, pages 4-22, April 1987.
- [14] Fahlman SE. An empirical study of learning speed in back-propagation networks. Technical Report CMU-CS-88-162, Carnegie-Mellon University, June 1988.
- [15] Draper NR and Smith H. *Applied regression analysis*. Wiley Series in Probability and Mathematical Statistics. Chichester, second edition, 1981.
- [16] Morrison DF. *Multivariate statistical methods*. McGraw-Hill Book Company, New York, second edition, 1976.
- [17] Murtagh F and Heck A. *Multivariate data analysis*. Kluwer, Dordrecht, Holland, 1987.
- [18] Vrckovnik G, Chung T, and Carter CR. Classifying impulse radar waveforms using principal component analysis and neural networks. In *International Joint Conference on neural networks*, volume I, pages 69-74, San Diego, CA, 1990.
- [19] Jain AK and Dubes RC. *Algorithms for clustering data*. Prentice Hall, Inc., Englewood Cliffs, NJ, 1988.
- [20] Frank O. Kritik der elastischen Manometer. *Z. Biol.*, 44:445-613, 1903.
- [21] Imholz BPM. *Noninvasive Finger Arterial Pressure Waveform Registration, evaluation of Finapres<sup>TM</sup> and Portapres*. PhD thesis, University of Amsterdam, Amsterdam, The Netherlands, 1991.
- [22] Weiss SM and Kulikowski CA. *Computer Systems that learn*. Morgan Kaufmann Publishers, Inc, 1991.
- [23] Refenes AN, Zapranis A, and Francis G. Stock performance modeling using neural networks : A comparative study with regression models. *Neural Networks*, 7(2):375-388, 1994.

- [24] Eberhart RC and Dobbins RW. *Neural Network PC Tools*. Academic Press, Inc., 1990.
- [25] Hush DR and Horne BG. Progress in supervised neural networks, what's new since Lippmann? *IEEE Signal Processing Magazine*, pages 8-39, January 1993.
- [26] Swets JA. Measuring the accuracy of diagnostic systems. *Science*, 240:1285-1293, June 1988.
- [27] Sebald AV. Use of neural networks for detection of artifacts in arterial pressure waveforms. In *Proceedings of the 11th Annual International Conference of the IEEE Engineering in Medicine and Biology Society*, volume 6, pages 2034-2035, Seattle, Washington, USA, November 9-12 1989.
- [28] Pike T and Mustard RA. Automated recognition of corrupted arterial waveforms using neural network techniques. *Computers in Biology and Medicine*, 22(3):173-179, 1992.
- [29] Klee G, Ackerman E, and Leonard A. Computer detection of distortion in arterial pressure signals. *IEEE Transactions on Biomedical Engineering*, pages 73-75, January 1974.
- [30] Hanson SJ and Pratt LY. Comparing biases for minimal network construction with back-propagation. In *IEEE Conference on Neural Information Processing Systems - Natural and Synthetic*, Denver CO, 28 Nov. - 1 Dec. 1989.
- [31] Miller AS, Blott BH, and Hames TK. Review of neural network applications in medical imaging and signal processing. *Medical and Biological Engineering and Computing*, 30:449-464, September 1992.
- [32] Wesseling KH and Smith TN. Availability of intraarterial pressure waveforms from catheter- manometer systems during surgery. *Journal of Clinical Monitoring*, 1:11-16, 1985.

# Chapter IV

## Models of brachial to finger pulse wave distortion and pressure decrement

*Paolo Gizdulich<sup>a</sup>, Andriana Prentza<sup>b</sup>, Karel H Wesseling<sup>b,c</sup>*

<sup>a</sup> Clinical Physiopathology Department, University of Florence, Viale Morgagni 85, 50134 Florence, Italy

<sup>b</sup> Department of Electrical Engineering, Technical University Eindhoven, P O Box 513, 5600 MB Eindhoven, The Netherlands

<sup>c</sup> TNO-TPD BioMedical Instrumentation, Academic Medical Centre, Suite L0-002, Meibergdreef 9, 1105 AZ Amsterdam, The Netherlands

*Cardiovascular Research; 33:698-705, 1997*

### Abstract

**Objective:** To model the pulse wave distortion and pressure decrement occurring between brachial and finger arteries. Distortion reversion and decrement correction were also our aims.

**Methods:** Brachial artery pressure was recorded intra-arterially and finger pressure was recorded non-invasively by the Finapres technique in 53 adult human subjects. Mean pressure was subtracted from each pressure waveform and Fourier analysis applied to the pulsations. A distortion model was estimated for each subject and averaged over the group. The average inverse model was applied to the full finger pressure waveform. The pressure decrement was modelled by multiple regression on finger systolic and diastolic levels. **Results:** Waveform distortion could be described by a general, frequency dependent model having a resonance at 7.3 Hz. The general inverse model has an anti-resonance at this frequency. It converts finger to brachial pulsations thereby reducing average waveform distortion from 9.7 (s.d. 3.2) mmHg per sample for the finger pulse to 3.7 (1.7) mmHg for the converted pulse. Systolic and diastolic level differences between finger and brachial arterial pressures changed from -4 (15) and -8 (11) to +8 (14) and +8 (12) mmHg, respectively, after inverse modelling, with pulse pressures correct on average. The pressure decrement model reduced both the mean and the standard deviation of

systolic and diastolic level differences to 0 (13) and 0 (8) mmHg. Diastolic differences were thus reduced most. **Conclusion:** Brachial to finger pulse wave distortion due to wave reflection in arteries is almost identical in all subjects and can be modelled by a single resonance. The pressure decrement due to flow in arteries is greatest for high pulse pressures superimposed on low means.

## Keywords

Finapres, Brachial-to-finger modelling, Waveform distortion, Blood pressure, Human.

## 1 Introduction

The brachial artery is often the clinical site for intra-arterial and for non-invasive Riva-Rocci cuff blood pressure measurements. For several years it has been possible for continuous finger arterial pressure waveforms to be recorded non-invasively. This has been used to follow changes in blood pressure in response to various stressors [1, 2, 3, 4, 5, 6] and during the course of the 24-h day [7] in persons in whom insertion of an arterial cannula is not accepted as ethical. However, for physiologic reasons (pulse wave reflection and pressure gradient due to flow), pressure pulsations in the finger differ in shape from and are depressed in level compared to those recorded in the brachial artery.

Therefore, since non-invasive arterial blood pressure has become feasible [8, 9], publications have appeared comparing finger arterial systolic, diastolic and mean pressure levels to levels recorded intra-arterially in the brachial or radial artery. Earlier studies concentrated on level comparisons sampled at various periodic intervals [10, 11, 5], while later studies compared beat-to-beat values [12, 2, 3, 13]. As a next step we decided to study the differences in the waveforms recorded in the brachial artery and at the finger, with the aim to find a distortion model and then to inverse-model the finger to the brachial pressure pulsations.

A previous study described pressure pulse propagation in the arterial system from the aorta to the radial artery and stated that application of a generalized filter could remove waveform distortion [14]. Since finger diastolic and mean pressure are clearly below intra-arterial [2], due to a pressure gradient in the arteries of the arm and hand and decrements that appeared to depend on the activity level of the subject [7] we suspected that waveform distortion to the finger might also depend on pressure gradient, mean pressure, heart rate and subject age.

## 2 Methods

### 2.1 Subjects

Pressure recordings were available from 4 previous studies [12, 1, 15, 13], chosen for our purpose because they cover a wide range of ages, blood pressures and conditions of the circulation. Study [15] provided pressures of 18 (suspectedly borderline) hypertensive patients aged 25–65 years. Eleven of the patients were on anti-hypertensive medication. Study [1] provided the pressures of 7 healthy resting volunteer subjects, aged 22–40 years. Studies [12] and [13] provided pressures of 28 subjects aged 52–83 years, 15 of whom were healthy elderly subjects, 13 suffered from therapy-resistant hypertension and 7 additionally from arteriosclerotic vascular disease. The original studies were approved by the respective ethical committees. Informed consent was obtained from all volunteer subjects and all patients prior to entering the protocol.

**Table IV.1:** Summary of patient and model characteristics. The parameters  $K$ ,  $f_1$ , and  $D$  refer to the forward model Eq. (IV.1). SDD = the standard deviation of the differences with the brachial reference waveform in mmHg per sample; 'original' refers to the original finger pulse, 'individual' to the individual inverse model, and 'general' to the general inverse model.

	Unit	Mean	s.d.	Range
Age	yr	54	15	22 – 83
HR	b.p.m.	68	11	50 – 95
$K$		0.84	0.09	0.63 – 0.98
$f_1$	Hz	7.34	1.34	4.26 – 10.58
$D$		0.36	0.16	0.07 – 0.83
Original SDD	mmHg	9.7	3.2	3.6 – 19.3
Individual SDD	mmHg	1.8	0.8	0.6 – 4.0
General SDD	mmHg	3.7	1.7	1.1 – 9.3

### 2.2 Pressure measurements

The non-dominant arm was used for cannulation. After local anaesthesia with a 1% lidocain solution, a Travenol Quick Cath, N1113, 20 gauge, 11 cm long Teflon cannula was inserted into the brachial artery. The cannula was connected through a short section of tubing to a fluid-filled pressure transducer installed with a continuous flush system and strapped to the mid-upper arm at heart level. The resonance frequency of these systems was checked with the fast flush or the tap method [16]. It ranged from 11 Hz

with 0.7 damping to 50 Hz underdamped and in all cases except one was at least "adequate" [16] in that instrumental resonance was well above physiological and well above the range where coherence between both blood pressure waveforms is significant. In the one case with resonance at 11 Hz it was "borderline" according to Gardner [16] due to a high damping factor which reduces instrumental oscillations. Pressure channel sensitivity (static accuracy) was checked against a well-maintained mercury manometer and against the Finapres. Differences were always less than 2 mmHg over the 0-300 mmHg range.

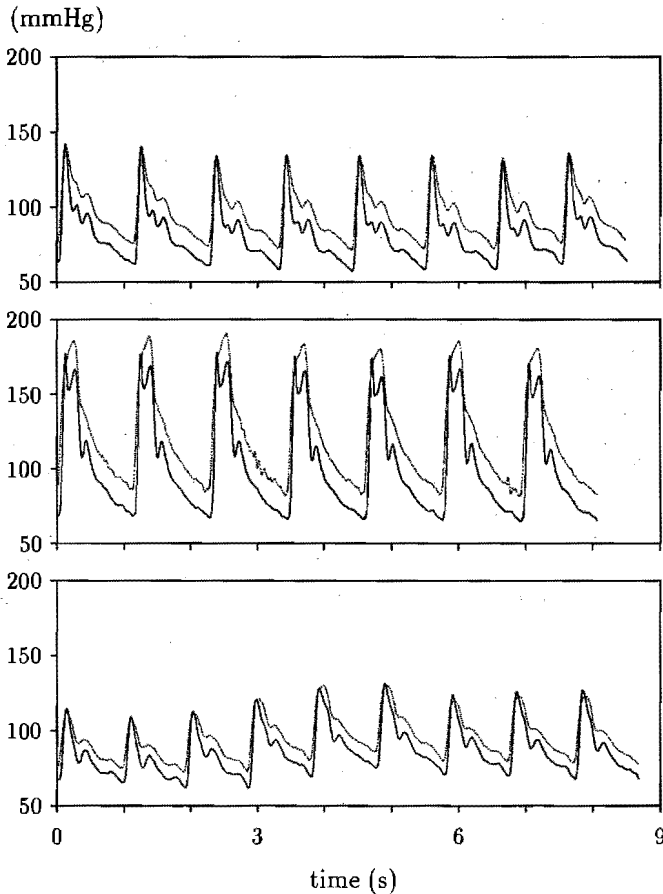


**Figure IV.1:** Three panels showing from above arterial pressure pulsations in a 22-, an 83- and a 40-year-old subject, the latter with a varying baseline. The dotted lines are brachial, the solid lines finger pressure.

TNO Finapres Model 5 devices and finger cuffs were used for the finger pressure recordings. A properly sized cuff (see Finapres manual) was wrapped around the middle



or index finger mid-phalanx of the ipsilateral hand, and supported at heart level. Using the ipsilateral hand may cause errors if the more proximal cannula partly blocks the radial artery [17]. However, in the studies whose results we used the much larger brachial artery was cannulated. No signs of damped brachial waves [18], or signs of blocking such as slow rising finger pressure pulses, could be detected.

### 2.3 Signal processing

The brachial and finger pressure signals were fed through identical Krohn-Hite Model 3750 40 dB/decade low pass filters at 30 Hz  $-3$  dB cut-off. A computer system digitized the simultaneous pressure signals with a resolution of 0.1 mmHg at a rate of 200 Hz. Next, the records were digitally filtered with a Hamming  $(-1 -5 -5 +20 +70 +98 +70 +20 -5 -5 -1)$  low pass filter, which is  $-3$  dB at 35 Hz. Every other sample was then deleted to have signals sampled at 100 Hz.

Epochs of approximately 10 s duration were selected from the recordings having an integer number of beats and an almost flat baseline. Selected epochs began and ended just before the beginning of a brachial upstroke, lasted on average 9 (s.d. 1.5) s, and contained  $n=10$  (s.d. 2), range 4-16 beats. Any slight remaining pressure differences between beginning and end of the records were linearly subtracted. This gave signal epochs ready for discrete Fourier analysis without further windowing.

### 2.4 Model identification

After subtraction of the mean pressure to obtain just the pulses Fourier analysis was used to establish each individual's and the geometric average "forward" (brachial to finger artery) complex frequency transfer function. We used MATLAB (The Math Works, Inc., South Natick, MA, USA) for this purpose. The amplitude transfer functions were suggestive of the existence of a resonance near 7 or 8 Hz and subsequent return to unity transfer at higher frequencies.

A model transfer function having such response is:

$$H(f) = K \frac{(1 + if/f_0)^2}{1 + 2iDf/f_1 - (f/f_1)^2} \quad (\text{IV.1})$$

with  $i$  the imaginary unit. This model is equivalent to a gain,  $K$ , a second-order aperiodic high emphasis section at frequency  $f_0$ , followed by a second-order underdamped low pass section at resonance frequency  $f_1$ , with damping  $D < 1$ . The transfer function was forced to unity transfer at high frequencies by linking  $f_0$  and  $f_1$  by the equation:

$$f_0 = f_1 \sqrt{K} \quad (\text{IV.2})$$

This avoided overtight fitting of the model to the high-frequency section of the response where coherence between brachial and finger pressure spectral components is low. Using

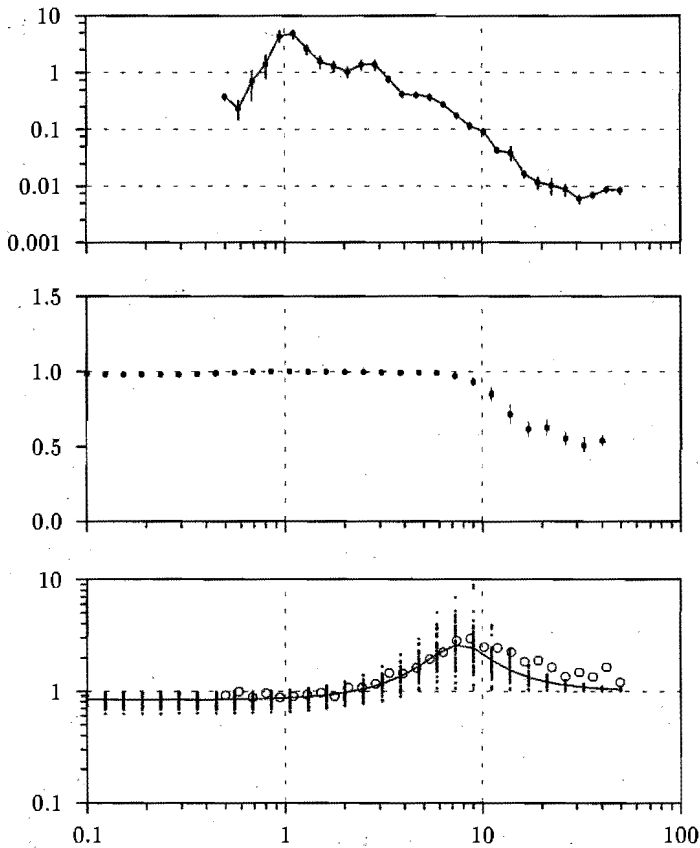


**Figure IV.2:** The upper panel shows the group average brachial pressure amplitude spectra and standard error bars (mmHg). The middle panel shows the average coherence between the brachial and finger pressure spectra and standard error bars. The bottom panel presents the measured geometric-average amplitude transfer function (circles) and the average model transfer function (drawn curve). The dots in vertical arrangement indicate the position of the individual model transfer functions. Note that some of the scales are logarithmic. Measured data start at a frequency of 0.5 Hz which was present in all subjects. Model data start at 0.1 Hz.

MATLAB, the complex model was least-squares-fitted to each subject's complex transfer function.

The fit program was free to change the relative delay of the two epochs per subject to obtain a best fit. Thus 3 model parameters were estimated: gain  $K$ , resonance frequency

$f_1$ , and damping  $D$ .

The model parameters obtained for each subject were entered into a table together with mean finger pressure, heart rate and age, and multiple regressions computed to verify interdependencies. A general model for the group was computed by taking the average of each model parameter. The result is the general forward model.

## 2.5 Inverse modelling

An inverse model amplifies the signal at frequencies where the forward model attenuates and vice versa. Each individual's own inverse model and the general inverse model for the group were applied to the finger pulses. The original finger pulse and the inverse-modelled finger pulse were compared to the corresponding brachial pulse and the standard deviation of the differences (SDD) obtained for the optimal delay. This provided a measure for the precision of brachial pulse approximation.

## 2.6 Level correction

Equally, the full finger pressure (without mean pressure subtracted) was inverse-modelled with the general inverse model to approach full brachial artery pressure. The remaining differences in systolic, diastolic and mean levels between finger and brachial, and between the inverse modelled finger and brachial pressures were computed. This provided a measure of the accuracy of the pressure level recovery by the inverse model. For the entire group we then checked if the level differences depended on measures obtainable non-invasively, such as finger pressure levels, heart rate, or age, by computing multiple regressions. When significant, we corrected the inverse modelled finger pressure levels by the value of the regression equation and recomputed level differences mean and standard deviation.

## 2.7 Random subgroups

Using the entire group for model analysis and inverse modelling provides for the best signal to noise ratio but does not allow the verification of selection effects. Therefore, 5 different random selections of 23–29 subjects and their complementary groups of 30–24 subjects were constructed. General distortion models for each of 10 subgroups were computed and compared to the general model for the entire group. Furthermore, the level differences multiple regressions for the 10 subgroups were computed and applied as a correction to their complementary group and the results compared.

# 3 Results

Some typical blood pressure records are shown in Fig. IV.1. Finger diastolic and mean levels are generally below intrabrachial; systolic levels tend to be at or above intrabrachial

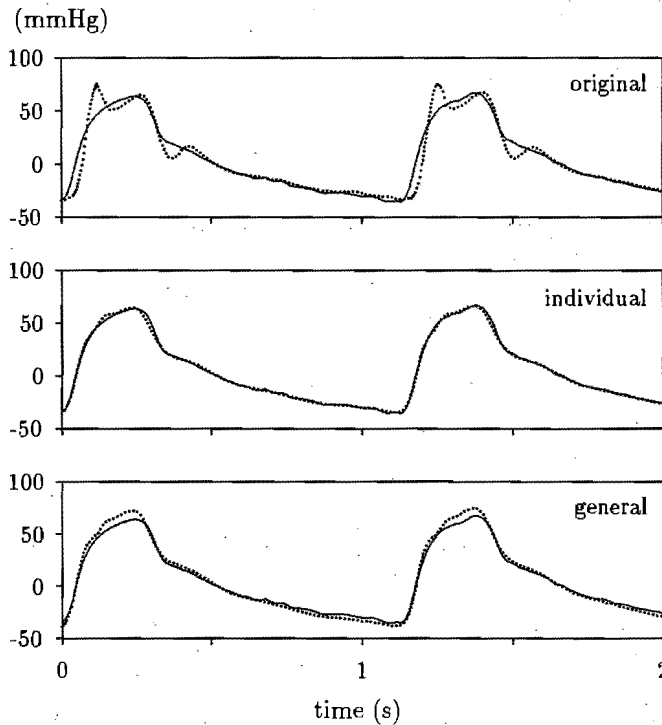


**Figure IV.3:** Comparison of the brachial pulse wave (solid curve) with (dotted), from above, the original finger pressure, and the inverse-modelled finger pressure for the individual and the general model in an 83-year old subject. Mean pressure was subtracted first.

pressures. At the finger, young subjects (top traces) tend to show a strong initial systolic peak and a deeper falling diastolic notch. Oscillations are more pronounced in the finger than in the brachial pressure. Older subjects (middle traces) tend to show two systolic peaks of approximately equal height. Baseline changes in intrabrachial pressure are tracked well by Finapres (bottom traces).

### 3.1 Waveform distortion model

Group average results of the spectral analyses are shown in Fig. IV.2. The amplitude spectrum for brachial pressure (upper panel) is high near the fundamental frequency of approximately 1 Hz. Towards higher frequencies the amplitude decreases quickly to below 0.1 mmHg at 10 Hz, or by a factor of 50 per decade of frequency.

Coherence between the brachial and finger pulsation spectra (middle panel) is near 1

up to about 10 Hz. Above 10 Hz coherence drops gradually to remain above 0.5 to 50 Hz.

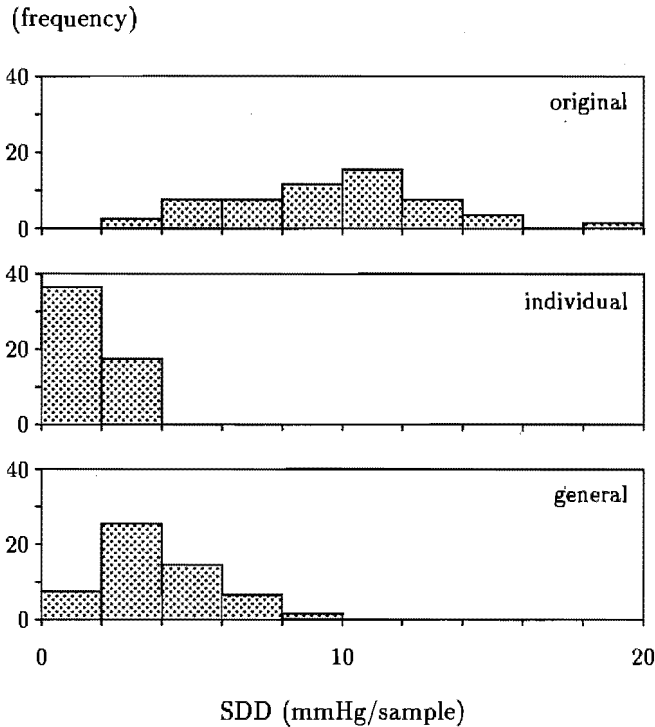


**Figure IV.4:** Histograms of the standard deviation of the differences (SDD) with the brachial pulsations of, from above, the original finger pressure, and the inverse-modelled finger pressure for the individual and the group average models in the 53 subjects of the study.

The geometric average forward amplitude transfer as a function of frequency (bottom panel) is shown together with the average forward model transfer function. Both transfers follow the same trace over the entire frequency range. Low frequencies are attenuated in the finger. Frequencies near the resonance peak at 7 Hz are amplified. The transfer function crosses unity level near 2 Hz. At high frequencies the model transfer function returns to unity slightly quicker than the computed forward transfer function since coherence is low at these frequencies and a tight fit not attempted. Individual transfer functions differ from the average, as can be observed in the figure, but not wildly so, as can be judged from the model statistics in Table IV.1. The model gain  $K$  has 10% standard deviation, the resonance frequency  $f_1$  has 18%, and the damping coefficient  $D$  has 45% standard deviation.

Various random selections of subjects from the pool of 53 and the remaining comple-

Table IV.2: Pressure levels and level differences (mmHg).

	Mean	s.d.	Range	Mean	s.d.	Range
<b>Brachial</b>						
Systolic	169	33	95 - 245			
Diastolic	89	17	46 - 127			
Mean	120	22	62 - 174			
Pulse	80	23	41 - 145			
<hr/>						
<b>Original finger</b>			<b>Fin-Bra</b>			
Systolic	165	30	89 - 241	-4	15	-37 - 28
Diastolic	81	17	40 - 128	-8	11	-33 - 18
Mean	107	21	53 - 164	-13	11	-37 - 14
Pulse	84	24	49 - 178	4	13	-31 - 33
<hr/>						
<b>Inverse-modelled</b>			<b>Inv-Bra</b>			
Systolic	177	34	93 - 252	8	14	-24 - 38
Diastolic	97	21	48 - 155	8	12	-18 - 36
Mean	128	25	63 - 194	8	12	-18 - 35
Pulse	80	25	44 - 166	0	9	-23 - 22
<hr/>						
<b>&amp; Level corrected</b>			<b>Cor-Bra</b>			
Systolic	169	33	96 - 261	0	13	-32 - 31
Diastolic	89	14	52 - 128	0	8	-19 - 20
Mean	119	21	66 - 168	-1	9	-23 - 19
Pulse	80	25	44 - 166	0	9	-23 - 22

mentary groups each had model parameter averages nearly equal to those in Table IV.1 and no random selection showed significant differences ( $P > 0.05$ ). No evidence of selection effects, therefore, is apparent.

### 3.2 Dependencies of model coefficients

Of the subject data, pulse pressure regressed significantly on age (correlation coefficient  $r=0.62$ ;  $P < 0.001$ ). Of the model coefficients,  $K$  did not regress on any other parameter. Resonance frequency,  $f_1$ , ( $r=0.48$ ;  $P < 0.001$ ) and damping coefficient,  $D$ , ( $r=0.41$ ;  $P < 0.01$ ) regressed significantly on mean finger pressure. Taking the regression into account the standard deviation of  $f_1$  decreased slightly from 18 to 16%. The standard deviation of  $D$  did not decrease appreciably after regression correction.

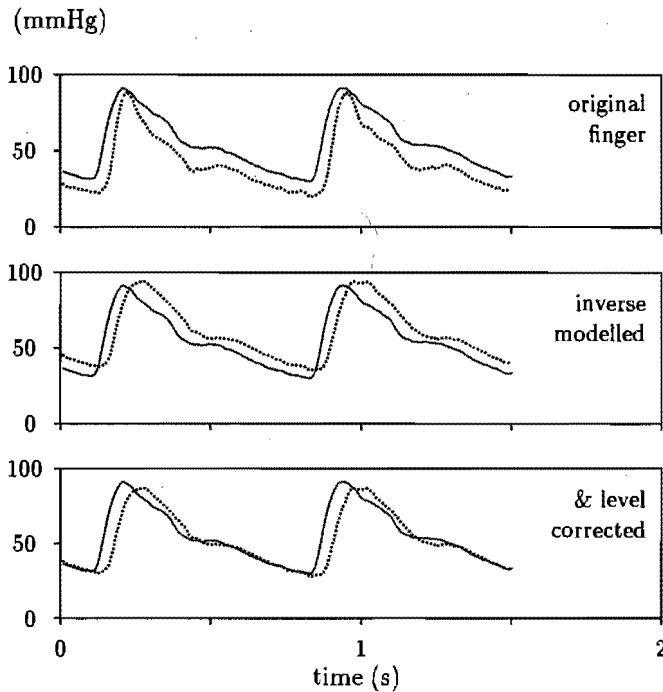


**Figure IV.5:** Demonstration of the process of inverse modelling and level correction on a waveform of a 53-year old subject. The original finger pressure (top panel) is distorted with respect to brachial (solid curve), and lower in level. After general inverse modelling (middle panel) the waveforms are nearly identical, but the level is still different. Level correction (bottom panel) shifts the waveform down by 7 mmHg in this case, after which it is nearly correct. The delay between waveforms was not modelled and, thus, not corrected, explaining the unchanged delays in the finger derived waveforms.

### 3.3 Inverse distortion model

The degree of pulse wave distortion removal can be judged from Fig. IV.3. The standard deviation of the differences (SDD) is reduced most by the individual inverse model (Table IV.1). Application of the general inverse model, since it is only correct on average, delivers less exact results. Still, most of the waveform distortion is removed by the general inverse model. Histograms of the SDD are shown in Fig. IV.4.

The general inverse model when applied to the full finger pressure waveform does the same conversion of the pulses, but in addition mean pressure is amplified by the model's inverse  $K$ -factor, which moves the pressure curve upwards. The systolic, diastolic, mean and pulse pressures in the brachial artery, at the finger, and at the finger after inverse modelling are shown in the first 3 panels of Table IV.2. Since mean pressure in the finger,

on average, is 90% of intrabrachial, but the inverse  $K$ -factor amplifies mean pressure by 1.19, the inverse-modelled mean pressure is higher than brachial, on average by 7%.

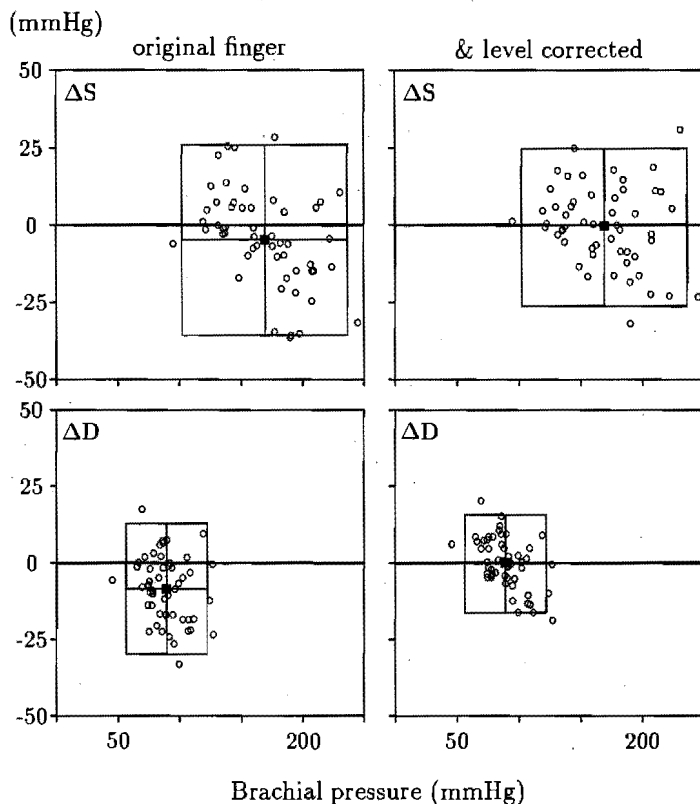


**Figure IV.6:** Systolic ( $\Delta S$ ) and diastolic ( $\Delta D$ ) level differences between brachial and finger (left panels) and between brachial and inverse modelled and corrected (right panels) finger pressures. The large squares indicate 95% confidence intervals, the centered solid squares the group average values.

### 3.4 Level correction

After application of the general inverse model pulse pressures were correct on average. The remaining differences of diastolic pressure with brachial,  $\Delta p_D$ , (Table IV.2, third panel: Inv-Bra) regressed significantly on inverse-modelled finger systolic ( $p_S$ ) and diastolic



( $p_D$ ) pressure ( $r=0.73$ ,  $P < 0.001$ ), and slightly less well on mean and pulse pressure. The differences in mean pressure also regressed on systolic and diastolic pressure ( $r=0.66$ ,  $P < 0.001$ ) although less closely. The differences in systolic pressure and pulse pressure did not correlate well. A level correction was applied to the inverse-modelled finger pressures using the regression model for the diastolic differences on inverse-modelled systolic and diastolic pressures:

$$\Delta p_D = -13.3 - 0.194p_S + 0.574p_D \quad (\text{IV.3})$$

Subtracting  $\Delta p_D$ , for each subject, from the systolic, diastolic and mean levels reduced both the mean and the standard deviation of the differences (Table IV.2, bottom panel).

The two-step process of inverse modelling and level correction is demonstrated in Fig. IV.5. Bland-Altman plots of the differences in systolic and diastolic pressure before and after correction are presented in Fig. IV.6. Improvement is greatest for diastolic pressure.

The 10 random selections from the 53 subjects on average provided very similar level correction effects (systolic 0.2 (s.d. 2), diastolic 0.4 (2), mean  $-0.2$  (2) mmHg) and reductions in standard deviation (systolic to 13, diastolic to 8, mean to 9 mmHg) on their complementary selections, suggesting the absence of selection effects.

## 4 Discussion

We found models for the distortion and level decrement of the pulse wave between the brachial artery and the finger. Similar studies [14, 19, 20] have appeared before, but the present one is the first on brachial to finger pressure and the first also to consider level depression. A two-step approach was used. First we modelled brachial to finger pulse waveform distortion by a frequency-dependent equation (Eqs.IV.1 and IV.2), then we modelled the remaining level differences between the two sites with a multiple regression equation (Eq.IV.3). Correction was done in the same two-step procedure. Major reductions in distortion and level decrement were obtained this way.

Finger pressure waveforms and levels are less familiar to clinicians than brachial or radial pressures. Radial artery pressures are used principally in surgery and intensive care situations. Here, monitoring changes in blood pressure levels is often more important than absolute accuracy. Brachial artery pressures are used frequently for diagnosis in the practice of internal medicine and cardiology. The accuracy of systolic and diastolic levels is of primary importance. To correct the differences of finger with intra-brachial pressures, both the pulse pressure and the mean pressure levels must be correct, which requires application of both our modelled effects.

Some authors mention the possibility of obtaining an estimate of arterial compliance from inspection of the aortic pressure wave, in particular the late systolic augmentation of the pulsation [19]. Some authors stress that such changes are age-related [21]. The present inverse model (from finger to brachial artery) does not allow for such inspection

of waveforms with clarity but would require extension of the inverse model to aortic pressures.

#### 4.1 Waveform distortion

Finger pressure is quite similar to radial artery pulsations [22, 20], whereas brachial pulsations appear as less resonant (Fig. IV.1). Using Fourier transformation, we determined individual linear forward transfer functions describing the waveform distortion that occurs when pulses travel in the arterial system between brachial and finger artery. Regardless of the individual differences in pulse shape, one major resonance near 7 Hz stood out (Fig IV.2). Since the model is linear, and since the finger pulses after individual inverse modelling approach the brachial pulse so closely (Table IV.1 and Figs. IV.3 and IV.4), this shows that pressure pulse propagation in the arm arterial system can be understood as a linear process. This confirms in humans earlier findings in animals [23], even for pulse pressures as high as 145 mmHg in the brachial artery (Table IV.2).

The resonance frequency depends most on the length of the arterial section considered. Karamanoglu, et al. [14], measured between aorta and radial artery, and detected a resonance near 4 Hz. We measured the shorter section between brachial artery and finger, and found a resonance near 7 Hz. Triedman and Saul [20] measured the even shorter section between radial artery and finger in children, and found a resonance near 10 Hz. Considering the arterial section as an organ pipe closed at the distal end (with reflection coefficient almost equal to 1 [23]), the shortest pipe indeed produces the highest tone.

Surprisingly, even the general inverse model provided a good approximation of the brachial from the finger pulse, although individual resonance frequency and damping showed substantial scatter and regressed significantly on mean blood pressure. An explanation is that at low frequencies the individual forward transfer functions are similar. It is at the lower frequencies that the harmonics in the finger pressure spectrum are strongest (Fig. IV.2) and thus have most influence on the shape of the pulse. What happens at higher frequencies has a lesser effect.

Karamanoglu et al. [14] stated recently that a generalized transfer function can be used to estimate central from peripheral pressure under different conditions in adult humans. It is not obvious, *a priori*, that Karamanoglu's conclusions remain valid for an acral site such as the finger since the small size of the peripheral arteries leading to the finger cause a pressure gradient due to flow, which dampens the pulse. We did find a significant pressure dependency of the model resonance frequency ( $f_1$ ) and damping ( $D$ ) coefficients. However, application of general inverse models with the model coefficients individually adapted applying the regression of each coefficient on mean pressure led to only insignificant individual and no changes on average in inverse modelling accuracy. This supports Karamanoglu's conclusion for transmission of pulses as far peripherally as the finger arteries.

## 4.2 Pressure levels

Finger pressures are not only distorted, but diastolic and mean pressures are depressed in level compared to brachial artery pressure. A notable pressure gradient in the arterial system exists caused by flow in the smaller resistive arteries. On applying the inverse model such mean level depressions on average are overcompensated, indicating that mean pressure is less affected by the resistance to flow than pulse pressure. The extra damping for pulsations at low frequencies could well be caused by the compliance of the small branches of the arterial system.

Thus, application of the general inverse model—although demonstrated earlier to improve tracking of blood pressure changes [24]—did not improve the accuracy of the estimation of systolic, diastolic and mean levels of brachial pressure by the finger even though pulse pressures were now correct on average (Table IV.2, bottom panels). The underestimation of brachial diastolic and mean levels by finger pressure turned into an overestimation of 8 mmHg for all levels. This overestimation could have been removed simply by subtracting 8 mmHg from all pressure levels but that would not have reduced the standard deviation of the differences. Correction by application of a multiple regression model, however, did reduce standard deviation. Diastolic pressure accuracy now meets AAMI criteria [25], but systolic does not. We applied the diastolic level correction since its regression equation showed the highest correlation and since diastolic levels showed the largest relative differences (8% for systolic versus 14% for diastolic, computed from Table IV.2) and needed correction most. After level correction relative differences distributed more equally at 8 and 9%, respectively.

This level correction shifts the waveform in an upwards direction when large pulsations are superimposed on a low diastolic pressure. Such large pulsations tend to indicate a large stroke volume and cardiac output, and a low diastolic pressure in addition indicates a low peripheral resistance and a high peripheral flow which would cause a high peripheral pressure decrement. The opposite situation of a small pulse superimposed on a high diastolic pressure we have often observed to occur in cold fingers under a supposedly high sympathetic tone and a generally low peripheral flow state [5]. Since a high aortic flow does not necessarily indicate a high peripheral flow in the arm and hand, the model is imperfect and the level shift correction helps but provides no perfect remedy.

We tested our general inverse model under experimental conditions of vasoconstriction and exercise to exertion that extrapolated to higher and lower heart rates and to higher blood pressures [24]. The inverse model not only produced more central blood pressure waveforms from non-invasive finger pressures, but changes in systolic blood pressure were followed with greater accuracy. To track systolic pressures in exercise stress testing and for the computation of baroreflex sensitivity, application of this model appeared essential [24].

Having pulse pressures correct on average after inverse modelling, it should suffice to calibrate just one of its levels (systolic, diastolic or mean) to the corresponding brachial level to have the entire waveform corrected. This was tried in another study [26]. Best results, clearly within AAMI criteria [25] for all levels, were obtained by adjusting inverse-

modelled finger systolic pressure to a return-to-flow systolic level detected with a Finapres mounted distal to the upper arm cuff. But extra equipment is needed for this important correction.

## 5 Conclusion

A simple, single resonance model describes waveform distortion in the arm arterial system between the brachial artery and the finger. A general inverse model converts non-invasively recorded finger pressure waveforms to brachial pulsations with precision independent of resting pressure, heart rate or age. A regression-based level correction procedure models the dependence of the pressure gradient on flow to further reduce group mean differences and standard deviations without taking an extra measurement.

## Appendix

### Spectral Analysis

Spectral analysis is the signal processing method that characterizes the frequency content of a measured signal. The basic motivation for developing and applying the frequency analysis tools is to provide a mathematical and pictorial representation for the frequency components that are contained in any given signal. The Fourier transform is at the foundation of spectral analysis. It is the mathematical method to relate a time varying signal to the frequency-domain representation.

Fourier transformation and inverse Fourier transformation are defined by the following pair of equations :

$$X(f) \equiv \int_{-\infty}^{\infty} x(t)e^{-i2\pi ft} dt$$

and

$$x(t) \equiv \int_{-\infty}^{\infty} X(f)e^{i2\pi ft} df$$

respectively, where  $t$  represents time,  $f$  represents frequency, and  $x(t)$  is the varying versus time signal.

It is shown by Fourier analysis that all reasonable (in a mathematical sense) waveforms can be represented mathematically as the summation of a number of sinusoidal waveforms, each with a specific amplitude and phase at its specific frequency [27]. Thus any waveform can be alternatively represented by a plot of amplitude versus frequency together with a plot of phase versus frequency. These plots are known as amplitude and phase spectra and provide a complementary way of representing the waveform, which more clearly reveals information about the frequency content of the waveform. They have a high value for the frequencies that are present to the waveform, and a low value for those frequencies that are not present in the waveform. The observed shapes of the spectra are often helpful in the understanding and interpretation of the waveforms. Amplitude and phase spectra often provide more useful information than the waveforms. The frequencies of the sinusoidal frequency components are harmonically related to each other, i.e. each is an integral multiple of the first harmonic frequency,  $f$ , where

$$f = 1/T_p$$

where  $T_p$  is the repetition period of the waveform.

In practice, the Fourier components of data are obtained by digital computation. A transform for use with discrete/sampled data, known as the discrete Fourier transform (DFT) is available, and is defined as follows [28]: Consider a finite sequence of numbers  $x_n = x_0, x_1, x_2, \dots, x_{N-1}$ . The DFT of this sequence is denoted by  $X_m = X_0, X_1, X_2, \dots, X_{N-1}$  and is defined by

$$X_m = \sum_{n=0}^{N-1} x_n e^{-i(2\pi/N)mn}, m = 0, 1, 2, \dots, N-1,$$

and the inverse DFT is defined by

$$x_n = 1/N \sum_{m=0}^{N-1} X_m e^{i(2\pi/N)nm}, n = 0, 1, 2, \dots, N-1.$$

The DFT  $X_m$  is the complex valued discrete density (scaled by  $N$ ) of sine wave components contained in the sequence  $x_n$ . The frequencies of the sine waves are  $0, 1/N, 2/N, \dots, (N-1)/N$ .

The inverse DFT is used to carry out transformation from the frequency to the time domain.

A large number of multiplications and additions are required for the calculation of the discrete Fourier transform. The fast Fourier transform (FFT) is an algorithm for computing this transform which eliminates most of the repeated complex multiplications in the Fourier transform, so its execution time is much shorter, in particular on large and/or multidimensional data. But in order to apply FFT, the signal must have a length equal to a power of 2, and thus zero padding or interpolation is necessary. When speed is not a problem, then discrete Fourier analysis is applied.

**Systems, models and transfer functions.** A *system* can be viewed as a "black box" where a signal is applied to its input, and a response results at its output. An example of such a system is the arterial system. To undertake an in-depth study of a system, it is very useful to have a *model* of the system, an assumed relationship among the signals. Models may be conceptual, physical or mathematical [29]. A *mathematical* (or *analytical*) model consists of a collection of equations describing the relationships between the signals appearing in the system, and it is usually an idealized representation of the system. The model should be simple, but also accurate. One way to develop a mathematical model is based on experimentation. Input and output signals from the system are recorded and subjected to data analysis in order to infer a model. One type of mathematical model is the transfer function, an input/output representation describing the relationship among the input and output signals of the system. The transfer function of a system can be determined from knowledge of the response  $y(t)$  to an input signal  $x(t)$ . It should be stressed that this result is valid only if the given system is (piecewise) linear. Thus, linearity is an important property of a system. In practice, a given nonlinear system is often approximated by a linear system so that analytical techniques for linear systems can be applied [30].

When a system with a transfer function  $H(f)$  is excited with an input signal that has a spectrum  $X(f)$ , the output of the system has the spectrum  $Y(f) = X(f)H(f)$ . The output signal is then determined from its spectrum via the inverse Fourier transform [31].

**Coherence.** The coherence between two signals is the degree of accuracy with which the two signals can be related to each other by a linear transformation. The coherence function expresses the amount of linear coupling between two signals in the frequency

domain. The coherence function can be viewed as the (frequency dependent) correlation coefficient between the input and output sequences. If this coefficient is 1 at a certain frequency, then there is perfect correlation between input and output at that frequency. There is consequently no noise interfering at that frequency [32].

The modulus or amplitude function (ratio between output and input signal) in the frequency domain is comparable to the regression coefficient in a linear regression equation in the time domain. If the explained variance in a linear regression is low there is a poor linear relationship between the two variables. In such a case the regression coefficient becomes unreliable and it is not worthwhile computing this coefficient. The same holds for the frequency domain, where if the coherence between two signals in a certain frequency region is low, the amplitude function becomes unreliable.

**Least-squares Method.** System identification is the process of determining the characteristics of the unknown system,  $H(f)$ , by a set of measurements performed on the system. The method of least-squares is a technique for performing system identification. In this method we postulate a model for the system and determine the parameters of the model that minimize, in the least-squares sense, the error between the actual system response and the response of the model.

**Resynthesis of a signal.** A transfer function derived from a model, as mentioned previously, can be used to resynthesize a signal,  $x_1$ , from another one,  $x_2$ . This procedure involves the following steps:

- 1/ The signal  $x_2$  is transformed into the frequency domain by use of a Fourier transform;
- 2/ With the use of the transfer function, the amplitude of each harmonic of the signal  $x_2$  is divided by the amplitude of the transfer function, and the phase of the transfer function is subtracted from the phase of the signal  $x_2$ ;
- 3/ this modified spectrum is transformed back into the time domain by use of an inverse Fourier transform.

**Practical Considerations.** Due to periodic nature of the pulsatile heart beat signals harmonics at the pulse rate are dominant. However, due to fluctuations in beat duration and pulse amplitude the side bands of the dominant harmonics are substantial, filling the intermediate harmonics. Using about 10 s epochs thus produces a finer spaced spectrum and improved signal-to-noise ratio, compared to single beat analysis.

There is no phase response fitted, since the fit program is free to change the relative delay between brachial and finger waveform due to pulse wave propagation to obtain least errors between the waveforms and thus the model does not correct for delay.

The phase shift between Fourier components depends on delay, causing a linear phase shift with frequency. The delay information is not considered relevant, since it can never be made up for in real-time.

## References

- [1] Idema RN, Van den Meiracker AH, Imholz BPM, Man in 't Veld AJ, Settels JJ, Ritsema van Eck HJ, and Schalekamp MADH. Comparison of Finapres non-invasive beat-to-beat finger blood pressure with intrabrachial artery pressure during and after bicycle ergometry. *Journal of Hypertension*, 7(suppl 6):S58-S59, 1989.
- [2] Imholz BPM, Van Montfrans GA, Settels JJ, Hoeven GMA, Karemaker JM, and Wieling W. Continuous non-invasive blood pressure monitoring: reliability of Finapres device during the valsalva manoeuvre. *Cardiovascular Research*, XXII(6):390-397, June 1988.
- [3] Imholz BPM, Settels JJ, Van den Meiracker AH, Wesseling KH, and Wieling W. Non-invasive continuous finger blood pressure measurement during orthostatic stress compared to intra-arterial pressure. *Cardiovascular Research*, 24:214-221, 1990.
- [4] Parati G, Casadei R, Gropelli A, Di Rienzo M, and Mancia G. Comparison of finger and intraarterial blood pressure monitoring in rest and during laboratory tests. *Hypertension*, 13:647-655, 1989.
- [5] Wesseling KH, Settels JJ, Van der Hoeven GMA, Nijboer JA, Butijn MWT, and Dorlas JC. Effects of peripheral vasoconstriction on the measurement of blood pressure in finger. *Cardiovasc. Res.*, 19:139-145, 1985.
- [6] Wieling W, ten Harkel ADJ, and van Lieshout JJ. Spectrum of orthostatic disorders: classification based on an analysis of the short-term circulatory responses upon standing. *Clin Sci*, 81:241-248, 1991.
- [7] Imholz BPM, Langewouters GJ, Van Montfrans GA, Parati G, Van Goudoever J, Wesseling KH, Wieling W, and Mancia G. Feasibility of ambulatory, continuous 24-hour finger arterial pressure recording. *Hypertension*, 21:65-73, 1993.
- [8] Peñáz J. Photoelectric measurement of blood pressure, volume and flow in the finger. In *Digest 10th Int. Conf. Med. Biol. End.*, Dresden, page 104, 1973.
- [9] Wesseling KH, de Wit B, van der Hoeven GMA, van Goudoever J, and Settels JJ. Physiological, calibrating finger vascular physiology for Finapres. *Homeostasis*, 36(2-3):67-82, 1995.
- [10] Molhoek GP, Wesseling KH, Settels JJ, Van Vollenhoven E, Weeda HWH, De Wit B, and Arntzenius AC. Evaluation of the Peñáz servo-plethysmo-manometer for the continuous and non-invasive measurement of finger blood pressure. *Basic Res Cardiol*, 79:598-609, 1984.



- [11] Smith NT, Wesseling KH, and De Wit B. Evaluation of two prototype devices producing noninvasive, pulsatile, calibrated blood pressure measurement from a finger. *Journal of Clinical Monitoring*, 1:17–29, 1987.
- [12] Bos WJW, Imholz BPM, Van Goudoever J, Wesseling KH, and Van Montfrans GA. The reliability of noninvasive continuous finger blood pressure measurement in patients with both hypertension and vascular disease. *Am. J. Hypertens.*, 5:529–535, 1992.
- [13] Rongen GA, Bos WJW, Lenders JWM, Van Montfrans GA, Van Lier HJJ, Van Goudoever J, Wesseling KH, and Thien T. Comparison of intrabrachial and finger blood pressure in healthy elderly volunteers. *Am. J. Hypertens.*, 8:237–248, 1995.
- [14] Karamanoglu M, O'Rourke MF, Avolio AP, and Kelly RP. An analysis of the relationship between central aortic and peripheral upper limb pressure waves in man. *European Heart Journal*, 14:160–167, 1993.
- [15] Van Montfrans GA, Van der Hoeven GMA, Karemaker JM, Wieling W, and Dunning AJ. Accuracy of auscultatory blood pressure measurement with a long cuff. *Br. Med. J.*, 295:354–355, 1987.
- [16] Gardner RM. Direct blood pressure measurements — dynamic response requirements. *Anesthesiology*, 54:227–236, 1981.
- [17] Kurki T, Smith NT, Head N, Dec-Silver H, and Quinn A. Noninvasive continuous blood pressure measurement from the finger: optimal measurement conditions and factors affecting reliability. *Journal of Clinical Monitoring*, 3:6–13, 1987.
- [18] Prentza A and Wesseling KH. Catheter–manometer system damped blood pressures detected by neural nets. *Medical and Biological Engineering and Computing*, 33:589–595, July 1995.
- [19] O'Rourke MF, Blazek JV, Morreels CL, and Krovetz LJ. Pressure wave transmission along the human aorta; changes with age and in arterial degenerative disease. *Circ. Res.*, 3:623–631, 1955.
- [20] Triedman JK and Saul JP. Comparison of intraarterial with continuous noninvasive blood pressure measurement in postoperative pediatric patients. *Journal of Clinical Monitoring*, 10:11–20, 1994.
- [21] Kelly R, Hayward C, Avolio A, and O'Rourke MF. Noninvasive determination of age-related changes in the human arterial pulses. *Circulation*, 80:1652–1659, 1989.
- [22] Settels JJ and Wesseling KH. FIN.A.PRES: Non-invasive finger arterial pressure registration. In Orlebeke JF, Mulder G, and van Doornen LJP, editors, *Psychophysiology of cardiovascular control. Models, Methods, and Data*, pages 267–283. Plenum, 1985.

- [23] Nichols WW and O'Rourke MF. *McDonald's Blood Flow in Arteries : theoretical, experimental and clinical principles*. Edward Arnold, London, third edition, 1990.
- [24] Gizdulich P, Imholz BPM, Van den Meiracker AH, Parati G, and Wesseling KH. Finapres tracking of systolic pressure and baroreflex sensitivity improved by waveform filtering. *Journal of Hypertension*, 14:243-250, 1996.
- [25] ANSI/AAMI SP 10-1992. *Association for the Advancement of Medical Instrumentation: Electronic or Automated Sphygmomanometers*. AAMI, Arlington, VA, 1992.
- [26] Bos WJW, Van Goudoever J, Van Montfrans GA, Van den Meiracker AH, and Wesseling KH. Reconstruction of brachial artery pressure from noninvasive finger pressure measurements. *Circulation*, 94(8):1870-1875, October 1996.
- [27] Oppenheim AV and Schafer RW. *Digital Signal Processing*. Englewood Cliffs : Prentice Hall, 1975.
- [28] Gardner WA. *Statistical Spectral Analysis, a nonprobabilistic theory*. Prentice Hall, New Jersey, 1988.
- [29] Eykhoff P. *System identification, parameter and state estimation*. John Wiley & Sons, 1974.
- [30] Kamen EW and Heck BS. *Fundamentals of Signals and Systems using Matlab*. Prentice Hall, New Jersey, 1997.
- [31] Proakis JG and Manolakis DG. *Introduction to digital signal processing*. Macmillan Publishing Company, 1988.
- [32] Ljung L. *System identification, theory for the user*. Prentice Hall, New Jersey, 1987.

# Chapter V

## Human age estimated from finger pressure waveforms

### 1 Human age estimated from finger pressure waveforms

*Andriana Prentza<sup>a</sup>, Willem Jan W Bos<sup>b</sup>, Gert A van Montfrans<sup>b</sup>, Wouter Wieling<sup>b</sup>, Karel H Wesseling<sup>a,c</sup>*

<sup>a</sup> Department of Electrical Engineering, Technical University Eindhoven, P O Box 513, 5600 MB Eindhoven, The Netherlands

<sup>b</sup> Department of Internal Medicine, Academic Medical Centre, Meibergdreef 9, 1105 AZ Amsterdam, The Netherlands

<sup>c</sup> TNO-TPD BioMedical Instrumentation, Academic Medical Centre, Suite L0-002, Meibergdreef 9, 1105 AZ Amsterdam, The Netherlands  
(submitted)

#### Abstract

**Objective:** To estimate a person's age from arterial pressure waveforms as a test of published aging waveform catalogs. **Methods:** The pressure waveforms of 106 subjects, recorded in earlier studies, were used. Aortic waveforms reconstructed from finger pressure were also tested. The group included healthy children, adults and elderly persons, (suspected borderline) hypertensives and subjects with additional cardiovascular disease. Measured under laboratory conditions in supine or semi-reclining position, employing a TNO Finapres, heart rates were between 49 and 99 BPM, and systolic, diastolic and pulse pressures between 83 and 239, 40 and 128, and 33 and 171 mmHg, respectively. The waveforms of 65 subjects aged 8 to 83 years formed the training selection, the waveforms of the other 41 subjects aged 9 to 75 years the test selection. Artificial neural networks of different layout estimated age. **Results:** Best results were obtained if the first 0.5 s of the once differentiated pressure pulse was presented to the neural net. Mean difference between estimated and calendar age in the test selection was -1 (SD 8) years and

the correlation coefficient was 0.92. There was no clear difference in accuracy between any of the healthy or patient groups, or between the use of finger or reconstructed aortic waveforms. **Conclusions:** An individual's age can be estimated from the finger arterial pressure waveform using an artificial neural net. However, some subjects with 'young' or 'old' waveforms for their age received a lower or higher estimated age. This suggests that an 'arterial' age was estimated which does not deviate far from calendar age.

## Keywords

Human age estimation, Finger pressure waveforms, Arterial waveform aging, Artificial neural nets, Reconstructed aortic pressure, Arterial age.

### 1.1 Introduction

Catalogs of human arterial pressure waveforms have been published [1] showing radial, carotid, and femoral waveforms averaged over a number of subjects per age decade (further called Kelly's catalogs). A clear change in the waveforms with increasing age is evident. We wondered if the reverse process of estimating a person's age from the arterial pulse would be possible on an individual person's basis. We call a person's true recorded age the 'calendar' age, and age estimated from an arterial waveform 'estimated' age. If such an estimate can be made to, say, within one year we consider that estimate perfect and would have demonstrated that cardiovascular aging is a process progressing linearly with calendar age, which process is precisely reflected in the arterial pressure pulse. If the estimate is essentially random either the age estimation technique is unsatisfactory or arterial aging is not present, and nothing has been demonstrated. If an age estimation technique would have an acceptable degree of imprecision but with clear outliers present, underlying causes for the outliers could be looked for. We could expect a subject's age to deviate from calendar age based on hypertension, vasoactive agents, or vascular disease since these factors might all affect the pressure pulse.

With the availability of Finapres [2, 3], the noninvasive measurement of arterial pressure waves in humans has become feasible from 6 years of age up. With increasing experience in finger pressure monitoring, we found that visual age estimation from the finger pressure waveform is possible and reasonably accurate. As a first approach, we tried a multiple regression prediction based on arterial systolic, diastolic, mean and pulse pressure levels and heart rate. This age estimation worked to some extent on the (train) selection of persons on which the pressures and multiple regression equations were obtained, but it did not work well on a different (test) selection. Thus, in view of Kelly's aging waveforms and the failure of the pressure level approach, we concluded that the principal information is not in the pressure levels with sufficient clarity. It could then only be present in the shape of the pressure wave.

Since we had good experience with the application of so-called "artificial neural networks" (neural nets) in detecting subtle differences in waveform [4], we decided to develop

**Table V.1:** *Statistics of common parameters. Age in years. Heart rate (HR) in beats per minute. Finger systolic, diastolic, mean and pulse pressures in mmHg. Note that heart rate ranges over a factor 2, blood pressure levels over a factor 3, pulse pressure over a factor 5.*

N(female/male)	All persons		Train selection		Test selection			
	Mean	Range	Mean	Range	Mean	Range		
106 (48 / 58)	46	8 - 83	65 (28 / 37)	47	8 - 83	41 (20 / 21)	45	9 - 75
	70	49 - 99		70	49 - 99		69	50 - 95
	153	83 - 239		154	89 - 239		152	83 - 221
	75	40 - 128		76	40 - 126		74	40 - 128
	100	53 - 164		101	53 - 164		98	53 - 162
	78	33 - 171		78	33 - 171		78	44 - 125

a neural net technique to estimate a person's age from finger arterial pressure waveforms.

## 1.2 Methods

### Subjects

Finger pressure waveforms from 106 persons, ranging in age from 8 to 83 years, were available from previous studies using Finapres. They spanned the range from healthy volunteers of various age ranges [5, 6, 7], to (borderline) hypertensive patients [8] with or without anti-hypertensive medication, to patients with additional arterial vascular disease [9], and were considered representative for the population on which finger arterial pressure measurements are used.

Study [5] provided the pressures of 17 healthy children aged 8 to 16 years. Study [6] provided 6 healthy volunteers, aged 28 to 40 years. Study [7] provided 14 healthy elderly subjects aged 72 to 83 years. Study [8] provided the pressures of 33 (suspectedly borderline) hypertensive patients aged 25 to 65 years. Study [9] provided 13 patients aged 52 to 79 years with vascular disease, of which 11 had therapy resistant hypertension. Finally, an unpublished study provided 23 healthy subjects aged 21 to 65 years whose waveforms were recorded to compare oscillometric, Riva-Rocci/Korotkoff and finger pressures (BP study). In this group, medication was not used on a regular basis.

The published studies requiring invasive instrumentation in volunteer subjects and patients were approved by the respective Ethics Committees, and all participants of the clinical studies had given their prior informed consent. The BP study involved only 15 min duration noninvasive blood pressure measurements in supine position for which nonsmoking medical doctors, medical trainees, nurses and medical physicists volunteered.

Table V.1 lists the principal subject characteristics.

The subjects were in a supine or semi-reclining position during the measurements. In the published studies all subjects except the children had an intrabrachial artery line. The children's recordings were taken before an intravenous line was inserted. All measurements were made in airconditioned rooms maintained at 22 degrees C. Except for the BP study which was carried out at arbitrary moments during the day, the measurements were made in the morning at least one hour after a light breakfast without coffee or tea. All subjects were asked to refrain from smoking and alcohol consumption for the 24 hours before the measurements began. The majority of the subjects were nonsmokers.

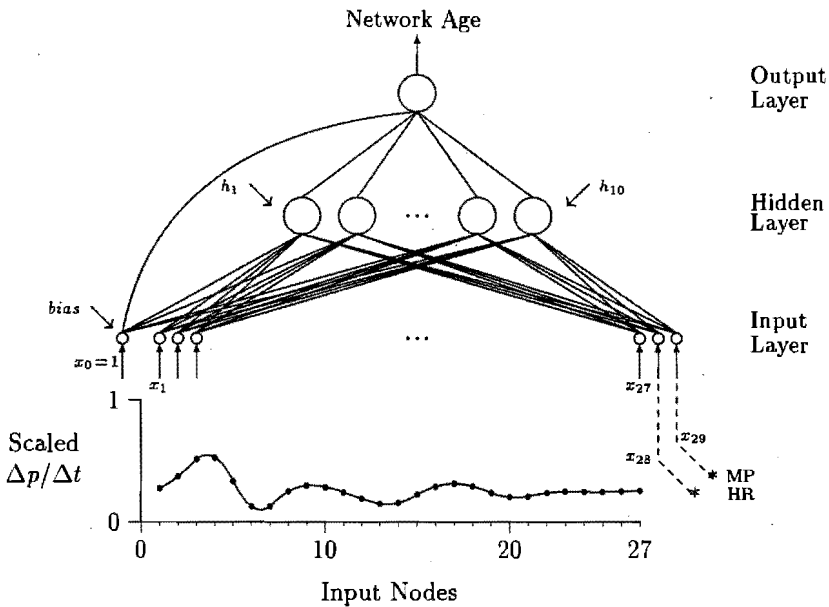


**Figure V.1:** Layout of neural net 3. The information flow is upwards. At the bottom is the input wave, which is a differentiated finger pressure pulse beginning just before the upstroke in the arterial pulse. The waveform is sampled at the dots and each sample value is fed to the input node just above it, 27 samples spanning 0.54 s in all. A bias value is added at the left, and heart rate and mean arterial pressure of the pulse are added at the right. The input samples are fed through line connections to the artificial neurons in the 'hidden layer' (hidden in the sense that they are not approached directly from the outside) multiplied by a numeric factor different in each line. The 10 hidden neurons increase their output when a certain threshold is exceeded. Their output is fed through similar line connections to one final neuron which, at its output at the top, presents a value proportional to age.

## Measurements

Finger arterial pressure was measured at the index or middle finger of the dominant arm with a TNO Finapres, model 4 or similar model 5. These devices are the non-commercial prototype of the Ohmeda Model 2300 Finapres. They measure blood pressure by means of the arterial volume clamp method of Peñáz [2, 3], and the Physiological criteria of Wesseling [10]. Waveform recording started when a stable finger pressure was obtained, usually after two or three minutes [11]. Finger pressure signals were recorded on a Hewlett-Packard (California, USA) Model 3964A FM Instrumentation Recorder and digitized off-line, or they were digitized on-line directly into a personal computer. In both situations sample rate was 100 Hz and sampling resolution was 0.25 mmHg. Epochs free from artifact, of about 10 s duration, were selected for each person to span at least one but usually two or three full respiratory cycles. Sections with arrhythmias were avoided.

## Neural nets

Artificial neural networks have a certain primitive similarity to networks of neurons. Several neural nets were investigated (see technical details in Appendix of this chapter). The artificial neural net giving best results in our study is shown in Fig. V.1. The signal to be analyzed, here the first derivative of a pressure pulse plus mean pressure and heart rate, is offered to the net on its 29 input nodes at the bottom. From there it passes through line connections, which implement multiplication factors or "weights", to artificial "neurons". Neurons sum their inputs and provide an output through a nonlinear threshold function. The threshold function is biased, and the bias can be optimized for best results. At the top of the neural net an output signal is generated by a final neuron representing an estimation of the person's age, which we rounded to the nearest year.

To use a network for age estimation, its weights and biases must be properly adjusted first. The process to do the adjustments is called "training". Training is done by presenting to the net a subset of the available persons' waveforms, observing the estimated age and comparing it with the labelled calendar age. Using the discrepancy, the weights and biases are adjusted until a better output is obtained. For these adjustments formalized (so-called back propagation) algorithms are available. The process is repeated until a certain (usually large) number of presentations, comparisons and adjustments has been done. Then, the network is "tested".

Testing is done by presenting to the net the remaining persons' waveforms, not used for training, and rating the net's performance. To quantitate performance we use the coefficient of correlation between calendar and estimated age. Training is continued on the train selection of persons and performance tested again on the test selection of persons until no further improvement on the test selection can be achieved. The test selection data is thus used only as a criterion to stop training on the train selection.

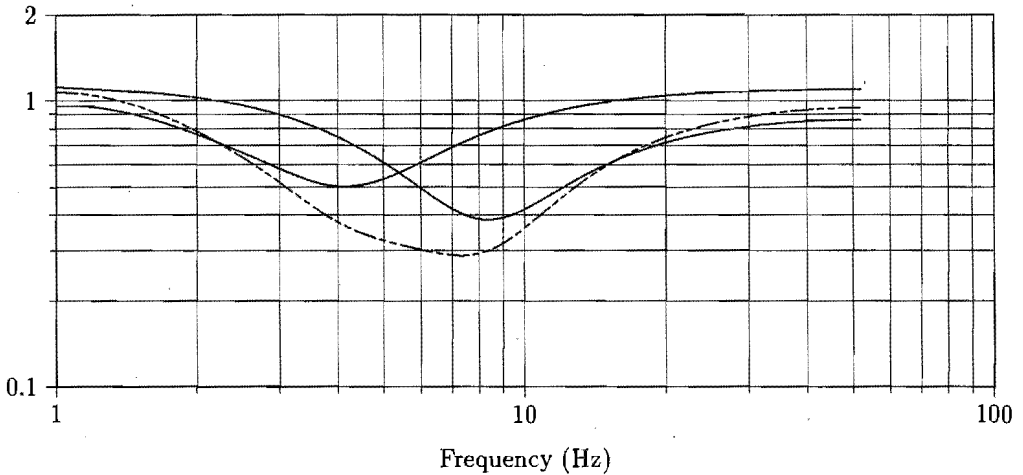


**Figure V.2:** Frequency responses of the filters used to transform finger to aortic waveforms. The filter response with the shallow dip near 8 Hz transforms from finger to brachial artery, the filter response dipping near 4 Hz transforms from brachial artery to aortic root. The deep dipping response (dashed line) is the combined response.

### Data processing

The selected blood pressure waveform epochs were segmented into beats using the BEAT-FAST program [12]. It identifies for each beat the instant of the beginning of the upstroke, the systolic, diastolic and mean pressure levels, pulse interval and heart rate. A total of 1282 beats were extracted, approximately 12 per subject. Each beat was labelled with the calendar age.

*Neural net 1:* Having hypothesized that the age information is in the waveform, we presented one entire arterial pulse to the neural net. Since an arterial pulsation of typically 1 s duration is represented by 100 samples, this leads to neural nets with a large number of inputs and thus weights. The greater the number of weights the more training is needed. It is thus advantageous to limit the number of data presented to a neural net. We based our data reduction on the frequency content of arterial waveforms. According to Frank [13], the highest frequency that is present in a 180 BPM human arterial pulse is 30 Hz, in a 100 BPM waveform (the highest recorded) not more than 15 Hz. According to the sampling theorem of Nyquist and Shannon, we can then limit the number of samples on a waveform to approximately 30, thus reducing the number of samples presented and the number of input nodes from 100 to 30 or by a factor 3. To allow for beats of long duration, the neural net could accept beats of maximally 1.8 s duration. The number of neurons in the hidden (middle) layer was varied. The best net had 25 neurons.

*Neural net 2:* The higher frequencies determine the fine pattern in the waveforms. They are small in amplitude and thus difficult to detect. It is possible to selectively em-



phasize the high frequency waveform components by differentiating the waveform. Sub-sampling this differentiated waveform by taking every other sample, reduced the number of inputs by a factor 2. By taking the derivative, only the pressure changes between consecutive sampled values are retained and information on mean pressure is lost. Mean pressure, therefore, is separately presented to the neural net. The maximal duration of beats was limited to 1.2 s, and 25 hidden neurons proved optimal.

*Neural net 3:* Finally, we reasoned that most of the waveform information is in the systolic portion since the diastolic portion simply approaches an exponential decay. Thus we took a fixed 540 ms portion of the initial part of the differentiated waveform and presented that, subsampled as before, to a third neural net having only 27 input nodes. In this case, both mean pressure and heart rate information are lost and therefore separately input to two further nodes, numbered 28 and 29 (Fig. V.1, bottom right). Ten hidden neurons gave the best age estimates.

### Reconstructed aortic waveforms

The arterial pulse is generated by the heart's pulsatile output into the aorta. The pulse is next passed through the arm arterial system to the finger, where we measure it. The peripheral arterial system behaves like a catheter-manometer system with a primary resonance frequency near 4 Hz [14, 15, 16]. Such a low frequency resonance distorts the peripheral pulse waveform which is why aortic and radial or finger pressure waveforms do not look alike. It was shown in recent years that aortic pulses can be reconstructed from radial ones [14, 16] and brachial pulses from finger ones [17]. We decided to use such filters, because they provide a clearer pressure wave to an observer, and for the same reason perhaps also to a neural net, by removing the resonances from the finger pulsations.

We reconstructed aortic from finger pulses in two stages. In a first stage, we used the model and filter published by Gizdulich et al. [17] to reconstruct brachial waves. The transformation from brachial to aortic waveforms is next done with an unpublished filter similar to that of Karamanoglu and colleagues [14]. The frequency response of our filters is shown in Fig. V.2. The finger to brachial filter amplifies frequencies to 2.5 Hz and attenuates above 2.5 Hz, with an antiresonance at 8 Hz. The brachial to aorta filter has an antiresonance at 4.2 Hz. Both filter responses return to near unity transfer at high frequencies. Their combined response is also shown in Fig. V.2. Aortic waveforms reconstructed from finger pressure waveforms were only used in differentiated form and applied to the third type neural net with 29 inputs.

### Composition of the train and the test selection

For training and testing, two subject selections were prepared from the pool of 106 subjects as shown in the age histograms of Fig. V.3. It appeared important to prevent the net from developing preferences for certain age ranges by providing it with an age-balanced train selection. Per decade, therefore, we selected persons randomly from the pool until an almost uniform age distribution was obtained (Fig. V.3b). In view of the number of

weights to be estimated the number of subjects in the train selection had to be maximized. The remaining persons were used as the test selection. The resulting test selection has a tri-modal distribution (Fig. V.3c) allowing testing of the neural nets at low, intermediate and high age. Thus, 65 persons are in the train selection and 41 in the test selection (Table V.1).

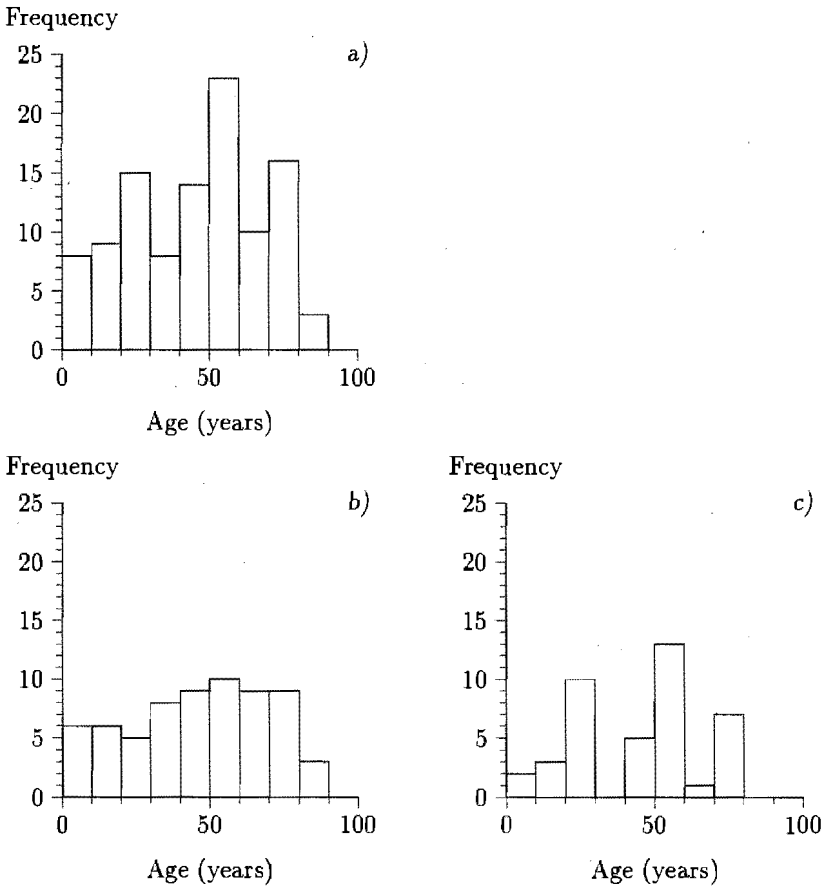


**Figure V.3:** Histograms of the distribution of subject age. The top panel (a) is the histogram of all 106 subjects. The bottom left panel (b) represents the train selection of 65 subjects, and the bottom right panel (c) the test selection of 41 subjects. It appeared important to train the neural nets with an equal number of subjects in each decade. The remaining test selection is tri-modal.

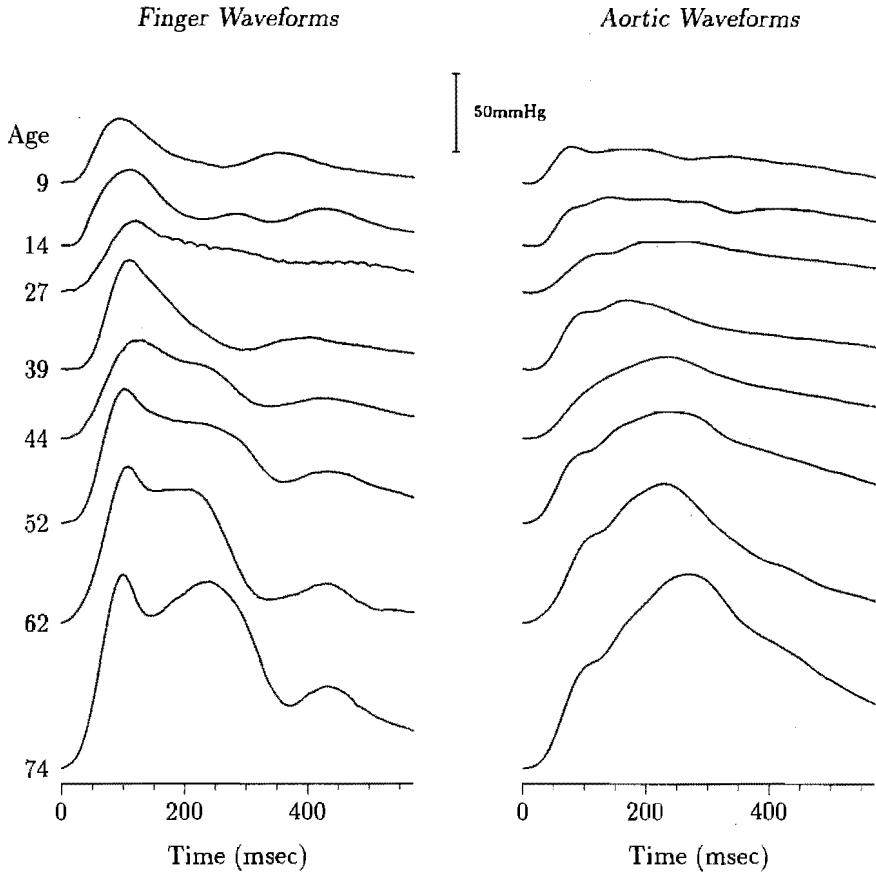


**Figure V.4:** A selection of finger and reconstructed aortic waveforms of eight subjects that received an estimated age identical to calendar age. It shows changes in the waveforms with age similar to those presented by Kelly et al., but presented here as individual, not group averaged per decade waveforms.

### Statistics

For each person the age estimates of the waveforms in a record were averaged. For the train and the test selection separately, each person's estimated age was plotted versus the calendar age and mean differences, standard deviations and correlations were computed and tested for significance. This was repeated for the three neural nets and the finger waveforms and for the third neural net and the reconstructed aorta waveforms.

We checked the significance of the correlation between the calendar age and the estimated age with Student's paired t-test. The accuracy of the age prediction is defined as the mean difference between the estimated age and the calendar age. The precision is defined as the standard deviation of that difference. Accuracies are compared using Student's paired t-test. Precisions are compared with Fisher's F-test for variance ratios. The estimated to calendar age differences grouped for the various studies were tested for significant differences by the Kruskal-Wallis one-way nonparametric and the parametric ANOVA. When both were significant, Peritz's F-test was used to compare results between the various studies. A  $P < 0.05$  is considered statistically significant.

**Table V.2:** Results of neural net age estimations. Age in years is given as mean (SD). All correlation coefficients between estimated and calendar age have  $P < 0.001$ , all differences from zero are not significant (at  $P = 0.05$ ).

	Train selection	Test selection
Calendar age	47 (22)	45 (20)
Neural net 1 age	47 (22)	44 (19)
Difference (Estim-Calend)	0 (4)	-1 (9)
Correlation coefficient	0.98	0.90
Neural net 2 age	47 (22)	44 (19)
Difference (Estim-Calend)	0 (3)	-2 (9)
Correlation coefficient	0.99	0.91
Neural net 3 age (finger)	47 (22)	44 (19)
Difference (Estim-Calend)	0 (5)	-1 (8)
Correlation coefficient	0.98	0.92
Neural net 3 age (aorta)	47 (21)	46 (19)
Difference (Estim-Calend)	0 (6)	0 (8)
Correlation coefficient	0.96	0.92

### 1.3 Results

Fig. V.4 presents typical pressure waveforms of subjects in which the age estimated on finger pressure by neural net 3 was identical to calendar age. The finger waveforms in the left panel show an initial high upstroke at all ages. The secondary systolic peak is low in relative amplitude for young, but high for older persons. The diastolic section is relatively uneventful with a broader and more pronounced early diastolic anacrotic wave in the young. The reconstructed aortic pulsations in the right panel show an initial systolic upstroke much less pronounced than in the finger waveforms. A late systolic

augmentation which follows advances in relative timing and increases amplitude with increasing age. An early diastolic anacrotic wave is seen only in young persons. A sharp dicrotic notch representing the high frequency components of aortic valve closure is not present in the reconstructed aortic waveform.

When these waveforms are compared with the ones in Kelly's catalogs, clearly, individual waveforms differ substantially from a group mean waveform in amplitude and shape although the general features can be recognized. The neural nets have the task of estimating age in the light of such inter-individual differences.

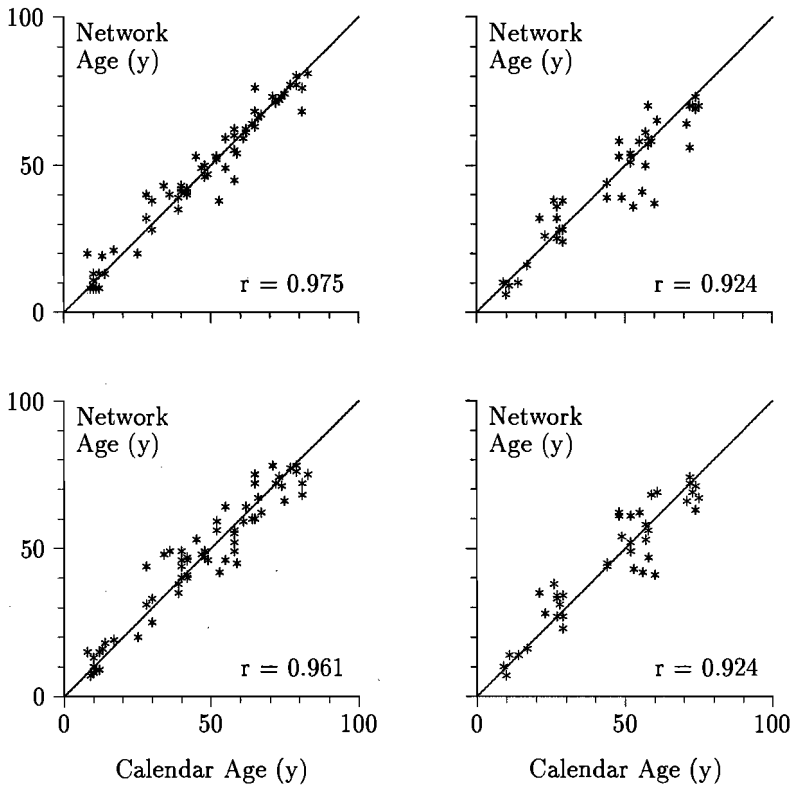


**Figure V.5:** Scattergrams of network estimated versus calendar age obtained with neural net 3. Each subject is represented by a star symbol. In the left panels the results obtained on the train selection, in the right panels the test selection. Top panels obtained for finger pressures, bottom panels for reconstructed aortic pressures. A line of identity is also shown.

### Performance of the neural nets

Table V.2 lists the results obtained with the three neural nets. Neural net 1 and 2 showed excellent performance on the train selection but their performance on the test selection degraded substantially. Neural net 3 showed a more balanced performance on the two selections. Mean error is not significantly different from zero (t-test) but the standard deviations for the finger waveforms only of both selections differ significantly (F-test).

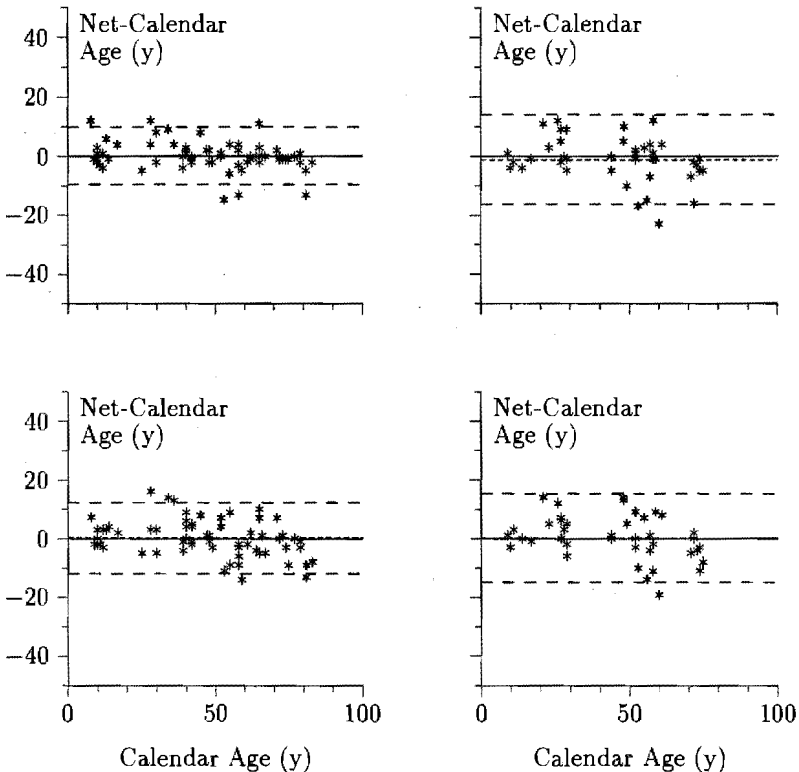


**Figure V.6:** Bland-Altman-like plots of the same estimated minus calendar age versus calendar age (not the usual mean of both ages). In the left panels are the results obtained on the train selection, in the right panels the test selection. Top panels for finger pressures, bottom panels for reconstructed aortic pressures. The dashes represent the 95% confidence limits. Mean error is almost zero.

Some persons had an estimated age lower, others higher than their calendar age. To check if finger and reconstructed aorta waveforms agreed on this deviation in direction and magnitude, we computed the correlation between the age differences of finger and aorta estimated age to calendar age. For the train and the test selection, respectively,

this correlation was 0.75 and 0.62. Expressed in terms of explained variance the waveforms agreed for 55 and 40% of the variance. Thus, approximately half of the variance is unexplained.

Fig. V.5 is a scattergram of the estimated versus the calendar ages for neural net 3. Fig. V.6 is a Bland-Altman-like diagram of this information, with calendar age on the horizontal axis. With the exception of one outlier, estimated age remains within 17 years of calendar age.

### Performance per subject group

In Fig. V.7 and Table V.3, we show the results of the age estimations per published study (see Methods) for the finger waveforms. The train and the test selections are pooled for this purpose. The healthy volunteers of study [6] received a relatively high estimated age and differed significantly from the healthy elderly group [7] whose ages were underestimated on average. No other between group difference was significant. A clear outlier is present in study [9]. This person in the test selection has a calendar age of 60 but an estimated age of only 37. His waveform and the waveform of a person with a calendar and an estimated age of 62 and 63, respectively, are plotted in Fig. V.8. By comparison, it appears that the outlier waveform is truly of a 'young' appearance, in terms of Kelly's catalogs, with virtual absence of a secondary late systolic peak. The subject (No 12 in Table 1 of [9]) is the only one from that group of patients with hypertension and cardiovascular disease who had normal intraarterial blood pressures (118/64 mmHg). He did not differ from the group in other aspects including vascular disease (ischemic cerebrovascular accident) and medication prescribed (ACE inhibitor, Calcium entry blocker, diuretic).

## 1.4 Discussion

We have automated the estimation of an individual's age from finger pressure waveforms recorded noninvasively with a Finapres device by training neural nets for the purpose. Age could be estimated with a standard deviation of approximately 8 years over an age range from 9 to 75 years (test selection) and without systematic error. Arterial pressure waveforms, therefore, clearly reflect subject age, even on an individual basis, even to a mathematical estimator. The accuracy of age estimation is not within one year and not random, but a definite and limited biological scatter between estimated and calendar age is present, including some apparent outliers.

### Generality of results

We consider this estimation procedure to be quite rugged and general, since we did not limit our selections to healthy, normotensive persons without the use of drugs. Healthy subjects and patients were both included. Heart rates varied over a 1:2 range, from 49 to 99 BPM, blood pressure levels ranged 1:3 and pulse pressures ranged 1:5. Female and male subjects were represented about equally (Table V.1). Drugs taken by some persons were

of the anti-hypertensive type and included ACE inhibitors, alpha-1 and beta blockers, Calcium entry blockers, diuretics, methyldopa and long acting nitrates [9], but did not have any apparent effect on the accuracy of the age estimation. No person complained of pain during the session. Arrhythmic beats were excluded from the waveform sets selected.

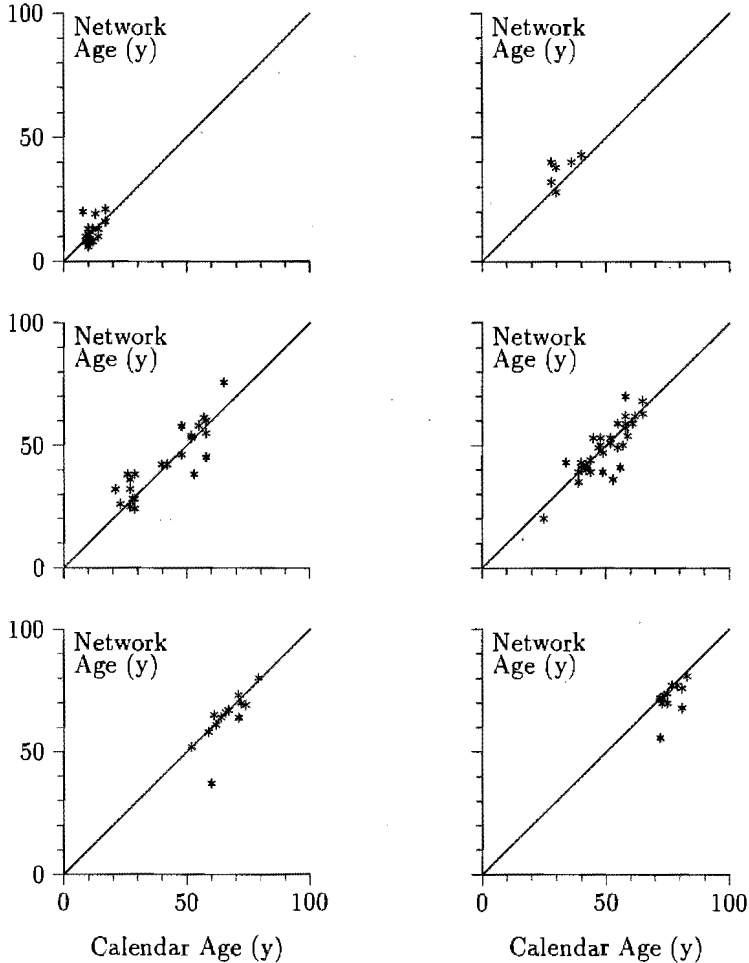


**Figure V.7:** Scattergrams for each of the subject groups of the published studies separately, and for the BP group. Subjects from the train and the test selection are combined. From left to right, from top to bottom are shown the subjects from De Jong et al [5], Idema et al [6], BP study, Van Montfrans et al [8], Bos et al [9], and Rongen et al [7].



However, all subjects were awake and resting and measurement conditions were standardized. It cannot be decided on the results presented that the estimation will work as well when measurement circumstances would differ substantially.

### Earlier efforts at age estimation with neural nets

Neural nets were used in an earlier study [18] to classify persons into three age categories: the third, fifth or seventh decade, based on radial artery plethysmographic (not pressure) waveforms. Persons were normotensive and five harmonics of the Fourier spectrum (not the time course) of the pulses were used as input. Into these age groups, separated by 20 years, 86% of the subjects were correctly classified. If we also accept a  $\pm 10$  year error limit, the present method correctly classifies 91% of the subjects in the train selection and 82% in the test selection. Thus, we obtained a similar score on a population with a wider range of blood pressures, heart rates, arterial condition and age.

### Comparison of finger and aorta waveforms

Results obtained with the neural nets on the finger and reconstructed aorta waveforms are not significantly different (Table V.2, bottom panels, and Fig. V.5 and V.6). Apparently, although the aorta waveforms tend to show a clearer picture to a human observer, the waveform resonances in the finger pressure do not confuse the properly trained neural net. The presence of the oscillations does not provide a better age estimation either.

Thus, the transmission of the pulse in the arm arteries to the finger provides no further clue to the age of a person. This is in agreement with the findings of Gizdulich et al. [17], that the model of pulse transmission from brachial to finger artery is not dependent on age. It also agrees with the observations of Karamonoglu et al. [14] and Chen [16] et al. that a single generalized filter may reconstruct the aortic pulse from the radial pulse for all adult ages.

### Causes for waveform changes with age

Young cardiovascularly healthy subjects typically show an aortic pressure waveform which is flat in systole and has a secondary anacrotic wave early in diastole (Fig. V.4, top right traces and more clearly in [1]). For older adults (Fig. V.4, bottom right traces), the secondary anacrotic wave moves forward in time with respect to the initial upstroke causing an aortic pressure with a late systolic augmentation and pressure falling after the incisura in an almost exponential fashion [19]. The secondary wave is a peripheral reflection of the primary systolic wave and its relative timing depends on the velocity with which pressure waves travel in the aorta and greater arteries. The amplitude of the reflected wave depends on the height of the peripheral resistance and on damping of the wave while travelling in the aorta.

With increasing age aortic wave velocity increases subsequent to stiffening of the aortic wall [19, 20]. A high velocity causes the reflected wave to already return early in systole

**Table V.3:** Age statistics per subgroup. Studies Idema: adult healthy, BP study: adult healthy, De Jong: healthy children, Van Montfrans: (suspected borderline) hypertensive, Bos: hypertension and cardiovascular disease, Rongen: aged healthy subjects.  $N$  is number of subjects in the group; mean difference between estimated and calendar age; variance ( $SD^2$ ) of difference. The groups are ordered according mean difference. The only significant difference ( $P < 0.05$ ) is between the top and the bottom group.

Study	N	mean dif	variance
Idema et al [6]	6	4.9	23
BP study	23	1.9	49
De Jong et al [5]	17	0.3	17
Van Montfrans et al [8]	33	-0.9	36
Bos et al [9]	13	-2.5	46
Rongen et al [7]	14	-3.6	24

thus modifying the systolic pulse in a way that is characteristic for the age of a subject [21].

According to Langewouters [22], aortic mechanical properties change almost exclusively with age. Although severe atherosclerosis compared to moderate tends to result in an aorta with slightly smaller Young's modulus of elasticity, this is compensated by a greater cross-section, resulting in equal compliance and no significant difference in wave velocity. Since lipid deposits and calcified plaques have little mechanical strength, certainly negligible compared to collagen fibers, this can be understood. Hypertension does not accelerate aortic aging [20]. Pulse wave velocity, however, linearly increases from an approximate 5 m/s at 30 to 14 m/s at 90 years of age.

### Vaso-active substances

In the past, it was demonstrated [23, 24, 25, 26, 27] that the administration of nitroglycerin, Calcium antagonists and ACE inhibitors affect pulsatility index, the amplitude of the reflected wave and systolic augmentation. This would have the effect of the pressure pulse looking 'younger' referring to Kelly's catalogs, and might affect age estimation. Some of our patients did indeed use these drugs [9], but the accuracy of their estimated ages did not degrade. Apparently, either the neural nets are not misled by such waveform changes or the waveform changes were only small. It is not known which information in the waveforms is used by the neural nets to estimate age, although the neural nets are exactly described in their algorithms. This is because of the large number of network weights and the nonlinear elements in the neurons, which make processing opaque. Our nets, having been trained with waveforms affected in some cases by vasoactive drugs but not in other cases, might have underemphasized the amplitude of the secondary wave or systolic augmentation and might have emphasized the relative timing of the secondary

wave with respect to the primary wave. This would explain the absence of a sensitivity for vasoactive drugs used.

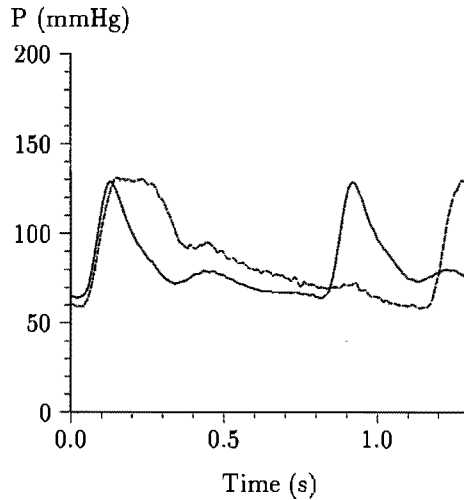


**Figure V.8:** *Finger blood pressure waveform of a 60 year old man with a 37 year young waveform (solid line) and of a 62 year old man with waveform corresponding to his age (dashed line). Note the low late systolic pulse amplitude typical for the young in the 60 year old subject.*

### The possible meaning of pressure pulse estimated age

The way we trained the neural nets was to estimate a subject's calendar age from a peripheral arterial pressure waveform. However, by looking at the arterial pressure waveforms of outlier subjects, it appears that our neural nets really estimate an 'arterial' age. If pulse shape is determined principally by aortic mechanical properties, as we argued and as supported in [28], an estimate of 'arterial' rather than calendar age is obtained. Arterial age, however, is probably determined principally by the calendar age of the subject, as suggested by the results of Langewouters [20] and others. In support of this finding argues that age was estimated with similar accuracy in young and old subjects, female or male, with or without hypertension, with or without cardiovascular disease, and with or without antihypertensive medication. Still, subjects with clearly 'young' waveforms for their age received a relative low age and vice versa. The causes of these differences in waveshape need to be determined.

The degree of certainty with which this deviating arterial age can be established depends on the inherent inaccuracies of this method. For the category of persons in this study, using finger pressure waveforms in combination with our neural net, we estimate

the inherent inaccuracy at  $\pm 5$  years. This is based on the correspondences and differences between finger and aortic estimated ages (Table V.2). We found that the difference between estimated and calendar age had a standard deviation between 5 and 8 years and thus a variance between 25 and 65. The finger and aorta trained neural nets agreed for approximately 50% of the variance leaving the other 50% unexplained. This results in an unexplained standard deviation of between 3 and 6 years, which we summarize to 5 years. A deviating arterial age is then detectable with 95% certainty when it differs more than 10 years from calendar age.

## 1.5 Conclusions

An artificial neural network can estimate the age of a person from the first derivative of its finger blood pressure waveform, mean pressure and heart rate. A large range of ages, blood pressures and resting heart rates, hypertension, vascular disease, and the use of vaso-active medication seem to pose no difficulty to the method. However, all subjects were measured under controlled circumstances, did not complain of pain, and arrhythmic beats were excluded from analysis. This work also confirms the conclusions of Avolio et al. [21], Kelly et al. [1] and O'Rourke et al. [28] of typical age-dependent changes in the arterial pulse, although it remains unknown exactly which aspects of the pressure waveforms are evaluated by the neural nets.

## 2 Is neural net estimated age stable during the 24 hour day?

### 2.1 Introduction

In the previous section, we trained neural nets to estimate subject age from 10 s epochs of finger arterial pressure waveforms. It appeared that neural nets could do this rather reliably on the basis of finger or reconstructed aorta waveforms. However, some subjects were outliers in the sense that they had too high or too low estimated age compared to their calendar age. We speculated that such deviations had to do with so-called 'arterial age', *ad hoc* defined as the speed with which the aorta – principally – aged. At the same time, we realized that certain vasoactive drugs such as nitroglycerin can alter the pressure and the waveform in the aorta and, subsequently, in the finger. It is possible that such changes in blood pressure and waveform affect the neural net estimated age, although

evidence in our subject base suggested that this was not the case.

During the 24 hour day blood pressure levels and pulse waveform change due to bouts of exercise or due to siesta or sleep. We had available the 24 hour waveforms of 24 subjects, which included 8 normotensive volunteer subjects and 16 hypertensive patients recorded partially at the Academic Medical Centre of the University of Amsterdam and at the University Hospital of Milan, Italy [29]. The patient recordings were performed with the simultaneous purpose to establish a proper blood pressure diagnosis and to compare noninvasive finger pressure with intrabrachial artery pressure during the 24 hour day, and were thus made with great care. During all recording sessions a strict protocol was followed with planned and well-timed activities and rest periods. These recordings seemed an ideal base to investigate the question of circadian stability of neural net estimated age.

**Table V.4:** *Group statistics. Age in years, heart rate (HR) in beats per minute, systolic, mean, diastolic and pulse pressures in mmHg.*

	Mean	Range
Age	36	19 – 58
HR	75	52 – 105
Systolic	137	109 – 172
Diastolic	74	55 – 102
Mean	93	70 – 129
Pulse	62	45 – 81

## 2.2 Methods

### Subjects

Of the 24 subjects of the study [29] two could not be used due to large periods of missing data for various instrumental reasons. Of the remaining 22 subjects we selected, simply to reduce the amount of work, at random 5 normotensive volunteers aged 19 to 32 years, and 7 hypertensive patients aged 20 to 58 years. Of the hypertensive patients selected one received anti-hypertensive combination therapy, the other received monotherapy, but treatment was discontinued at least two weeks before the measurement. Compared to our original database this represents a narrow age range and a small number but our first aim was to investigate stability of the age estimation. The original study was approved by the ethical committees at both hospitals and prior informed consent was obtained from all volunteer subjects and patients. Table V.4 lists some of their principal characteristics.

Subjects were hospitalized during the recordings but were free to engage in the usual activities of in-patients not confined to bed. Recordings started at 13:00 hrs. An afternoon siesta was taken from 14:00 to 15:30 hrs, followed by 30 minutes of recreative cycling on

**Table V.5:** Calendar age (Age) and neural net estimated age using finger pressure waveforms each half hour averaged during the 24 hour (24h), the day (day), the night (nit), the morning (mor), and during the siesta (sie), and their differences, D24h (Age-24h), Dday (Age-day), Dnit (Age-nit), Dmor (Age-mor), and Dsie (Age-sie).

Nr	Age	24h	day	nit	mor	sie	D24h	Dday	Dnit	Dmor	Dsie
1	41	55	56	54	63	61	14	15	13	22	20
2	58	47	45	51	42	50	-11	-13	-7	-16	-8
3	43	38	36	43	29	49	-5	-7	0	-14	6
4	42	37	36	39	31	40	-5	-6	-3	-11	-2
5	55	44	45	44	43	37	-11	-10	-11	-12	-18
6	32	25	25	26	27	29	-7	-7	-6	-5	-3
7	19	33	33	33	37	32	14	14	14	18	13
8	22	18	18	19	15	18	-4	-4	-3	-7	-4
9	26	26	28	22	32	26	0	2	-4	6	0
10	21	34	35	32	34	36	13	14	11	13	15
11	20	30	33	23	34	39	10	13	3	14	19
12	51	44	42	47	46	51	-7	-9	-4	-5	0
Mean	36	36	36	36	36	39	0	0	0	0	3
SD	14	10	10	12	12	12	10	11	8	14	12

a bicycle ergometer set to 50 W at 50 to 60 RPM. The subjects stayed in bed from 22:00 to 06:00 hours. Two periods of outside walk were scheduled in the morning from 10:00 to 10:30 and from 11:00 to 11:30 hrs.

### Measurements

Pressures were recorded with a combination of noninvasive finger arterial pressure with Portapres and intrabrachial artery pressures with an Oxford device. Portapres is the portable, battery operated version of Finapres. It has an internal 4-channel analog tape recorder of which one channel was used for flutter compensation, one for recording hydrostatic height and two channels for recording finger and brachial pressures. For the present analysis we only used the finger pressure tracings. After every 30 min the recording of finger pressure was switched from one finger to a neighboring finger of the same hand to avoid discomfort and to relieve venous congestion of the finger tip. The hand was protected from the environment when walking outside in the cold. The arm was carried in a mitella to avoid undue movements of the measurement arm, although a hydrostatic height correction system was in place to measure and compensate for such height changes as are caused by hand movements. At regular times during the recording the quality of

the blood pressure signals was inspected.

**Table V.6:** *Calendar age and neural net estimated age using reconstructed aorta pressure waveforms, and their differences.*

Nr	Age	24h	day	nit	mor	sie	D24h	Dday	Dnit	Dmor	Dsie
1	41	54	56	50	61	61	13	15	9	20	20
2	58	51	48	55	48	47	-7	-10	-3	-10	-11
3	43	37	36	37	30	49	-6	-7	-6	-13	6
4	42	40	39	41	35	46	-2	-3	-1	-7	4
5	55	48	49	47	45	38	-7	-6	-8	-10	-17
6	32	25	26	22	26	29	-7	-6	-10	-6	-3
7	19	26	27	24	27	23	7	8	5	8	4
8	22	18	20	14	16	21	-4	-2	-8	-6	-1
9	26	24	27	19	22	26	-2	1	-7	-4	0
10	21	29	29	29	28	32	8	8	8	7	11
11	20	28	30	23	34	33	8	10	3	14	13
12	51	57	56	59	61	60	6	5	8	10	9
Mean	36	36	37	35	36	39	1	1	-1	0	3
SD	14	13	12	15	15	14	7	8	7	11	10

## Data processing

Epochs of 10 seconds of good quality recordings were extracted each half hour, free from arrhythmias and artifact. This resulted in 48 epochs per subject.

The finger pressures were filtered to aortic waveforms as before and finger and reconstructed aortic waveforms were segmented into beats using the BEATFAST program [12]. Their first derivative waveform was computed and the first 540ms of each beat together with heart rate and mean pressure were presented to the already trained finger and aorta neural nets described in the previous section. For the beats of each epoch a mean age was computed and used for evaluation.

## Statistics

For each person the 48 age estimates for each waveform type were averaged over the 24 hour period and compared to calendar age. This process was additionally carried out separately for the day from 13:00 to 22:00 hrs and from 06:00 to 13:00 hrs of the next day, for the night from 22:00 to 06:00 hrs, for the morning from 06:00 to 10:00 hrs, and for the siesta from 14:00 to 15:30 hrs. Estimated ages for the various periods were compared

to calendar age and to the 24 hour average estimated age using a two-way ANOVA. The morning period was separately considered since in these hours a disproportionately large number of cardiovascular accidents occur in a population which might be due to waveform and blood pressure level changes.

Significance of the correlation between the calendar age and the estimated mean ages were checked with Student's paired t-test.

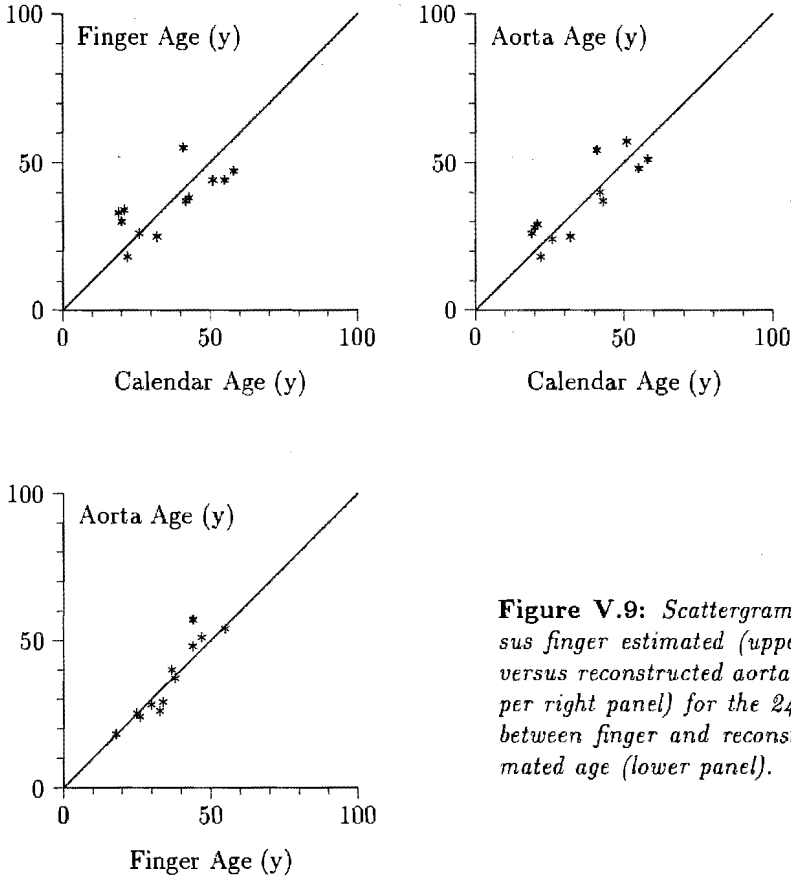


**Figure V.9:** Scattergrams of calendar versus finger estimated (upper left panel), and versus reconstructed aorta estimate age (upper right panel) for the 24 hour period, and between finger and reconstructed aorta estimated age (lower panel).

### 2.3 Results

In Table V.5 we present the estimated ages per subject for the various periods using finger pressure and the finger pressure neural net. Mean differences between calendar age and estimated age remain within one year except for the siesta period when the estimated age



is three higher than calendar age. This difference is not significant. In fact, a two-way ANOVA reveals no significant differences between columns.

Table V.6 lists similar data for the ages estimated from reconstructed aorta waveforms and the aorta neural net. Again, no difference between columns is significant.

Table V.7 presents all the correlations between calendar age and neural net estimated ages for the various periods. The correlation between morning and calendar age for the finger pressure is the only non significant one. Generally, correlations are higher for reconstructed aorta than for finger pressures. Correlations between estimated ages for the various periods are much higher than between any estimated and calendar age. In other words, the neural net estimated ages are consistently higher or lower than calendar age, regardless the period they were taken from.

This is further exemplified by Fig. V.9 which shows in three panels the scattergrams of calendar versus finger estimated, and versus reconstructed aorta estimated age for the 24 hour period, and between finger and reconstructed aorta estimated age. The latter has the highest correlation of 0.93, compared to 0.73 for the first and 0.86 for the second comparison.

**Table V.7:** Correlation coefficients between calendar age (*Age*) and neural net estimated age during the 24h, the day, the night (*nit*), the morning (*mor*), and the siesta (*sie*). The lower left triangle numbers are for finger, the upper right triangle for reconstructed aorta pressure waveforms.

	age	24h	day	nit	mor	sie
age		.86	.83	.89	.72	.73
24h	.73		.99	.99	.96	.91
day	.66	.99		.96	.97	.90
nit	.82	.96	.91		.92	.89
mor	.48	.90	.94	.78		.88
sie	.63	.92	.89	.89	.81	
	age	24h	day	nit	mor	sie

## 2.4 Discussion

We took samples of the finger pressure waveforms of 12 subjects every half hour during the 24 hours they were recorded with Portapres for another purpose. The subjects differed from the selection in the previous study. The techniques used were the same as in the previous study for the best neural net (neural net 3), but the neural nets were not retrained. Yet the results were comparable. This suggests once more the robustness of the neural net and its ability to generalize, as often claimed in the literature [30] and as mentioned in section 1 of chapter II of this thesis.

We averaged the resultant age estimates obtained each half hour over various periods during the day and over the full 24 hours. We were not able to demonstrate any significant differences in the estimated ages over any period, and no significant difference was found between estimated and calendar age. More importantly, differences in estimated age between periods of the day were much smaller than between the subjects. This is remarkable since substantial day-night changes in blood pressure and rest-exercise changes in heart rate and cardiac output were present.

## **2.5 Conclusions**

It appears that neural nets estimate an age, which we suggested to call 'arterial' age, quite independent from the state the subject is in. We could thus not refute the concept suggested in the previous section that neural nets indeed estimate a subject's arterial age, even though the exact meaning of this concept is not entirely clear. This arterial age may deviate (moderately) from calendar age and the deviation remains nearly constant during a 24 hour day under the conditions of this study.

## Appendix

**Neural nets.** MATLAB Neural Network Toolbox (The MathWorks, Massachusetts, MA) was selected, as a development tool for the neural nets of the age estimation study.

*Neural net 1* (see section 1.2, chapter V) : these neural nets consisted of a 60 node input layer for the variable length beats. The input values were normalized to a range of 0.05–0.95 (which corresponds to the 40–300 mmHg range). The normalized values were placed in the beginning of a 60 element array and unused places for any particular heart beat were filled with minimal values.

*Neural net 2* (see section 1.2, chapter V) : these neural nets also consisted of a 60 node input layer. The input values (samples of the derivative waveforms) were normalized to the range 0.05–0.95 (which corresponds to the -1400 – 4600 mmHg/sec range). The number of derivative values per beat was variable and a 60 elements array was used. The empty positions were set to 0.05. Mean Pressure (also included as input to the net) was normalized to the range 0.05–0.95 (corresponding to the 40–300 mmHg).

*Neural net 3* (see section 1.2, chapter V) : The fixed length derivative waveform was presented to 27 nodes. Both heart rate and mean pressure (also included as input to the net) were normalized to the range 0.05–0.95, – corresponding to 40–300 beats/min and to 40–300mmHg, respectively.

All neural nets were fully connected, i.e. all connections were present with finite weights. For initialization of the weights and biases, Nguyen and Widrow initial conditions (described in section 4.2 of chapter II) were used. The backpropagation algorithm was used to train the neural nets with momentum and adaptive learning rate (details in section 4.2 of chapter II). The sigmoid nonlinear function was used in the intermediate and output layers.

## References

- [1] Kelly R, Hayward C, Avolio A, and O'Rourke MF. Noninvasive determination of age-related changes in the human arterial pulses. *Circulation*, 80:1652–1659, 1989.
- [2] Peñáz J. Photoelectric measurement of blood pressure, volume and flow in the finger. In *Digest 10th Int. Conf. Med. Biol. End.*, Dresden, page 104, 1973.
- [3] Wesseling KH, de Wit B, Settels JJ, and Klawer WH. On the indirect registration of finger blood pressure after Peñáz. *Funkt. Biol. Med.*, 1:245–250, 1982.
- [4] Prentza A and Wesseling KH. Catheter–manometer system damped blood pressures detected by neural nets. *Medical and Biological Engineering and Computing*, 33:589–595, July 1995.

- [5] De Jong-De Vos van Steenwijk CCE, Wieling W, Johannes JM, Harms MP, Kuis W, and Wesseling KH. Incidence and hemodynamic characteristics of near-fainting in healthy 6- to 16-year old subjects. *J. Am. Coll. Cardiol.*, 25(7):1615-1621, 1995.
- [6] Idema RN, Van den Meiracker AH, Imholz BPM, Man in 't Veld AJ, Settels JJ, Ritsema van Eck HJ, and Schalekamp MADH. Comparison of Finapres non-invasive beat-to-beat finger blood pressure with intrabrachial artery pressure during and after bicycle ergometry. *Journal of Hypertension*, 7(suppl 6):S58-S59, 1989.
- [7] Rongen GA, Bos WJW, Lenders JWM, Van Montfrans GA, Van Lier HJJ, Van Goudoever J, Wesseling KH, and Thien T. Comparison of intrabrachial and finger blood pressure in healthy elderly volunteers. *Am. J. Hypertens.*, 8:237-248, 1995.
- [8] Van Montfrans GA, Van der Hoeven GMA, Karemaker JM, Wieling W, and Dunning AJ. Accuracy of auscultatory blood pressure measurement with a long cuff. *Br. Med. J.*, 295:354-355, 1987.
- [9] Bos WJW, Imholz BPM, Van Goudoever J, Wesseling KH, and Van Montfrans GA. The reliability of noninvasive continuous finger blood pressure measurement in patients with both hypertension and vascular disease. *Am. J. Hypertens.*, 5:529-535, 1992.
- [10] Wesseling KH, de Wit B, van der Hoeven GMA, van Goudoever J, and Settels JJ. Physiological, calibrating finger vascular physiology for Finapres. *Homeostasis*, 36(2-3):67-82, 1995.
- [11] Wesseling KH. Finger arterial pressure measurement with Finapres. *Z Kardiol.*, 85(Suppl 3):38-44, 1996.
- [12] Wesseling KH. *FAST system User Manual*. TNO-Biomedical Instrumentation, Academic Medical Centre, Amsterdam, The Netherlands, 1993.
- [13] Frank O. Kritik der elastischen Manometer. *Z. Biol.*, 44:445-613, 1903.
- [14] Karamanoglu M, O'Rourke MF, Avolio AP, and Kelly RP. An analysis of the relationship between central aortic and peripheral upper limb pressure waves in man. *European Heart Journal*, 14:160-167, 1993.
- [15] Gizdulich P and Wesseling KH. Reconstruction of brachial arterial pulsation from finger arterial pulsation. In *Proceedings of the 12Th International Conference of the IEEE Engineering in Medicine and Biology Society*, volume 12(3), pages 1046-1047, 1990.
- [16] Chen CH, Nevo E, Fetis B, Pak PH, Yin FCP, Maughan LW, and Kass DA. Estimation of central aortic pressure waveform by mathematical transformation of radial tonometry pressure; validation of generalized transfer function. *Circulation*, 95:1827-1836, 1997.

- [17] Gizdulich P, Prentza A, and Wesseling KH. Models of brachial to finger pulse wave distortion and pressure decrement. *Cardiovascular Research*, 33:698–705, March 1997.
- [18] Passoni LI, Fritschy J, Introzzi A, and Clara F. Clustering algorithms as classifiers of blood pressure recordings. In Power H and Hart RT, editors, *Third International Conference on Computer Simulations in Biomedicine - BIOMED 95*, pages 513–520. Wessex Institute of Technology, UK, Computational Mechanics Publications, 21-23 June 1995.
- [19] Nichols WW and O'Rourke MF. *McDonald's Blood Flow in Arteries : theoretical, experimental and clinical principles*. Edward Arnold, London, third edition, 1990.
- [20] Langewouters GJ, Wesseling KH, and Goedhard WJA. The static elastic properties of 45 human thoracic and 20 abdominal aortas in vitro and the parameters of a new model. *Journal of Biomechanics*, 17:425–435, 1984.
- [21] Avolio A. Ageing and wave reflection. *Journal of Hypertension*, 10(suppl 6):S83–S86, 1992.
- [22] Langewouters GJ. *Visco-elasticity of the human aorta in vitro in relation to pressure and age*. PhD thesis, Free University, Amsterdam, The Netherlands, 1982.
- [23] Yaginuma T, Avolio A, O'Rourke M, Nichols WW, Morgan JJ, Roy P, Baron D, Branson J, and Feneley M. Effect of glyceryl trinitrate on peripheral arteries alters left ventricular hydraulic load in man. *Cardiovascular Research*, 20:153–160, 1986.
- [24] London GM, Pannier B, Guerrin AP, Marchais SJ, Safar ME, and Cuche JL. Cardiac hypertrophy, aortic compliance, peripheral resistance, and wave reflection in end stage renal disease; comparative effects of ACE inhibition and Calcium Channel Blockade. *Circulation*, 90:2786–2796, 1994.
- [25] Chen CH, Ting CT, Lin SJ, Hsu TL, Yin FCP, Siu CO, and et al. Different effects of fosinopril and atenolol on wave reflections in hypertensive patients. *Hypertension*, 25:1034–1041, 1995.
- [26] Ting CT, Chen JW, Chang MS, and Yin FCP. Arterial hemodynamics in human hypertension; effects of calcium channel antagonist nifedipine. *Hypertension*, 25:1326–1332, 1995.
- [27] Ting CT, Yang TM, Chen JW, Chang MS, and Yin FCP. Arterial hemodynamics in human hypertension; effects of angiotensin converting enzyme inhibition. *Hypertension*, 22:839–846, 1993.
- [28] O'Rourke MF, Blazek JV, Morreels CL, and Krovetz LJ. Pressure wave transmission along the human aorta - changes with age and in arterial degenerative disease. *Circulation Research*, XXIII:567–579, October 1968.

- [29] Imholz BPM, Langewouters GJ, Van Montfrans GA, Parati G, Van Goudoever J, Wesseling KH, Wieling W, and Mancia G. Feasibility of ambulatory, continuous 24-hour finger arterial pressure recording. *Hypertension*, 21:65–73, 1993.
- [30] Maren A, Harston C, and Pap R. *Handbook of neural computing applications*. Academic Press, London, 1990.

# Summary

The objective of this thesis is to assess qualities of arterial pressure waveforms using spectral analysis and artificial neural networks. We investigated such diverse aspects as instrumental waveform damping, physiological distortion of peripheral arterial pressure waveforms, and the estimation of human age from arterial pressure pulsations.

**Damping.** Catheter-manometer systems are routinely used to measure intra-arterial pressure. During blood pressure monitoring, instrumental waveform damping often develops very gradually over time. It affects the form of the arterial pulse recorded, its upper—systolic—pressure level, as well as other derived parameters such as computed stroke volume. Thus monitoring a patient may become compromised without warning. In *Chapter III.1*, we tried to provide an early warning of the development of instrumental waveform damping before damping affects monitoring quality to a clinically significant degree. Artificial neural networks of varying architecture have been developed to detect degradation in dynamic performance. The networks were trained by the back propagation algorithm on sets of brachial arterial pressure waveforms obtained from a group of normotensive or (borderline) hypertensive subjects. For each patient and category 5–10 waves were available. A second order digital simulation of a catheter-manometer system was used to cause a known amount of waveform damping, varying from slight to moderate. Each beat in the waveforms was represented by an 11 parameter vector representing various pressure levels, instants of events and rates of change on the waveforms. The best design neural nets correctly classified about 75–85% of the individual beats as either adequate or damped. Using a single majority vote classification per subject per damped or adequate situation, the best neural nets correctly classify at least 16 of the 18 situations in nine test subjects (binomial  $P=0.001$ ). More importantly, these neural nets detected damping before clinically relevant parameters such as systolic pressure and computed stroke volume were reduced by more than 2%. Neural nets seem remarkably well adapted to solving such subtle problems as detecting slight damping of arterial pressure waves before it affects waveforms to a clinically relevant degree. The best neural nets do this reliably, continuously, and easily in real time.

In *Chapter III.2*, we demonstrate the feasibility of neural nets to classify catheter-manometer system arterial pressure waveforms to adequate and damped even during physical exercise when large increases in blood pressure and heart rate occur. Physical exercise is used, for example, in the revalidation of heart patients where adequate monitoring of ECG and blood pressure is necessary.

In *Chapter III.3*, finally, we compare the performance of experts and neural nets in detecting waveform damping. It appears that neural nets easily outperform human experts. Human expert observers detected only quite severely damped waveforms. However, since

slight damping already causes significant degradation of systolic pressure and stroke volume computation accuracy, human experts are too slow. This does not take into account that it can hardly be asked of an expert to perform the dull task of detecting damping, and in addition quickly retires from such repetitive tasks. We conclude that the developed neural nets could prove useful clinically.

**Physiological distortion.** Brachial artery pressure is used for diagnosis in the practice of internal medicine and cardiology. Recently, Finapres has become a well-accepted method to measure arterial pressure continuously in a noninvasive manner. However, blood pressure levels and pulse measured at the finger differ from those measured intra-brachially. We applied Fourier analysis and modelled the brachial to finger pulse wave distortion and pressure decrement (*Chapter IV*). Brachial artery pressure was recorded intra-arterially and simultaneous finger pressure was recorded non-invasively by Finapres in 53 adult human subjects. Mean pressure was subtracted from each pressure waveform and Fourier analysis applied to the pulsations. A distortion model was estimated for each subject and averaged over the group. This average inverse model was applied to the full finger pressure waveform to correct the distortion. The remaining pressure level difference was modelled by multiple regression on finger systolic and diastolic levels. It appeared that waveform distortion could be described by a general, frequency dependent model having a resonance at 7.3 Hz. The general inverse model has an anti-resonance at this frequency. It converts finger to brachial pulsations, thereby reducing average waveform distortion from 9.7 (s.d. 3.2) mmHg per sample for the finger pulse to 3.7 (1.7) mmHg for the converted pulse. Systolic and diastolic level differences between finger and brachial arterial pressures changed from -4 (15) and -8 (11) to +8 (14) and +8 (12) mmHg, respectively, after inverse waveform modelling, with pulse pressures correct on average. The pressure decrement model next reduced both the mean and the standard deviation of systolic and diastolic level differences to 0 (13) and 0 (8) mmHg. Diastolic differences were reduced most. Thus, we are able to reconstruct brachial pulse waveforms from finger waveforms that closely resemble invasive intrabrachial blood pressure registrations, satisfying a clinical need.

**Age estimation.** During life, the shape of the arterial pulse shows characteristic changes, and catalogs have been formed showing group mean arterial pulsations per age-decade. These changes differ between central and peripheral waveforms. We investigated if the inverse process of estimating age from the pressure pulse was also possible. We further required this to be done on an individual, not a group mean, basis. We trained multilayer perceptron artificial neural networks with the back propagation algorithm to develop age estimator models. We used the pressure waveforms of 65 subjects aged 8 to 83 years of varying clinical condition (*Chapter V.1*). Once trained, the network's performance was tested on the waveforms of another 41 subjects aged 9 to 75 years. Patients were measured under laboratory conditions in supine or semi-reclining position. Blood pressure was recorded employing a TNO Model 4 or 5 Finapres on the dominant hand. Most of



the adult subjects had arterial invasive instrumentation. Best results were obtained if the first 0.5 s of the once differentiated pressure pulse was presented to the neural net. Differences between estimated and calendar age for the subjects in the test selection were  $-1$  (SD 8) years on average and correlation between estimated and calendar age was 0.92. Seven of the 41 test subjects had an estimated age differing more than 10 years from calendar age. A large range of ages, blood pressures and resting heart rates, the presence of hypertension and vascular disease, and the use of vaso-active drugs seemed to pose no difficulty to the method. There was little difference in accuracy between any of the healthy and patient groups. Thus, the changes in the waveform during the aging process could be attributed largely to the age of a subject, but not entirely. Some subjects appear to have young waveforms for their age and some appear with rather older waveforms. This differentiation seems absent below 30 years of age.

Blood pressure waveforms and levels differ substantially during the day and the night. If we estimated age, the network age should be constant during the 24 hour day. In *Chapter V.2*, we investigate the diurnal stability of the estimated age. The 24 hour recording of blood pressure with a TNO Model 1 Portapres device took place during a strict protocol including well timed bouts of exercise, walking outside the hospital, siesta and sleep. We were not able to demonstrate any significant differences in the estimated ages over any period, and no significant difference was found between estimated and calendar age in this new group, using the neural net developed earlier without change. More importantly, differences within a subject in estimated age between periods of the day were much smaller than between the subjects. This is remarkable since substantial day-night changes in blood pressure and rest-exercise changes in heart rate and cardiac output were present. It appears, therefore, that neural nets estimate an age, which we suggest to call arterial age, quite independent from the state the subject is in. This arterial age may deviate (moderately) from calendar age, and the deviation remains nearly constant during a 24 hour day under the conditions of this study.

**Conclusion.** Neural nets appear able to detect subtle changes in arterial pressure waveform and, subject to training, can attach meaning to such changes. The detection of instrumental damping has an obvious clinical application. The detection of human arterial age, as yet, does not have an immediate clinical application but new research on the basis of this technique has been started. Presently attracting most intense clinical attention is the possibility to record continuous brachial artery pressure at a finger with Finapres by inverse waveform filtering and level correction.

# Samenvatting

In dit proefschrift wordt over het onderzoek gerapporteerd naar zekere eigenschappen of kwaliteiten van arteriële bloeddrukcurven, ook wel golfvorm, polsgolf of drukpols genoemd. Hierbij wordt voornamelijk gebruikt gemaakt van twee technieken: spectrale analyse en kunstmatige neurale netwerken. We onderzoeken de mogelijkheid om golfvormdemping te detecteren zoals die veroorzaakt kan worden door inadequate meetinstrumenten. We onderzoeken de vervorming van perifere arteriële drukcurven door fysiologische oorzaken met het doel voor deze vervorming te corrigeren. Tenslotte onderzoeken we of de leeftijd van een persoon tot uitdrukking komt in zijn (v/m) arteriële drukpulsaties en in hoeverre deze leeftijd met een goed geoefend neuraal netwerk geschat kan worden.

**Demping.** Catheter-manometer systemen worden routinematig ingezet om de arteriële druk bij patiënten te meten. Bij deze bloeddrukbewaking treedt instrumentele golfvormdemping op die zich vaak zeer geleidelijk, bijna onmerkbaar, in de tijd ontwikkelt. Dit beïnvloedt de vorm van de gemeten arteriële puls, en daarmee de bovendruk (systolische druk), en andere afgeleide parameters zoals het berekende slagvolume. De gemeten bloeddruk kan hierdoor fout, veelal te laag, zijn zonder waarschuwing. In *hoofdstuk III.1* is geprobeerd om een vroegtijdig waarschuwingssignaal te genereren voor het ontstaan van instrumentele golfvormdemping, voordat demping de bloeddruk zover vervormt dat het klinisch relevant en dus gevaarlijk wordt.

Kunstmatige neurale netten van verschillende architecturen zijn ontwikkeld om deze afname in de dynamische prestatie van het catheter-manometer systeem vroegtijdig te detecteren. De neurale netten werden getraind door middel van het zogenaamde 'back propagation' algoritme. Wij gebruikten hiervoor verzamelingen van brachiale arteriële bloeddrukcurven verkregen bij patiënten met normale of met een licht verhoogde bloeddruk. Van elke patiënt waren 5 tot 10 pulsaties beschikbaar. Een digitale simulatie van een catheter-manometer systeem is gebruikt om in exact doseerbare en bekende grootte een golfvormdemping aan te brengen, variërend van gering tot middelmatig. Elke slag in de golfvormen werd daarna gerepresenteerd door een elf-dimensionale parameter vector, die de verscheidene drukniveaus, tijdstippen van gebeurtenissen, en snelheden van verandering van de golfvormen bevat.

Het beste neurale net dat we ontwikkelde classificeerde 75% tot 85% van de individuele slagen correct hetzij als gedempt of ongedempt. Dit net classificeerde bovendien met een 'bij meerderheid van stemmen' algoritme waarbij alle golfpatronen van een patiënt betrokken worden, 16 van de 18 situaties bij de negen patiënten correct. Dat is statistisch significant veel beter dan een beslissing op basis van het opwerpen van een muntstuk ( $P < 0.001$ ). Nog belangrijker is de overweging dat deze neurale netten in staat blijken demping te detecteren nog voordat klinische relevante bloeddrukparameters zoals systo-

lische druk en berekend slagvolume echt zijn aangetast.

Neurale netten zijn blijkbaar zeer geschikt voor het detecteren van geringe demping van arteriële bloeddrukcurven voordat de golfvormen tot een klinisch relevant niveau zijn beïnvloed. Ons beste net doet dit betrouwbaar, continu en in real time.

In *hoofdstuk III.2* worden arteriële bloeddrukcurven die verkregen zijn tijdens lichamelijke inspanning met succes geklassificeerd als gedempt of ongedempt. Dit is belangrijk en lastiger omdat hierbij grote toenames in bloeddruk en hartslag optreden. Lichamelijke inspanning wordt bijvoorbeeld gebruikt in de revalidatie van hartpatiënten waarbij een adequate bewaking van ECG en bloeddruk nodig is.

In *hoofdstuk III.3* tenslotte worden de prestaties van menselijke experts en neurale netten in het detecteren van golfvorm-demping met elkaar vergeleken. Het blijkt dat neurale netten beter presteren dan menselijke experts. Menselijke experts blijken nauwelijks in staat zwak gedempte golfvormen te herkennen. Omdat geringe demping al een klinisch significante onderschatting van systolische drukniveaus en berekend slagvolume kan veroorzaken, is de menselijke expert daardoor meestal te laat. Wij vinden dit opmerkelijk omdat meestal de menselijk expert patronen veel beter herkent dan een machine of computer algoritme. En daarbij hebben we nog niet eens rekening gehouden met het feit dat het van een expert nauwelijks gevraagd kan worden om de geestdodende taak van het continu bewaken van een drukgolfvorm op het optreden van demping uit te voeren. We concluderen uit dit alles dat de ontwikkelde neurale netten klinisch toepasbaar zijn.

**Fysiologische vervorming.** De bloeddruk aan de bovenarm gemeten, de brachiale arteriële druk, wordt gebruikt voor diagnoses in de Inwendige Geneeskunde en de Cardiologie. Finapres is recentelijk een geaccepteerde methode geworden om arteriële druk continu en onbloedig te meten. De gemeten bloeddruk-niveaus en bloeddruk-pulsaties aan de vinger gemeten verschillen echter van die in de brachiale slagader. Door middel van Fourier analyses hebben we deze verschillen tussen de brachiale en vinger polsgolf gemodelleerd (*hoofdstuk IV*).

Bij 53 volwassen proefpersonen werd de brachiale arteriële druk bloedig gemeten en tegelijkertijd de vingerdruk onbloedig door middel van de Finapres. De gemiddelde druk werd afgetrokken van elke drukgolfvorm en Fourier analyses werden toegepast op de pulsaties. Een vervormingsmodel werd geschat voor elk proefpersoon en daarna werd een gemiddeld model berekend voor de groep. Vervolgens werd een model berekend dat exact de omgekeerde lineaire vervorming geeft. Dit inverse model werd toegepast op de volledige vingerdruk met het doel de vervorming te corrigeren. Het overgebleven drukniveauverschil werd gemodelleerd via multi-pele regressie analyse.

Het blijkt dat golfvervorming beschreven kan worden door een algemeen, frequentie afhankelijk model met een resonantie bij 7.3 Hz. Het inverse model heeft een anti-resonantie bij deze frequentie. Het converteert vinger naar brachiale pulsaties waarbij de gemiddelde golfvervorming gereduceerd wordt van 9.7 (SD 3.2) mmHg per genomen monster op de vinger golfvorm naar 3.7 (1.7) mmHg voor de geconverteerde puls. Door toepassing van het inverse model wordt de normale drukonderschatting aan de vinger veranderd in een

overschatting als volgt: de systolische niveauverschillen veranderen van -4 (SD 15) naar +8 (14) en de diastolische verschillen van -8 (11) naar +8 (12) mmHg. Het multi-pele regressie model reduceerde daarna zowel de gemiddelden als de standaard deviaties van de verschillen tot 0 (13) en 0 (8) mmHg. Diastolische verschillen blijken het sterkste verminderd.

We zijn dus in staat om uit de vingerdruk brachiale golfvormen te reconstrueren die sterk lijken op de intra-brachiale bloeddruk. Daarbij wordt aan een klinische behoefte tegemoet gekomen.

**Leeftijdsschatting.** De arteriële polsgolf vertoont karakteristieke veranderingen met het ouder worden. Geofende waarnemers zijn dan ook in staat aan de hand van de polsgolf de leeftijdscategorie van een persoon in te schatten. In het verleden zijn er zelfs catalogi van gemiddelde polsgolven samengesteld per decade van tien jaar ouderdom waaruit de gemiddelde veroudering van de polsgolf duidelijk blijkt. We wilden onderzoeken of het inverse proces van leeftijdsschatting aan de hand van de polsgolf door een computer kon worden uitgevoerd. Verder wilden we dit doen op individuele basis.

We trainden daartoe kunstmatige neurale netten met behulp van het back propagation algoritme om modellen voor het schatten van de leeftijd te ontwikkelen (*hoofdstuk V.1*). We gebruikten de drukgolfvormen van 65 proefpersonen in de leeftijd van 8 tot 83 jaar waarbij zowel gezonde personen als patiënten met hypertensie en cardiovasculaire aandoeningen werden geïnccludeerd. Na de training werd het net getest met behulp van de golfvormen van 41 andere proefpersonen variërend in leeftijd van 9 tot 75 jaar met overigens een vergelijkbare verdeling van gezond of ziek, vrouw of man. Alle metingen zijn verricht onder laboratorium omstandigheden in liggende houding. De bloeddruk werd geregistreerd aan de dominante hand waarbij gebruik werd gemaakt van een Finapres model 4 of 5 van TNO.

De beste resultaten werden verkregen als de eerste 0.5 seconden van de gedifferentieerde polsgolf werd aangeboden aan het neurale net. Verschillen tussen de geschatte en de werkelijke leeftijd van de proefpersonen in de test groep bedroegen gemiddeld -1 (SD 8) jaar. De correlatiecoëfficiënt tussen de geschatte en de werkelijke leeftijd bedroeg 0.92. Een groot verschil in leeftijd, bloeddruk en hartslag, hypertensie of vaatlijden, en het gebruik van vaso-actieve medicatie lijken de nauwkeurigheid van de leeftijdsschatting niet te beïnvloeden. Sommige proefpersonen blijken voor hun leeftijd jonge golfvormen te hebben terwijl anderen juist oude golfvormen blijken te hebben. Deze verschillen lijken afwezig te zijn bij personen jonger dan 30 jaar.

De golfvormen en de hoogte van de bloeddruk verschillende gedurende de dag en de nacht maar de leeftijd van de persoon blijft (vrijwel) gelijk. In *hoofdstuk V.2*, onderzoeken we de stabiliteit van de geschatte leeftijd gedurende de 24-uurs dag.

De 24-uurs registratie van de bloeddruk met een Portapres Model 1 draagbare bloeddrukmeter van TNO vond plaats volgens een streng protocol met ondermeer vaste periodes van fietsergometrie, wandelen buiten het ziekenhuis, middagdut en slaap.

We bleken niet in staat significante verschillen in geschatte leeftijden over enige pe-

riode gedurende de dag aan te tonen. Ook werd er geen significant verschil gevonden tussen geschatte en werkelijke leeftijd in deze nieuwe groep. Nog belangrijker was dat verschillen in geschatte leeftijd voor verschillende perioden van de dag per proefpersoon kleiner waren dan verschillen tussen proefpersonen. Dit is opmerkelijk omdat er aanzienlijke veranderingen optraden in bloeddruk voor dag en nacht en in hartslag en cardiac output voor rust- en inspanningsperioden.

Hieruit blijkt dat neurale netten een leeftijd schatten—die we arteriële leeftijd zouden willen noemen—die nagenoeg onafhankelijk is van de toestand waarin de persoon verkeert. Deze arteriële leeftijd kan (gemiddeld) afwijken van de werkelijke leeftijd maar de afwijking is vrijwel constant gedurende de 24 uur die een dag telt.

**Conclusie.** Neurale netten blijken in staat te zijn om subtiele veranderingen in de vorm van de arteriële drukgolf te detecteren en, indien goed geoefend, deze veranderingen te kunnen waarderen. Het detecteren van instrumentele demping heeft een duidelijke klinische toepassing. Het detecteren van de ouderdom van de menselijke arteriën heeft nog geen directe klinische toepassing, maar nieuw onderzoek naar deze techniek is reeds aangevangen. Op dit moment is de aandacht van klinici vooral gericht op de nu gerealiseerde mogelijkheid om met Finapres continu de brachiale arteriedruk aan de vinger te registreren. Dit met behulp van inverse filtering van de golfvorm en na hoogte correctie.

# Curriculum vitae

Andriana Prentza was born on the 20th of May, 1968, in Sydney, Australia, and moved to Greece in 1972. After graduating from secondary school in Athens, Greece, in 1986, she attended the University of Patras, Patras, Greece and received her diploma degree from the Department of Computer Engineering and Information Sciences in July 1991.

In the following one year, she attended a european postgraduate course in Biomedical Engineering, organized by the university of Patras, Patras, Greece, supported by the ERASMUS Program of the European Union.

In October 1992 she started research as a Ph.D student at the Eindhoven University of Technology under the guidance of prof.ir. K. H. Wesseling. The work finally resulted in this thesis.

# **Stellingen**

behorende bij het proefschrift

## **Blood pressure waveform characteristics exposed by spectral analysis and neural nets**

door

**Andriana Prentza**

1.

Artificial neural networks are possibly ten orders of magnitude more simple than networks of neurons. They are simply no comparison.

2.

The arterial pulse is the same nowhere: it distorts and degrades travelling in the arterial system.

3.

Relying on human experts impedes the training of artificial neural networks.

*this dissertation, chapter III*

4.

A person is as old as his pulse.

*this dissertation, chapter V*

5.

A person's age is stable during the 24 hour day although his blood pressure is not.

*this dissertation, chapter V*

6.

The human arm arterial system to the finger does not show its age.

*this dissertation, chapter V*

7.

Arteries are akin to organ pipes. The shorter length produces the higher tone.

*this dissertation, chapter IV*



8.

Special measures are needed for thermodilution cardiac output estimation to achieve clinical reliability, which could receive clinical recognition.

*J.R.C. Jansen - The thermodilution method for the clinical assessment of cardiac output, Intensive Care Med, 21:691-697, 1995*

9.

Both in secure communications protocols and in artificial neural nets back propagation is a most useful idea.

10.

Taking risks comes before luck.

11.

In a male predominant environment as the faculty of Electrical Engineering in Eindhoven, the requirement that for early or late access to the workplace two persons of the same sex need to be present, is next to impossible to obey for the female minority. What's wrong with the opposite sex?

12.

If you were to say to the grown-ups: 'I saw a beautiful house made of rosy brick, with geraniums in the windows and doves on the roof', they would not be able to get any idea of that house at all. You would have to say to them : 'I saw a house that cost \$20,000'. Then they would exclaim : 'Oh, what a pretty house that is!'

*Antoine de Saint-Exupery - The Little Prince*

Eindhoven, July 3, 1997

